"Description of Finn MacCool and his people, being a humorous or quasi-humorous incursion into ancient mythology:

Too great was he for standing. The neck to him was as the bole of a great oak, knolled and seized together with muscle-humps and carbuncles of tangled sinew, the better for good feasting and contending with the bards. Each thigh to him was to the thickness of a horse's belly, narrowing to a green-veined calf to the thickness of a foal. Three fifties of fosterlings could engage with handball against the wideness of his backside, which was wide enough to halt the march of warriors through a mountain pass.

On the kerseymere of the gutted jacket to his back was the dark tincture of the ivory sloes and the manivaries whortles of the ditches of the east of Erin; for it was here that he would spent a part of the year with his people, courting and rummaging generous women, vibrating quick spears at the old stag of Slieve Gullian, hog-baiting in thickets and engaging in sapient dialectics with the bag-eyed brahons.

The knees and calves to him, swealed and swathed with soogawns and Thomond weed-ropes, were hardened by stainings of mead and trickles of metheglin and all the dribblings and drippings of his medher, for it was the custom of Finn to drink nightly with his people.

I am a bark tor buffeting, said Finn,
I am a hound for thornypaws.
I am a doe for swiftness.
I am a tree for wind seige.
I am a windmill.
I am a hole in a wall."

At Swim-Two-Birds.
Flann O'Brien

DEDICATION

To my parents

To my brothers and sisters

and to Jackie DeRoo.

THE ABSORPTION SPECTRUM OF CARBONYL SELENIDE

THE ABSORPTION SPECTRUM OF CARBONYL SELENIDE

by

EOIN JUSTIN FINN, B.Sc.

A Thesis

Submitted to the School of Graduate Studies

in Partial Fulfillment of the Requirements

for the Degree

Doctor of Philosophy

McMaster University

April 1973

DOCTOR OF PHILOSOPHY (1973)
CHEMISTRY

McMASTER UNIVERSITY
Hamilton, Ontario.

TITLE: The Absorption Spectrum of Carbonyl Selenide

AUTHOR: Eoin Justin Finn, B.Sc. (National University of Ireland)

SUPERVISOR: Dr. G. W. King

NUMBER OF PAGES: ix, 153, a(x)

SCOPE AND CONTENTS:

The absorption spectrum of gas-phase carbonyl selenide (OCSe) in the infrared, ultraviolet and vacuum ultraviolet regions of the electromagnetic sprectrum has been recorded under high resolution. A method of synthesis of the compound, which has been used in the preparation of selenium-isotope OCSe, has been described. A description of a novel light source, the emission continuum produced by which is suitable for absorption spectroscopy of the ultraviolet and vacuum ultraviolet spectral regions, has been included.

The ground state fundamental vibrational frequencies of carbonyl selenide have been determined. The spectrum in the ultraviolet and vacuum ultraviolet regions has been assigned to correspond to seventeen electronic transitions of OCSe. Vibrational analyses have been accomplished for each of these, and the symmetries and electron configurations of the excited electronic states have been assigned. The ionization potential of OCSe has been measured.

The majority of these transitions have been shown to be Rydberg in nature. Quantum-mechanical calculations have been performed to predict the term values for Rydberg series members and to aid the analysis of the spectrum. The spin-orbit coupling in Rydberg states of OCSe has been

shown to be intermediate between the cases (Λ,S) and (Ω_c,ω), and to tend to the latter case as the ionization limit is approached.

Some details of the spectra of the isoelectronic molecules OCS and CS_2 have been included to support the analysis of the OCSe spectrum.

ACKNOWLEDGEMENTS

I wish to thank most sincerely my research colleague, Frank Greening, whose help and advice contributed in no small measure to the subject matter of this thesis. Also, I especially thank my colleague, Bob McLean, for his kind help in converting a rusty sewer pipe to a vacuum spectrograph. I am grateful to my other research colleagues: M. Danyluk, E. R. Farnworth, D. Grangé, Dr. H. E. Howard-Lock, R. Judge, Dr. K. G. Kidd, Z. B. Lemanczyk, R. C. Meatherall, Dr. J. P. McBride, Dr. K. I. Shrikameswaran, Dr. S. P. So, Dr. C. R. Subramaniam, A. A. van Putten and Dr. C. H. Warren. I thank them all for their kindness, advice and assistance during my stay at McMaster, and I take this opportunity to wish them the very best for the future.

I would like to express my appreciation to Dr. G. N. King for his many helpful criticisms of the manuscript of this thesis.

To the staff of the electronic and machine shops of McMaster University, I offer my gratitude. I am grateful to Mr. J. Bradford for technical assistance and to Susan Hawley, who typed this thesis.

I am indebted to the people of Ontario who, through their government, provided financial assistance during the course of this work.

Finally, I thank my friends of the McMaster University Climbing and Caving Club for preserving my life and limbs during many enjoyable ups, downs and danglings in the truly beautiful wildernesses of this continent.

TABLE OF CONTENTS

LIST OF TABLES

LIST OF TABLES (cont'd)

LIST OF FIGURES

LIST OF FIGURES (cont'd)

CHAPTER I

INTRODUCTION

In this thesis, the investigation of some electronic states and structures of the triatomic molecule, carbonyl selenide (OCSe), by use of the experimental technique of gas phase absorption spectroscopy, is reported. An elementary knowledge of quantum mechanics and group theory is assumed throughout.

1.1. Separation of the Wave Equation

A molecule is a system of electrons and nuclei, in which the nuclei are separated by distances of the order of 10^{-9} - 10^{-10} m. The time-independent Schrödinger equation for a system in which energy is conserved may be written as

$$H\psi_T = E_T\psi_T \qquad [1.1]$$

where H is the quantum-mechanical Hamiltonian operator, E_T are the energy eigenvalues and ψ_T are the corresponding energy eigenfunctions. The latter characterize the stationary states of the system. If nuclear and electronic spin, and translation of the molecule as a whole, are neglected, the molecular Hamiltonian, H, may be written as

$$H = -\sum_i \frac{\hbar^2}{2m_i}\nabla_i^2 - \sum_A \frac{\hbar^2}{2M_A}\nabla_A^2 - \sum_{A,i} \frac{Z_A e^2}{r_{Ai}} + \sum_{A>B} \frac{Z_A Z_B e^2}{r_{AB}} + \sum_{i>j} \frac{e^2}{r_{ij}}$$

where: $h = 2\pi\hbar$ is Planck's constant,

m_i and M_A are the masses of the i^{th} electron and the A^{th} nucleus, respectively,

∇^2 is the Laplacian operator,

Z_A is the atomic number of nucleus A,

$r_{\alpha\beta}$ is the distance between particles α and β, and

e is the absolute value of the electronic charge.

Because of the mass difference between electrons and nuclei, classical electronic motion occurs much more rapidly than nuclear motion. The Born-Oppenheimer[1] approximation assumes that these motions can be separated, i.e., the electron distribution is an instantaneous function of any nuclear conformation. ψ_T may, in this approximation, be written as the product

$$\psi_T = \psi_e \cdot \psi_N \qquad [1.2]$$

where ψ_e are eigenfunctions of the electronic Hamiltonian H_e with eigenvalues E_e and ψ_N are eigenfunctions of the nuclear Hamiltonian H_N, where

$$H_e = -\sum_i \frac{\hbar^2}{2m_i} \nabla_i^2 - \sum_{A,i} \frac{Z_A e^2}{r_{Ai}} + \sum_{i>j} \frac{e^2}{r_{ij}} \qquad [1.3]$$

for a fixed nuclear configuration. The equation

$$H_e \psi_e = E_e \psi_e \qquad [1.4]$$

is the Schrödinger equation of the electrons moving in the field of the fixed nuclei and having a potential energy U_e, which is a function of electronic coordinates. U_e varies as the internuclear separations are changed, and therefore the eigenfunctions ψ_e and the eigenvalues E_e of equation [1.4] depend on the nuclear coordinates as parameters.

The nuclear Hamiltonian, H_N, is given by

$$H_N = -\sum_A \frac{\hbar^2}{2M_A} \nabla_A^2 + \sum_{A>B} \frac{Z_A Z_B e^2}{r_{AB}} + E_e \qquad [1.5]$$

The kinetic energy term, $-\sum_A \frac{\hbar^2}{2M_A} \nabla_A^2$, contains both vibrational and rotational contributions. In the rigid rotor[2] approximation, rotational and vibrational motions may be separated.

The total wavefunction and the total energy may then be written as

$$\psi_T = \psi_e \psi_{VIB} \psi_{ROT} \qquad [1.6]$$

and

$$E_T = E_e + E_{VIB} + E_{ROT} \qquad [1.7]$$

respectively.

Where small interactions occur among these components, the methods of perturbation theory may be applied to obtain closer approximations to ψ_T and E_T. Where interactions are large, the partitionings represented by equations [1.6] and [1.7], and the approximations on which the latter are based, are no longer valid.

1.2. Spectroscopic Transitions

Transitions between the stationary states of a molecule may be induced by interaction with an oscillating electromagnetic field[3]. If a term representing this interaction is included in the molecular Schrödinger equation, it may be shown[4] that, for a system originally in a state characterized by the quantized energy E_m, a non-zero probability arises of finding the system in a state of energy E_n if radiation of energy

$$\nu = \frac{E_m - E_n}{hc} \quad (E_m > E_n) \qquad [1.8]$$

was present. If E_m and E_n are given in ergs, h in erg.sec, and c, the velocity of light in vacuo, in $cm.sec^{-1}$, then ν is given in wavenumber units (cm^{-1}).

The quantized energies associated with the motions of the electrons

and nuclei in a molecule extend over a wide range and the quanta emitted or absorbed by a molecule in transitions between the various energy levels associated with these motions differ considerably in magnitude. The spectra corresponding to these transitions are roughly divided in energy and description as follows:

1. Pure Rotational Spectra: These correspond to transitions between the rotational energy levels associated with a vibrational energy level of the ground electronic state. They occur in the microwave region (~0.1-100 cm^{-1}).
2. Vibrational Spectra: Transitions between vibrational levels of the ground electronic state give rise to vibrational spectra in the infrared region of the electromagnetic spectrum (~100-4000 cm^{-1}). Accompanying changes in rotational energy give rise to rotational fine structure in these spectra.
3. Electronic Spectra: Spectra observed in the visible, ultraviolet and vacuum ultraviolet regions (~10^4-2×10^5 cm^{-1}) are associated with electronic excitation in molecules. Changes in vibrational and rotational energies may also occur in these excitations.

1.3. Selection Rules

The probability of an electric dipolar transition between two states described by the total eigenfunctions ψ_n and ψ_m is proportional to the square of the transition moment integral M, defined by

$$\overline{M} = \int \psi_m^* \overline{P} \psi_n d\tau \qquad [1.9]$$

where the integral is taken over the whole configuration space of the molecule

and $\bar{P}$ is the electric dipole moment operator. Excluding the rotational eigenfunction, the total eigenfunction of any state of a system may be approximated[1] as (c.f. equation [1.6])

$$\psi_T = \psi_e \psi_v \qquad [1.10]$$

and $\bar{P}$ may be separated as

$$\bar{P} = \bar{P}_e + \bar{P}_N \qquad [1.11]$$

where $\bar{P}_e$ and $\bar{P}_N$ are the electric dipole moment operators associated with the charge distributions of the electrons and nuclei, respectively. Equation [1.9] may be rewritten as

$$\bar{M} = \int \psi_v' \bar{P}_n \psi_v'' d\tau_n \int \psi_e' \psi_e'' d\tau_e + \int \psi_v' \psi_v'' d\tau_n \int \psi_e' \bar{P}_e \psi_e'' d\tau_e \qquad [1.12]$$

where the single and double prime symbols refer to the upper and lower energy states of a vibronic transition, respectively. For a common nuclear conformation, ψ_e' and ψ_e'' are orthogonal if they refer to different electronic states, and the first term of equation [1.12] vanishes. The purely electronic transition moment, given by

$$\bar{M}_e = \int \psi_e'(r,Q) \bar{P}_e \psi_e''(r,Q) d\tau_e \qquad [1.13]$$

depends upon the electronic coordinates r and the nuclear coordinates Q in the combining states. The approximation generally made is that this integral is calculated at the equilibrium position, Q_o, of the nuclei in the initial state. $\bar{M}_e$ then becomes independent of nuclear coordinates, and equation [1.12] becomes

$$\bar{M} = \bar{M}_e(Q_o) \int \psi_v' \psi_v'' d\tau_n \qquad [1.14]$$

The symmetry classification of electronic and vibrational eigenfunctions has been given by several authors[5,6,7]. The methods of group theory may be applied to the determination of those transitions for which $\bar{M}$ is non-zero[8].

The quantity $\bar{M}_e(Q_o)$ is non-zero only if the direct product of the irreducible representation (I.R.) of ψ_e' and ψ_e'',

$$\Gamma(\psi_e') \times \Gamma(\psi_e'') \qquad [1.15]$$

contains the I.R. $\Gamma(\bar{P}_e^x)$, $\Gamma(\bar{P}_e^y)$ or $\Gamma(\bar{P}_e^z)$. $\bar{P}_e^x$, $\bar{P}_e^y$ and $\bar{P}_e^z$ are the vector components of $\bar{P}_e$ in the axis system (x, y, z) of the molecule. The quantity

$$\int \psi_v' \psi_v'' d\tau_n \qquad [1.16]$$

in equation [1.14] gives the magnitude of the overlap for the vibrational eigenfunctions in the combining electronic states. It is non-zero only if

$$\Gamma(\psi') \times \Gamma(\psi'') \qquad [1.17]$$

contains a component which transforms as the totally symmetric representation of the molecular point group.

Where $\bar{M}_e(Q_o)$ is zero or non-zero, the electronic transition is commonly denoted as forbidden or allowed, respectively. The magnitude of the quantity in [1.16] determines the intensity distribution among vibronic components of an allowed electronic transition[9].

Electric dipolar transitions between different electronic states of molecules classified under the symmetry point groups C_{2v} and C_s, where the molecules belong to the same point group in the combining electronic states, are shown in Table 1.1. The orientations of the dipole moments for allowed

transitions are also indicated.

Inclusion of the electronic spin eigenfunction in equation [1.6] leads to the spin selection rule for electronic transitions

$$\Delta S = 0 \qquad [1.18]$$

where S is the quantum number of the total electronic spin.

1.4. Previous Work on Carbonyl Selenide

1.4.1. General

Some information on OCSe, known prior to the present investigation, is listed in Table 1.2.

1.4.2. Previous Investigations of the Electronic Spectrum of OCSe

Stiles, Tyerman, Strausz and Gunning[11] have reported the ultraviolet gas-phase absorption spectrum of OCSe under low resolution. Two distinct regions of absorption were observed: (1) a weak diffuse absorption in the 2800 Å-2250 Å region, and (2) a much stronger, apparently banded, system in the 2150 Å-(1900 Å) region. No assignments were made.

M. Bavia, G. D. Lonardo, C. Galloni and A. Trombetti[12] have recorded the gas-phase absorption spectrum of non-isotopic OCSe both in the infrared (300-5000 cm^{-1}) and in the ultraviolet (2600-1350 Å) regions. No fewer than seventeen electronic origins have been assigned. Except for the first system in the 2500 Å region, where the bending vibration, ν_2, is reported active, the vibrational structure associated with these systems has been analyzed in terms of the totally symmetric normal modes ν_1 and ν_3. The electron configurations and symmetries of the states were, in general, not given. These workers could not identify the Rydberg states associated with the frequencies observed in

TABLE 1.1

TRANSITION MOMENTS OF ELECTRONIC TRANSITIONS

OF MOLECULES BELONGING TO THE POINT GROUPS $C_{\infty v}$ AND C_s

$C_{\infty v}$	Σ^+	Σ^-	π	Δ	Φ	.....
	P_z	f.	P_x, P_y	f.	f.	Σ^+
		P_z	P_x, P_y	f.	f.	Σ^-
			P_z	P_x, P_y	f.	π
				P_z	P_x, P_y	Δ
					P_z	Φ
						⋮

C_s	A'	A"
	P_y, P_z	P_x A'
		P_y, P_z A"

NOTES: (i) f. denotes an electric dipolar forbidden transition.

(ii) The molecule-fixed Cartesian coordinates x and y have been chosen to define the molecular plane in the C_s symmetry group, and the z coordinate to define the molecular axis in the $C_{\infty v}$ point group. These are in accord with international convention[10].

the vacuum ultraviolet spectrum. A summary of these results is given below. The spectra were recorded in the U.V. and V.U.V. regions at reciprocal linear dispersions of 2.5 Å/mm and 8 Å/mm, respectively.

TABLE 1.2

INFORMATION ON OCSe KNOWN PRIOR TO THE PRESENT INVESTIGATION

(i) Colour: Colourless (gaseous and liquid phases), white crystalline (solid phase).

(ii) Physiological: Foul odour, toxic[13].

(iii) Melting point: -122.1°C[14].

(iv) Boiling point: -22.9°C/725 torr[14].

(v) Dipole moment: 0.59×10^{-18} e.s.u.[15].

(vi) Density: 1.812 gs/cc (liquid phase/4.1°C)[13].

(vii) Latent heat of vaporization: 49.3 cal/gm[14].

(viii) Vapour pressure[14]:

T (°C)	-95	-83.4	-63.3	-45.5	-30.6	-22.9
P (mm)	10.0	23.1	91.2	254.7	505.0	722.9

(ix) Miscellaneous: Decomposes (i) when heated to 500°C, (ii) in the presence of moisture, and (iii) in an electric discharge, to carbon monoxide and selenium[13].

(x) Geometrical structure in the ground electronic state[16,17,18]:

O—C bond length = 1.160 Å

C—Se bond length = 1.711 Å

OĈSe angle = 180°

(xi) Vibrational frequencies of the ground electronic state (gaseous phase):

Symmetry	Vibrational Assignment	Frequency (cm^{-1})
σ	ν_1	2021.2[18,20], 2022.3[12]
π	ν_2	466.1[20], 474[16], 465.5[12]
σ	ν_3	642.1[20,18], 643.0[12]
σ	$2\nu_1$	4020.2[12]
σ	$\nu_1 + \nu_3$	2664.0[12]
σ	$2\nu_2$	927.1[12]

TABLE 1.2 (continued)

(xii) Rotational constants in the ground electronic state[16]:

O^{16}-C^{12}-Se^{80}	$^{*}B_{ooo} = 0.1340\ cm^{-1}$
O^{16}-C^{12}-Se^{78}	$B_{ooo} = 0.1348\ cm^{-1}$
O^{16}-C^{13}-Se^{80}	$B_{ooo} = 0.1328\ cm^{-1}$

(xiii) Mean square amplitudes of vibration in the G.E.S.[19] (T = 298°K):

σ_{CO} stretch = 0.001224 Å

σ_{CSe} stretch = 0.001594 Å

*The subscript ooo indicates the zeroth vibrational energy level.

TABLE 1.3

SUMMARY OF OBSERVED STATES* OF OCSe

State	T_o	ν_1	ν_2	ν_3
$\tilde{X}$ ($^1\Sigma^+$)	0	2022.3	465.5	643.0
$\tilde{A}$ (A' or A")	39480		440	
$\tilde{B}$ ($^1\Sigma^+$ or $^1\Pi$)	47055			490
$\tilde{C}$	55588			585
$\tilde{D}$	56021			567
$\tilde{E}$	56865	(1500)[a]		565
$\tilde{F}$	58365			565
$\tilde{G}$	60155			570
$\tilde{H}$	64386	(1828)[b]		537
$\tilde{I}$	64539	(1750)[c]		511
$\tilde{L}$	66214			531
$\tilde{M}$	66298			510
$\tilde{N}$	67587	(1916)[d]		529
$\tilde{O}$	68151			548
$\tilde{P}$	68296	(1963)[e]		530
$\tilde{Q}$	69503			511
$\tilde{R}$	70259			527
$\tilde{S}$	72044			503

*all data in cm^{-1}.

[a]origin of $\tilde{F}$ may be $T_o(\tilde{E}) + \nu_1(\tilde{E})$.

[b]origin of $\tilde{L}$ may be $T_o(\tilde{H}) + \nu_1(\tilde{H})$.

[c]origin of $\tilde{M}$ may be $T_o(\tilde{I}) + \nu_1(\tilde{I})$.

[d]origin of $\tilde{Q}$ may be $T_o(\tilde{N}) + \nu_1(\tilde{N})$.

[e]origin of $\tilde{R}$ may be $T_o(\tilde{R}) + \nu_1(\tilde{R})$.

CHAPTER II

EXPERIMENTAL WORK

2.1. Previous Syntheses of Carbonyl Selenide

The synthesis of isotopically-natural carbonyl selenide has been reported by several authors[13,15,21,22]. Pearson and Robinson[13] prepared OCSe by flowing carbon monoxide over selenium heated to 500°C. The reported yield was 3.6% by volume of OCSe. Glemser and Risler[15] prepared OCSe in 36% yield by the reaction $Al_2Se_3 + 3COCl_2 \rightarrow 3OCSe + 2AlCl_3$. In this method, phosgene was flowed at 1.75 litres/hour over Al_2Se_3 heated to 219°C. The other methods reported only trace quantities of OCSe.

2.2. Synthesis of Carbonyl Selenide from Natural Selenium

The method of Glemser and Risler[15] was attempted, but a thick-walled sealed pyrex reaction tube was used instead of a flow method. The reaction of 20 mg. Al_2Se_3 (Alfa Inorganics) and phosgene at 100 torr yielded the products, CO, CO_2, Cl_2 and traces of OCSe.

With natural selenium, the methods of Pearson and Robinson[13] was employed in order to obtain sufficient sample for a preliminary investigation of the spectrum of OCSe. Fig. 2.1 is a schematic illustration of the apparatus used. Carbon monoxide gas (Matheson, 99% purity) was flowed from a cylinder at a rate of 3 litres/hour over Se powder (Sargent) heated to ~500°C. The products were collected in cold traps kept at liquid nitrogen temperature. Infrared absorption measurements confirmed that the major product was OCSe, with traces of CSe_2 and CO_2. Fractional trap-to-trap distillation at -96°C largely removed these impurities.

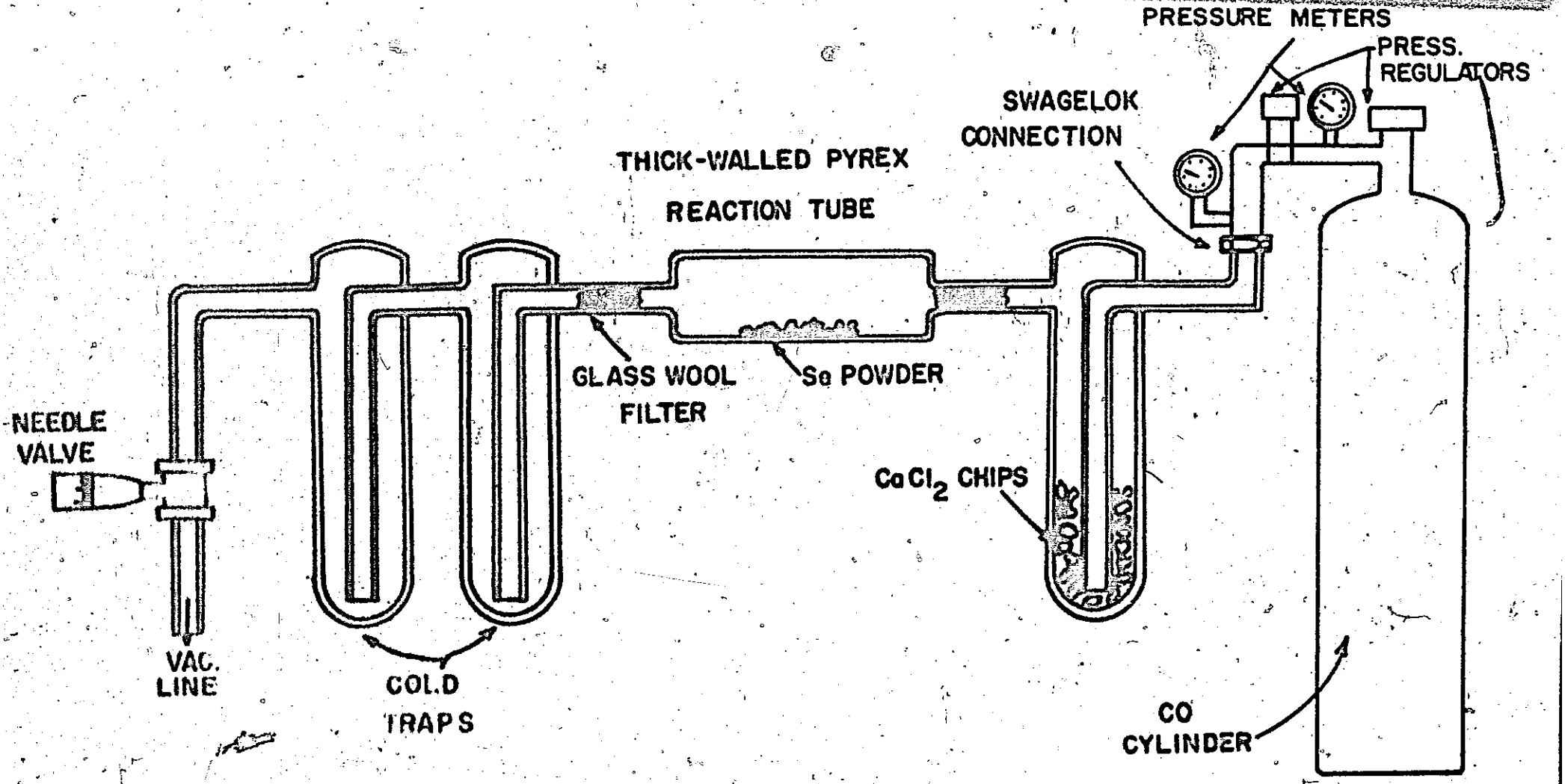

Fig. 2.1.. Apparatus for synthesis of $OCSe^{nat}$ (schematic).

Carbonyl selenide is stable when stored, at room temperature, in a closed glass container. It decomposes on contact with mercury or stopcock grease (Apiezon N).

2.3. Synthesis of Carbonyl Selenide from Selenium Isotopes

Selenium has six stable isotopes, the natural abundances of which are: Se 82, 88%; Se 80, 49.9%; Se 78, 23.6%; Se 77, 7.5%; Se 76, 9.12%; Se 74, 0.96%. Synthetic methods previously described did not prove suitable for the isotopic synthesis of OCSe because of their low efficiency. Also, the offensive odour and toxicity of Se and OCSe required that the synthesis be conducted in a closed system. A new synthesis was developed and is described here. The isotopes Se^{80} and Se^{78}, obtained from Oak Ridge National Laboratory of the United States Atomic Energy Commission, were used in the synthesis. They had isotopic purities of 97% and 96% respectively. Fig. 2.2 is a schematic illustration of the apparatus used.

3 ml. of 1,2,3,4-tetrahydronaphthalene (Matheson, Coleman and Bell) and 15 mg. Se isotope were placed in reaction tube A. After evacuation, the tube was sealed at the constriction. Similarly, 1-2 g. of p-bromophenylisocyanate (Eastman Kodak Reagent grade M.PT. 42°C) were placed in reaction tube B. The reactants in tube A, upon careful heating to 500°C, produced isotopic H_2Se. The breakseal was then broken and the H_2Se condensed into reaction tube B, kept at liquid nitrogen temperature, while tube A was kept at -23°C to reduce the vapour pressure of both naphthalene and 1,2,3,4-tetrahydronaphthalene. Reaction tube B, isolated by sealing at the central constriction, was then heated to 100°C for 1-2 hours to ensure complete reaction of the H_2Se. (This impurity absorbs strongly in the U.V. and V.U.V. regions.) After

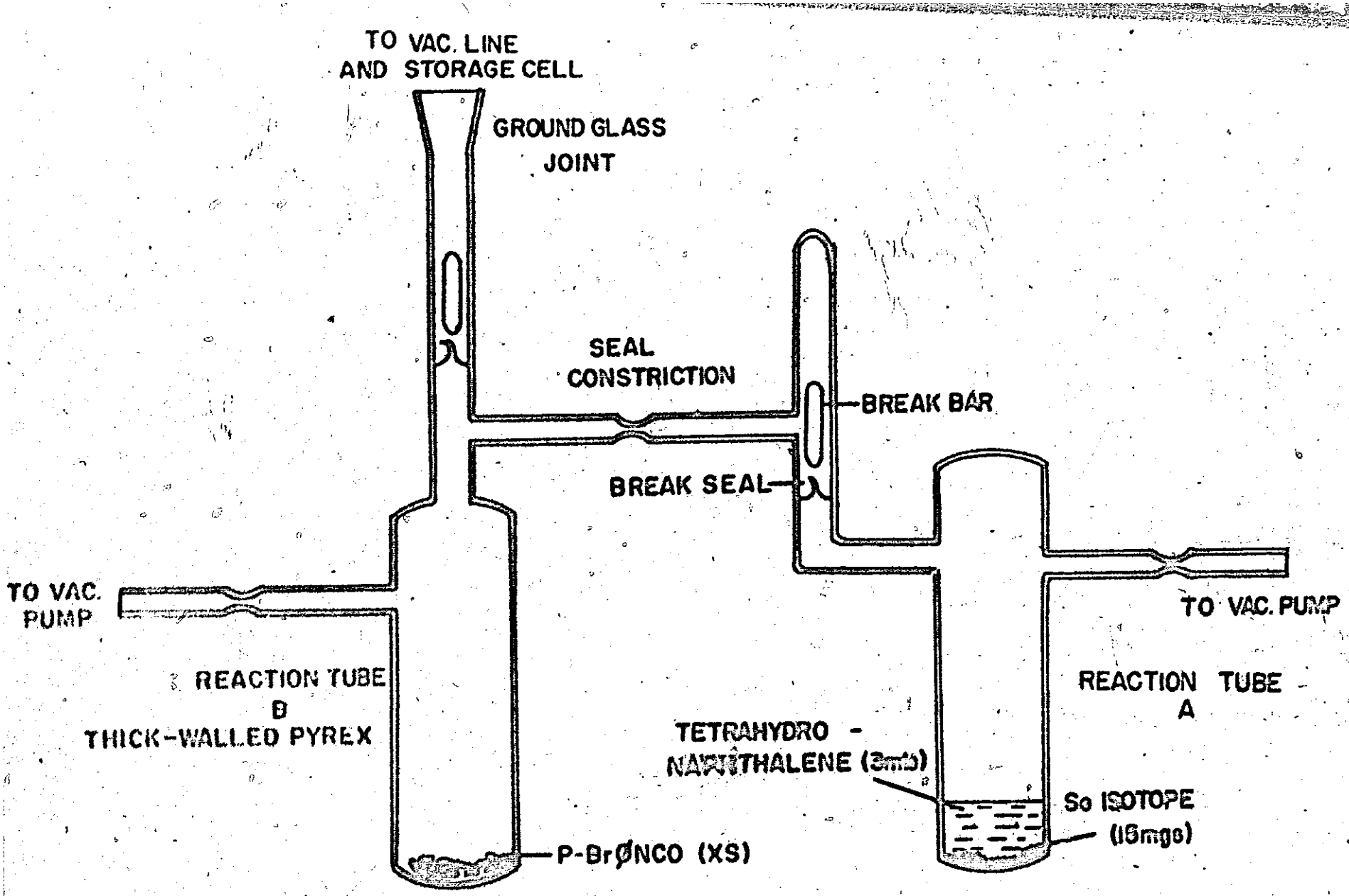

Fig. 2.2. Apparatus for synthesis of $OCSe^{i}$ (schematic).

breaking the breakseal on tube B, the hydrogen and carbon monoxide were pumped off at liquid nitrogen temperature. Vacuum distillation of the products at -96°C yielded high purity OCSe, though some traces of CO and CO_2 were noted in the I.R. spectrum of the products. The yield of OCSe was calculated to be in the range 70-80%.

A variation of this synthetic method has been tested for the production of $O^{18}CSe$ (and $O^{18}CS$) from $O_2{}^{18}$ gas. This variation is described in Appendix A.1.

2.4. Preparation of Carbonyl Sulfide and Carbon Disulfide

Carbonyl sulfide gas, supplied by Matheson (96% purity), was purified by repeated distillation from a cold trap kept at -130°C until no bands, which could be attributed to either CO_2 or CS_2, could be observed in the spectrum in the 2000 Å - 1600 Å region.

Reagent grade carbon disulfide was degassed and used without further purification.

2.5. Infrared Spectra

Infrared absorption spectra in the 4000 cm^{-1} - 250 cm^{-1} region were recorded using a Perkin Elmer model 521 grating spectrophotometer. All spectra were recorded at room temperature. The vacuum wavelengths of absorption features were determined with respect to the vacuum wavelengths of absorption peaks due to a thin polystyrene film. The infrared cells were 10 cm long and were fitted with KBr windows. Cell pressures were not measured directly but were estimated from pressure-volume relationships to be of the order of 10-15 torr. The uncertainty on the measured frequencies was estimated to be ±2.0 cm^{-1}.

2.6. Low Resolution Electronic Spectra

All spectra reported here were measured in the gas phase. The ultraviolet absorption spectrum of carbonyl selenide vapour was recorded at room temperature on each of three low-resolution instruments: a Cary Model 14 spectrophotometer, a Bausch and Lomb Model 11 1.5 metre concave grating spectrograph, and a Hilger and Watts Model 492 1.5 metre Littrow-mounted quartz prism spectrograph. With the Cary instrument, the scan region was 4000 Å - 1850 Å. Five and 10 cm quartz absorption cells were used, with cell pressures of from 5-15 torr of OCSe. The Bausch and Lomb and Hilger and Watts spectrographs were used to record spectra photographically in the 3000 Å - 2200 Å region. A 50 cm long quartz absorption cell, filled with OCSe to a pressure of about 2 torr, was used. The Bausch and Lomb spectrograph, which was used in the second order of the grating, had a dispersion and resolving power of 7.5 Å/mm and 70,000, respectively. The source, a 250 w Xenon arc (Osram XBO high pressure lamp), provided an emission continuum in the 4000 Å - 2200 Å region. Photodecomposition of the sample was observed when this source, which emits radiation continuously to 1500 Å, was used, and two methods were employed to select wavelengths of $\lambda > 2200$ Å:

(1) a Corning 9-54 ultraviolet transmitting filter placed between the source and the cell unit; and

(2) a Schoeffel 700 mμ-200 mμ monochromator which, at its largest slit width, transmitted radiation of 100 Å bandwidth in the 2500 Å region.

No sample decomposition could be observed visually when either of these methods were in use.

The low-resolution vacuum ultraviolet absorption of OCSe, OCS and CS_2 vapours were obtained using a McPherson Model 225 1-metre double beam scanning

monochromator. This was equipped with a concave grating of one metre radius of curvature ruled with 1200 lines/mm and blazed at 1500 Å in the first order. The reciprocal linear dispersion of the instrument in the first order was 8.3 Å/mm. A McPherson model 630 (Hinteregger-type) vacuum U.V. lamp was used as the radiation source, the lamp being operated with a stream of hydrogen, at 2 torr pressure, flowing through the capillary. The outputs of a matched pair of E.M.I. type 9635B photomultipliers, mounted behind windows coated with a thin layer of sodium salicylate, were connected to a Burr-Brown model 1665/16 log ratio amplifier and thence to a Hewlett-Packard Moseley 7100 strip chart recorder. The deflection of the recorder pen gave directly the absorbance A of the sample at a given wavelength, where

$$A = \text{Log } I_o/I \quad , \qquad [2.1]$$

and where I_o was the intensity of light incident upon the reference photomultiplier and I was the intensity of light transmitted to the absorption cell photomultiplier. A wavelength counter attached to the grating drive mechanism was calibrated against known absorption features of ammonia and oxygen to an accuracy of ±1 Å. Cell pressures of from 10 torr to 1 μ were measured with Vacustat McLeod gauges, models 1G and 2G, attached to the absorption cell which was of stainless steel, 10 cm long, and was fitted with LiF windows. The accuracy of measurement of absorption features varied with the sharpness of the spectra, but was generally of the order of ±1.0 Å to ±3.0 Å.

2.7. High Resolution Electronic Spectra

High resolution absorption spectra of OCSe were recorded in the

ultraviolet region (4000 Å-2200 Å) using a 21 ft Ebert spectrograph of the type described by King[23]. The cell, cell pressure and source were identical to those used in the low resolution photographic recordings in this region. This spectrograph, used in the second order of the grating, had a dispersion and resolving power of 0.298 Å/mm and 320,000, respectively.

High resolution vacuum ultraviolet spectra were recorded using a 21 ft off-plane Eagle-mounted spectrograph. The design, construction, calibration and operation of this instrument has been described by Richardson[24]. The concave grating, ruled with 1200 lines/mm, was used primarily in the second order, in which the dispersion and theoretical resolving power were 0.6 Å/mm and 300,000, respectively. The practical resolving power was considerably lower. The absorption cell was 75 cm in length. Cell pressures in the 1 μ-1000 μ range were measured with an uncalibrated Consolidated Vacuum Corporation thermocouple vacuum gauge, Type 6 T.C. 100. Order sorting was accomplished by means of a LiF foreprism situated between the cell and the spectrograph slit.

2.8. Helium Emission Source

The Lyman source, described by Richardson[24], was not used in the present work as a continuum background for absorption studies in the vacuum U.V. (Schumann) region. A new source, superior in spectroscopic "cleanliness" and ease of maintenance, and comparable in emission intensity to the Lyman source, was developed and is described in detail here.

The well-known Hopfield[25] emission continuum of helium, ascribed to a transition from the upper $^1\Sigma_u^+$ state to the unstable $^1\Sigma_g^+$ ground state of He_2, extends from 600 Å to 1000 Å. More recently, Huffmann, Hunt, Tanaka and Larrabee[26] have reported a new continuum extending from 1050 Å-4000 Å,

excited by a condensed discharge through high pressure of helium gas. The new source is based on this information.

The source, a modified Hinteregger-type gas discharge tube, was built in the McMaster University machine shop and was designed to be accommodated on an optical bench and attached directly to the absorption cell. A schematic diagram of the source and electrical circuit is shown in Fig. 2.3. A legend for this figure is listed in Table 2.1.

The high-voltage power supply, a Universal Voltronics type BAC-22-160, variable through the range 0-25 kV, 0-160 mA, was used to charge the Sprague Model D4495, 16 kV, 0.045 μF, oil-filled capacitor through a fan-cooled resistor bank of 70 kΩ (Marvelohm 20kΩ and 30 kΩ resistors). The polarity of the voltage output was reversible, and was used in the earth-positive mode throughout this work. The earth terminal was connected to both the capacitor and the preslit of the spectrograph, which acted as the (ground) anode.

The quartz capillary, supplied by McPherson Instrument Corp., was 8.5 cm long × 7 mm I.D. with a surrounding jacket for cooling-water. The electrodes were also cooled by a fan installed in the base of the lamp housing directly under the cooling vanes. Two slits were inserted between the preslit and the cell window as aperture stops. The large separation of the preslit and the cell window very effectively reduced deposition on the window of the brown polymeric material characteristic of such sources.

High-purity helium gas, supplied by Canadian Liquid Air Co. (purity 99.995%), was bled from the tank through a needle-valve connected by copper tubing to an inert gas purifier (R. D. Mathis Co., California, Model GP100). In this, a titanium metal strip, enclosed in a quartz tube, was heated by furnace to 900°C, at which temperature its chem-absorption properties for such

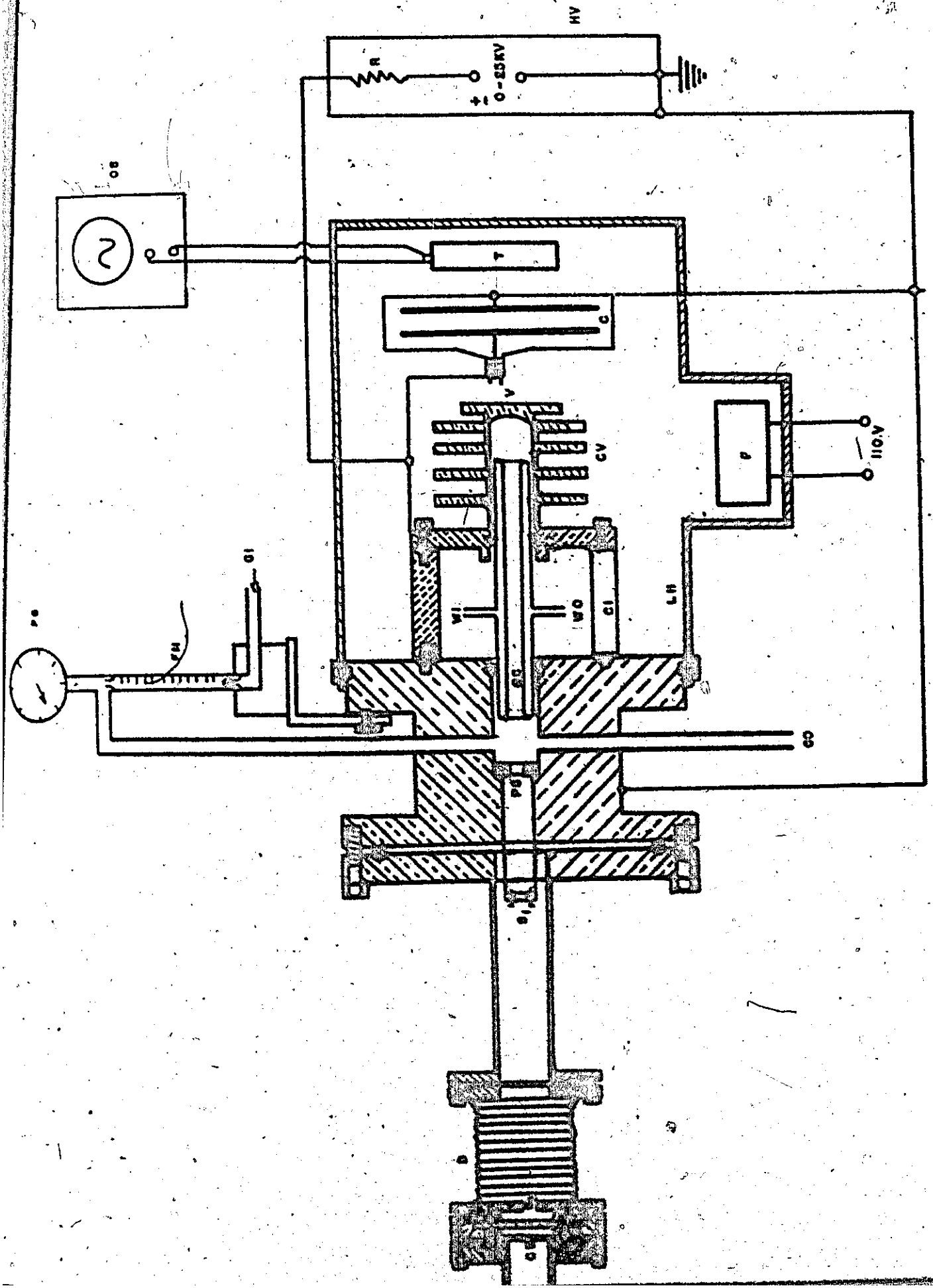

Fig. 2.3. Hollim emission source (vertical section).

TABLE 2.1

LEGEND FOR FIG. 2.3

AC	absorption cell, 75 cm
B	extendable brass bellows
C	storage capacitor 0.06 μF, 15 kV
CI	ceramic insulator
CS	"covar" glass-metal joint
CV	cooling vanes
CW	cell window, CaF_2, 1" × 2 mm
F	fan
FM	flow meter
GI	gas inlet
GO	gas outlet
HV	high voltage power supply
LH	lamp housing, perforated for better cooling
OS	oscilloscope
PG	pressure gauge, 0-760 torr, aneroid type
PS	preslit, also ground electrode
QC	quartz capillary, 8.5 cm × 2.5 cm (O.D.), 7 mm (I.D.)
R	ballast resistors, 70 kΩ, fan-cooled
S_2	slits, horizontal, 2 mm × 8 mm, stainless steel
S_1	slits, horizontal, 2 mm × 12 mm, brass
T	Pearson transformer, model 110
V	high-voltage electrode, aluminum
WI	water in
WO	water out

Overall length, cell window to rear: 57.5 cm ± 1.5 cm

inert gas impurities as N_2, O_2, CO, CO_2 and hydrocarbons, are excellent. The outlet of the purifier was connected by flexible stainless steel tubing to a Brooks "Sho-Rate 150" flowmeter mounted on top of the lamp. A needle valve was connected between the gas outlet and an Edwards Rotary Pump (Model ES75) to allow control of the gas pressure in the lamp. The flow rate was ~ 2 litres/hour. The entire system was vacuum-tested using a helium-leak detector, as it was found that even small leaks resulted in a complete loss of continuum in the spectral region of interest.

The lamp was operated at helium pressures of 500-600 torr, with the charging voltage and current at 10 kV and ~90 mA, respectively. At pressures of greater than 100 torr, the discharge became self-triggering, and increased in intensity with increasing pressure. The firing rate was measured by connecting the output of a Pearson Model 110 wide band pulse transformer mounted in the rear of the lamp housing, to an oscilloscope, triggering at 250-300 cps.

The continuum has been observed in this work to extend from 6000 Å - 1300 Å. While the pressure-broadened and self-absorbed emission lines of HeI and HeII appear in the visible region of the continuum, the ultraviolet and vacuum U.V. regions are comparatively line-free. Weak emission lines of NI, OII, CI, CII, absorption bands of CO, and the very strong pressure-broadened first member of a Lyman series of HeII at 1640.4 Å are the principal features in the continuum in these latter spectral regions. A quantitative study of the wavelength/intensity properties of the emission was not attempted. However, Fig. I of Reference 26 is considered a reasonable approximation.

Usable photographic plate densities in the V.U.V. region could be obtained with exposure times of from 5 min. (2200 Å) to 40 min. (1300 Å), with the spectrograph slits set at 50 μ. Fig. 2.4 shows the source and cell

FIG. 2.4 The Source and Cell Arrangement.

21b

arrangement and Table 2.2 is a list of the emission features observed in the continuum in the 2100 Å-1300 Å region.

The origin of the continuum is not certain. It has been found[26,27] that the emission intensity varied directly with that of the HeII emission features at 1640.4 Å and 1215.2 Å. The conclusion was drawn that the relationship of this continuum to the 1640.4 Å emission line is similar to that of the continuum of rare gases to their resonance lines[28], and that the species He_2^+ or perhaps He_2^{++} are involved.

The McPherson model 630 hydrogen emission source, modified so as to be accommodated on the optical bench of the spectrograph, was also used for photography in the 2200 Å-1725 Å region. Exposure times were in the range of from 2-4 hours.

2.9. Photographic Materials

Spectra in the ultraviolet region were recorded on Kodak Spectrum Analysis No. 1 photographic emulsion, while those in the V.U.V. region were recorded on Kodak Special Film Type 101-01.

2.10. Measurement

The positions of spectral features were measured by two methods:

(1) By a McPherson travelling microscope, which had a precision of 0.001 mm. This was connected to a digital encoder and a card punch. Computer programmes were then used to interpolate, by a least squares method, to the positions of the various absorption features observed.

(2) By use of spectral traces obtained on a Joyce-Loebl MK IIIC microdensitometer, employing direct interpolation between known vacuum frequencies of Iron arc lines[29]. In these interpolations, Edlen[30]

TABLE 2.2

PERSISTENT* IMPURITY FEATURES OBSERVED IN THE HELIUM CONTINUUM

Wavelength (Å)	Intensity**	Origin
1988.05	w	CII
1962.2	w	OII
1930.9	m	CI
1862.5	vw	NII ?
1862.2	s	NII ?
1857.5	vw	NI
1854.1	s	?
1767.6	vw	?
1670.0	s	ArIII ?
1658.126	s	CI
1657.9	s	CI
1657.38	s	CI
1657.005	s	CI
1656.28	s	CI
1640.4	vvs (diffuse)	HeII
1611.5	m	?
1605.5	m	?
1561.4	w	CI
1561.3	w	CI
1560.7	w	CI
1560.3	w	CIV
1545.5 (in absorption)	w band	CO 4th + ve
1509.86 (in absorption)	w band	CO 4th + ve
1494.6	m	NI
1492.8	vvw	NI
1492.63	m	NI
1477.65 (in absorption)	vw band	CO 4th + ve
1467.45 (in absorption)	vw	CO 4th + ve
1463.33	vw	CI

* The intensity of the various emission features varied considerably, depending on the condition and treatment of the gas purifier and the care taken in degassing the source and metal tubing.

** w = weak, m = moderately strong, s = strong.

and order corrections were applied.

The variation in film sensitivity and source intensity with wavelength in the vacuum U.V. region and use of the predispersion unit made uniform photographic emulsion densities difficult to achieve. Instead, intensities in this region were measured off spectra taken on the McPherson model 225 scanning monochromator. Several advantages were thereby gained over the method of emulsion densities: (1) the quantum efficiency of the sodium salicylate windows is approximately constant in the 1200 Å-2000 Å region[28]; (2) fluctuations in the source emission intensity were compensated for in the double beam operation; and (3) decomposition effects were minimal as the absorption cell was placed after the monochromator.

Absorption intensities of spectral features recorded in the U.V. region were measured as follows: Microdensitometer traces of all the bands were taken. The Joyce-Loebl instrument measured the optical density of the photographic image, which was approximately proportional to the log of the transmission coefficient of the sample at the wavelength in question. The intensity data quoted for spectral features observed in this region are proportional to the log of the intensity of the absorption features.

2.11. Temperature-Dependence Work

The temperature dependence of the intensities of bands appearing in both the U.V. and V.U.V. regions of the spectrum was investigated. A 5 cm long quartz cell was used, which was wound with 1.5 ohm/ft nichrome wire, wrapped with asbestos paper and heated electrically to 250°C. For the U.V. investigations, the cell was placed in the light path of the Cary 14 instrument. The McPherson instrument was used for these studies in the V.U.V.

region, but, due to the danger of cracking of the LiF windows, the absorption cell on this instrument was not heated. Rather, the 5 cm cell was attached directly to this cell, and the spectrum was recorded immediately upon introduction of the heated gas. This method of studying the temperature-dependence of absorption proved quite efficient.

2.12. Spectral Observations

A brief description of the observed spectra is given in table 2.3.

TABLE 2.3

NOTES ON SPECTRAL OBSERVATIONS

CARBONYL SELENIDE

2800 Å - 5000 Å: No absorption spectra observed in this region. Hilger Quartz instrument used. Pressure-path length $\leq$ 0.02 meter-atmospheres.

2700 Å - 2200 Å: Weak system of diffuse absorption bands. Photographed on low-resolution instruments (Hilger Quartz and Bausch and Lomb). Assigned to a bent-linear transition. The possibility that two electronic transitions are involved is discussed.

2150 Å - 1800 Å: A series of strong discrete red-degraded absorption bands. "Forbidden" pseudo-origin due to strong vibronic (Hertzberg-Teller) coupling. Assigned to a linear-linear intravalence shell transition. Also, two series of weak bands and a series of very intense bands all of which are very diffuse. These are assigned to Rydberg transitions of linear OCSe. The upper states arise from the configuration --- $(\pi)^3$ (so).

1550 Å - 1425 Å: Four very strong series of absorption bands. Assigned to Rydberg transitions of linear OCSe.

1450 Å - 1210 Å: Several series of very intense absorption bands. Assigned to Rydberg transitions of linear OCSe on the basis of comparisions of experimental and calculated Rydberg term values. The analysis is made from McPherson monochromator recordings of the spectrum.

TABLE 2.3 (cont'd.)

CARBONYL SULFIDE

1565 Å - 1440 Å: Three series of absorption bands observed in this region:

(i) a very intense, very diffuse series;

(ii) a weak diffuse series; and

(iii) a short series of weak sharp-headed bands.

Series (i) and (ii) are assigned to Rydberg transitions and (iii) is an intravalence shell transition. All are linear-linear transitions. The analogy between these series and those of OCSe in the 1820 Å - 1600 Å regions is discussed.

CARBON DISULFIDE

1625 Å - 1575 Å: Very strong doublet with some sequence bands. Assigned to two linear-linear Rydberg transitions.

CHAPTER III

THEORETICAL CONSIDERATIONS

The general theory of the classification of electronic states and the theory of electronic transitions have been discussed by various authors[5,31]. In this chapter the electronic energy states of OCSe and such details of the above theory as are essential to the vibrational analyses of the observed spectra will be discussed. The chapter is intended to be complementary to the analysis of the spectra reported in Chapter V.

3.1. Electronic States of OCSe

3.1.1. General

The molecules CO_2, OCS, CS_2, OCSe and CSe_2 form an isoelectronic series in that they each contain sixteen valence electrons. The molecules OCS and OCSe belong to the point groups $C_{\infty v}$ and C_s in the linear and bent conformations, respectively. By the adiabatic principle, the electronic states of the two conformations can be correlated.

Neither molecular orbital nor valence bond calculations have been reported for OCSe. Accordingly, the discussion of the electronic states and electronic energies of this molecule is based on analogies with the calculations available for the isoelectronic molecule OCS.

3.1.2. Molecular Orbitals for the Linear Conformation of OCS, OCSe

The ground state electron configurations of carbon, oxygen, sulfur and selenium atoms are:

C:	K	$2s^2 2p^2$	S:	KL	$3s^2 3p^4$
O:	K	$2s^2 2p^4$	Se:	KLM	$4s^2 4p^4$

Of the sixteen valence electrons of the molecules OCS/OCSe, four are contributed by carbon and six each by oxygen and sulfur/selenium. The electrons in closed shells of the atoms contribute little to the bonding or antibonding characteristics of the molecular orbitals.

The relative energies and atomic orbital compositions of the molecular orbitals of OCS have been calculated by McLean and Yoshimine[32] and by Rabalais, McDonald, Scherr and McGlynn[33]. The former authors used an iterative SCF methods of calculation, which employed a large basis set of s, p, d and f functions. The latter authors used a Mulliken-Wolfsberg-Helmholz (MWH) or "extended Hückel" treatment, employing only s and p atomic functions. In both calculations, the atomic functions used were the double-zeta functions of Clementi[34]. Though the calculated energies differed substantially, the energy ordering of the molecular orbitals was identical in both calculations. The energies and ordering of the molecular orbitals of reference 32 are given in Fig. 3.1. The lowest-lying σ orbitals, viz. 1σ, 2σ and 3σ, are not shown, being essentially sulfur, oxygen and carbon 1s atomic orbitals, respectively. The 4σ, 5σ and 1π M.O.'s are essentially 2s, $2p_z$ and $2p_{x,y}$ A.O.'s respectively on sulfur. The following is a rough description of the A.O. composition and the bonding and antibonding characteristics of the valence electron M.O.'s, as calculated by McLean and Yoshimine.

6σ: 2s(C) and 2s(O). Bonding.

7σ: A combination of 3s(S), 2s(C) and 2s(O). Bonding between sulfur and carbon and weakly antibonding between carbon and oxygen.

8σ: 3s(S), 2s(O), $2p_z$(C), 2s(O) and $2p_z$(O), weakly antibonding between sulfur and carbon and strongly bonding between carbon and oxygen.

2π: $2p_{x,y}$(C) and $2p_{x,y}$(O). Weakly bonding.

TIGHT. BINDING

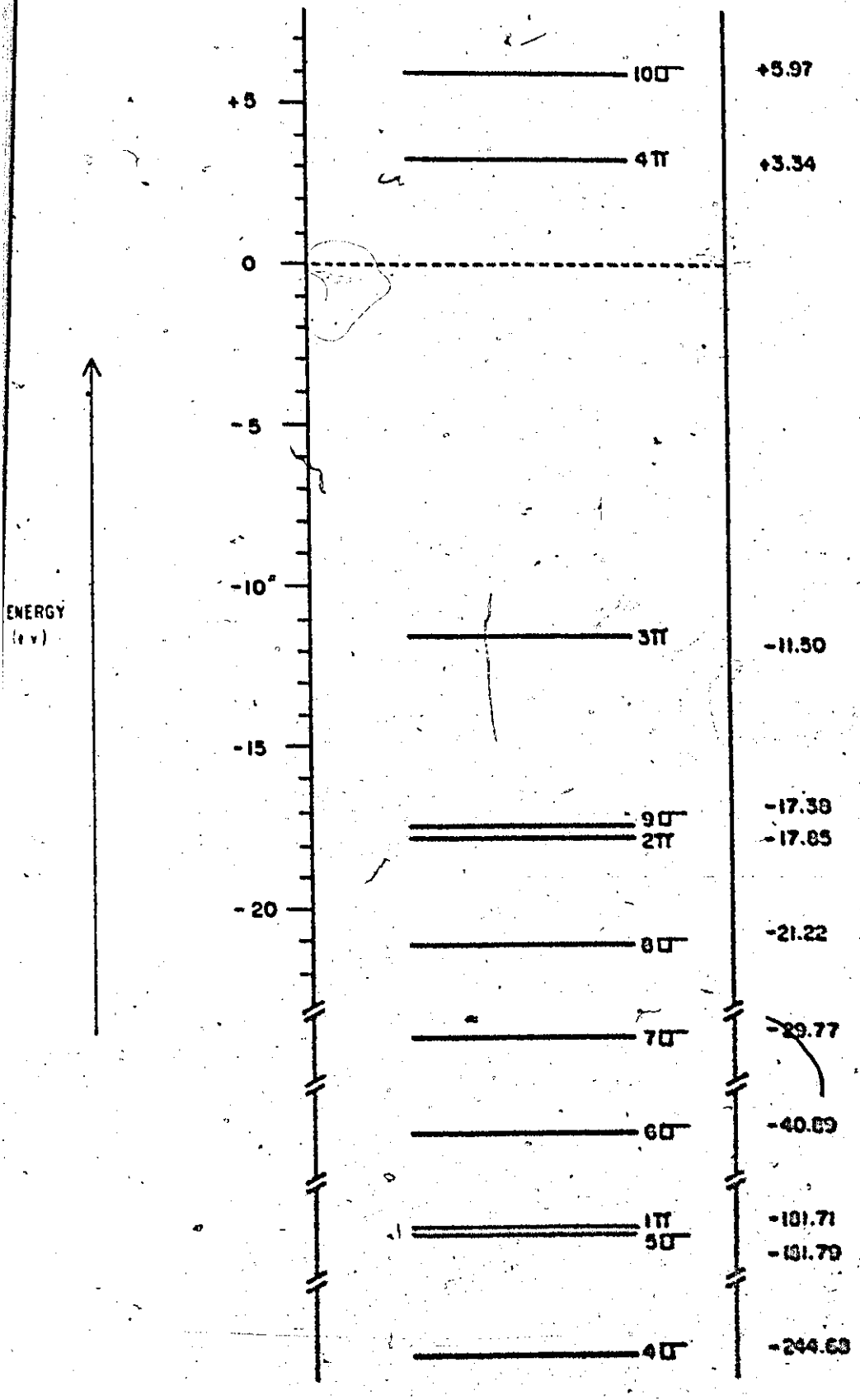

Fig. 3.1. Molecular orbital energies for OCS (adapted from Ref. 32).

9σ: Complex composition. Weakly antibonding between S and C and weakly bonding between C and O.

3π: A combination of $3p_{x,y}(S)$ and $2p_{(x,y)}(O)$. Weakly bonding.

This is the most loosely-bound filled M.O. Its bonding and antibonding characteristics and stability in the linear conformation of the molecule largely determine the molecular geometry in various electronic states of the molecule. This is a particularly valid approximation for Rydberg states, as the Rydberg orbital is non-bonding.

Of the unfilled (virtual) M.O.'s of OCS, the 4π lies at lower energy than the 10σ. The former, composed of $3p_{x,y}(S)$, $2p_{x,y}(C)$ and $2p_{x,y}(O)$ A.O.'s is weakly antibonding between S and C and C and O. The latter is composed of 3s(S), $3p_z(S)$, 2s(C) and $2p_z(O)$ A.O.'s and is strongly antibonding between S and C, and weakly antibonding between C and O.

The approximation is now made that the energy ordering of the molecular orbitals of OCS and OCSe or at least that of the M.O.'s 9σ, 3π, 4π and 10σ, is similar. The inclusion of the 3d electrons of selenium is considered unlikely to affect this ordering[35]. The phenomenal similarity in both the appearance and the intensity distribution of the spectra of OCS and OCSe supports this approximation. In further discussion, the 1s and 3d electrons of selenium are disregarded so that the same numbering scheme can be employed for the M.O.'s of OCS and OCSe.

3.1.3. Ground Electronic State of OCSe

To obtain the ground state electron configuration, the molecular orbitals are filled according to the Aufbau Principle. The ground state configuration is then

$$.....(8\sigma)^2(2\pi)^4(9\sigma)^2(3\pi)^4.....^1\Sigma^+$$

Each non-degenerate (σ) orbital is doubly occupied by electrons of opposite spin whereas each two-fold degenerate (π) orbital is occupied by four electrons. This configuration represents a closed-shell arrangement and only one electronic state can result[36]. The eigenfunction of this state must transform as the totally symmetric representation of the $C_{\infty v}$ point group, i.e., as $^1\Sigma^+$. This is denoted, by convention, as $\tilde{X}\ ^1\Sigma^+$. The linearity of the molecule in the ground state has been confirmed by microwave work[16].

3.1.4. Excited States of OCSe

An excited electronic state of a molecule, in which one or more electrons are promoted to higher energies usually result in a rearrangement of electrons and nuclei with respect to their coordinates in the ground state. In unsymmetrical triatomic molecules (type ABC), the stable equilibrium conformation of the nuclei in an excited state may be either linear or bent. The eigenfunctions are then classified under the $C_{\infty v}$ or C_s symmetry point groups, respectively.

The lower excited electronic states of OCSe most probably result from the electron excitation $4\pi \leftarrow 3\pi$. The methods of group theory or the vector addition of the axial components of the orbital and spin angular momenta may be applied to obtain the symmetries and angular momenta of the electronic states resulting from this $(3\pi)^3(4\pi)$ electron configuration. The symmetries of the electronic states resulting from this electron configuration are then obtained in the following fashion[37]. The triple antisymmetric product of (π, $E\frac{1}{2}$) is

$$\pi \times E\frac{1}{2}$$

Since electrons in the 3π and 4π M.O. are non-equivalent, the direct product

$$\pi \times E\frac{1}{2} \times \pi \times E\frac{1}{2}$$

is taken. Six electronic states (of the linear conformation) result, viz. $^{1,3}\Delta$, $^{1,3}\Sigma^-$ and $^{1,3}\Sigma^+$. By application of Hund's Rules[38] the energy ordering of these electronic states would be expected to be

$$^3\Delta < {}^3\Sigma^-,\ {}^3\Sigma^+ < {}^1\Delta < {}^1\Sigma^-,\ {}^1\Sigma^+,$$

i.e., the energy, relative to that of the ground electronic state, increases from left to right in this ordering. The electron configuration

$$.....(3\pi)^3(10\sigma)$$

resulting from the single electron promotion

$$10\sigma \leftarrow 3\pi$$

yields the electronic states $^{1,3}\Pi$ of the linear conformation. The calculated energy separation of the M.O.'s 9σ and 3π is large (~6 e.v.). Transitions to electronic states resulting from electron promotion from the 9σ M.O. are then expected to occur at high energies.

3.1.5. Molecular Orbitals for the Bent Conformation of OCSe

A qualitative correlation of single electron molecular orbital energies in a triatomic molecule of the type AB_2, between bent and linear conformations, has been given by Walsh[39]. This author suggested that the correlation diagram, called a Walsh diagram, may also apply to ABC-type molecules. This diagram is shown in Fig. 3.2. Each M.O. of π symmetry correlates with two non-degenerate orbitals, of a' and a'' symmetry, of the bent confirmation, while each σ M.O. correlates with one of a' symmetry. The M.O.'s of the bent confirmation are

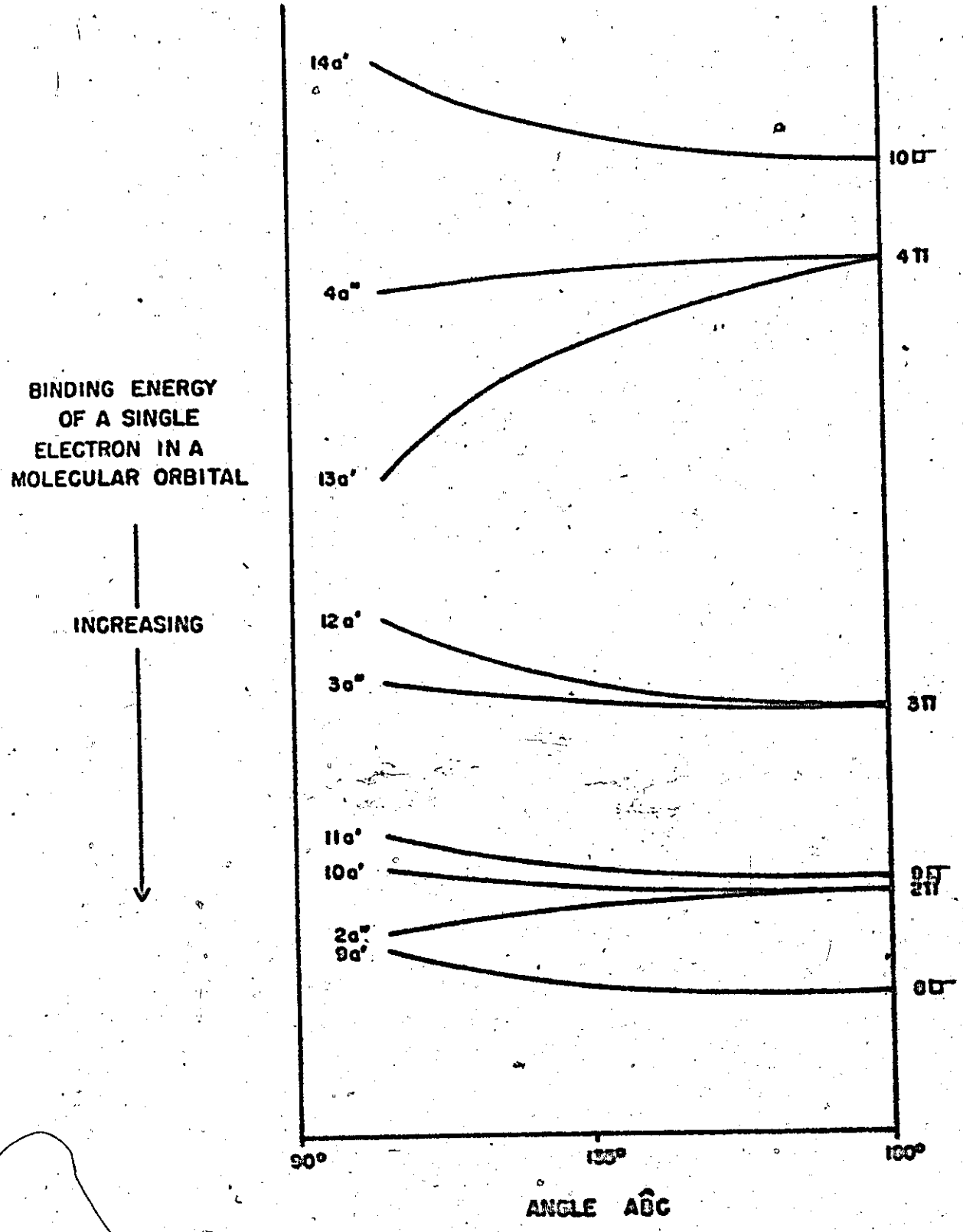

Fig. 3.2. Walsh Diagram for AB$_2$-type molecules.

numbered in the order of increasing energy under the assumption that cross-overs do not occur for bond angles greater than 120°. Fig. 3.2 shows that changes in energy occur for each orbital as the bonding angle is varied. Although no quantitative estimates are possible, some qualitative arguments based on this diagram may be advanced regarding the probable equilibrium conformations of the excited states of ABC-type sixteen valence-electron molecules.

3.1.6. Electronic States of the Bent Conformation of OCSe

The Aufbau Principle is again applied in the filling of the molecular orbitals of the bent conformation. The electron configuration of the ground electronic state is then

$$.....(3a'')^2(12a')^2,$$

and the resulting electronic state is of symmetry $^1A'$. This correlates with $^1\Sigma^+$ of the linear conformation. Both orbitals have energy minima corresponding to the linear geometry and the molecule is expected to be linear in the ground state.

If the lower excited states result from the single electron promotion $4\pi \leftarrow 3\pi$, the following electron configurations and electronic states of the bent conformation are obtained:

	Configuration	Electronic States	
Ground State	$...(3a'')^2(12a')^2$	$^1A'$	
Excited States	$...(3a'')^2(12a')(13a')$	$^1A', ^3A'$	1 and 2
	$...(3a'')(12a')^2(13a')$	$^1A'', ^3A''$	3 and 4
	$...(3a'')^2(12a')(4a'')$	$^1A'', ^3A''$	5 and 6
	$...(3a'')(12a')^2(4a'')$	$^1A', ^3A'$	7 and 8

Those states resulting from an electron configuration in which the 13a' M.O. is singly or doubly occupied are expected to have bent equilibrium geometry, viz. states 1, 2, 3 and 4 which correlate with the states $^1\Delta$ and $^3\Delta$ of the linear conformation. A prediction of the equilibrium geometry of the molecule in the electronic states 5 and 6 is difficult since the energies of the M.O.'s 12a' and 4a" vary oppositely with change in bond angles ABC. These latter states correlate with the states $^1\Sigma^-$ and $^3\Sigma^-$ of the linear conformation. States 7 and 8, which correlate with $^1\Sigma^+$ and $^3\Sigma^+$, are expected to be stable in the linear conformation, as are the states $^{1,3}\Pi$ resulting from the electron promotion $10\sigma \rightarrow 3\pi$.

A calculation of the total energies of the lower electronic states of the isoelectronic molecule NCS^- has been published by Rabalais, McDonald, Scherr and McGlynn[33]. These results are shown in Fig. 3.3. The ground state is linear, as expected. Of the electronic states arising from the $\ldots(3\pi)^3(4\pi)$ configuration, the molecule is predicted to be bent in the states $^1\Delta(^1A')$, $^1\Sigma^-(^1A'')$ and $^1\Delta(^1A'')$ and linear in the $^1\Sigma^+(^1A')$ state.

The electron configurations and symmetry species of the ground and lower excited electronic states of OCSe, in both linear and bent conformations, are given in Table 3.1, together with the molecular conformation predicted for each of these states. Electric dipolar transitions that are allowed or forbidden by the selection rules (Chapter I, Section 1.3) are indicated as such.

3.2. Vibronic Coupling

The selection rules outlined in Chapter I, Section 1.3 are derived through application of the Born-Oppenheimer Approximation. In polyatomic molecules, interactions of vibrational and electronic motions occur which

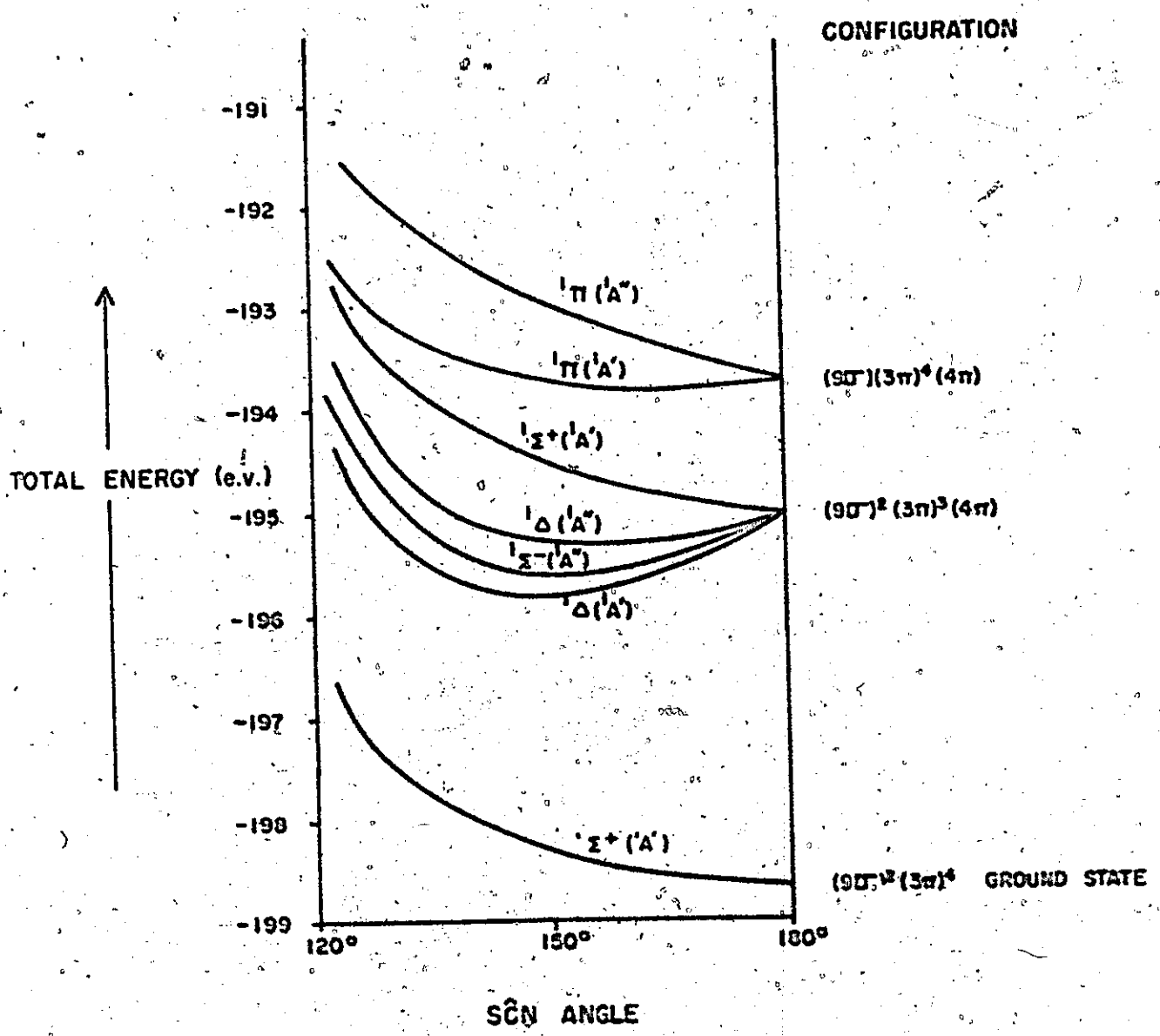

Fig. 3.3. Total energies of the lower electronic states of NCS^- as a function of angle (adapted from Ref. 33).

TABLE 3.1

ELECTRON CONFIGURATIONS AND ELECTRONIC STATES OF OCS, OCSe

LINEAR			BENT			
Configuration	$\Gamma(\psi_e)$	$\Gamma(\psi_e\psi_s)$	Configuration	$\Gamma(\psi_e)$	$\Gamma(\psi_e\psi_s)$	Form
$\ldots(3\pi)^3(10\sigma)$	$^1\Pi$	Π	$\ldots(3a'')(12a')^2(14a')$	$^1A''$	A''	Linear
			$\ldots(3a'')^2(12a')(14a')$	$^1A'$	A'	
	$^3\Pi(sf)$**	Σ^+, Π, Δ	$\ldots(3a'')(12a')^2(14a')$	$^3A'(sf)$	$A' + 2A''$	Linear
			$\ldots(3a'')^2(12a')(14a')$	$^3A''(sf)$	$A'' + 2A'$	
	$^1\Sigma^+$	Σ^+	$\ldots(3a'')(12a')^2(4a'')$	$^1A'$	A'	Linear
	$^1\Sigma^-(f_{LIN})$*	Σ^-	$\ldots(3a'')^2(12a')(4a'')$	$^1A''$	A''	(Bent)?
	$^1\Delta(f_{LIN})$	Δ	$\ldots(3a'')(12a')^2(13a')$	$^1A''$	A''	Bent
			$\ldots(3a'')^2(12a')(13a')$	$^1A'$	A'	Bent
$\ldots(3\pi)^3(4\pi)$	$^3\Sigma^+(sf)$	$\Sigma^- + \Pi$	$\ldots(3a'')(12a')^2(4a'')$	$^3A'(sf)$	$A' + 2A''$	Linear
	$^3\Sigma^-(sf)$	$\Sigma^+ + \Pi$	$\ldots(3a'')^2(12a')(4a'')$	$^3A''(sf)$	$A'' + 2A'$	(Bent)?
	$^3\Delta(sf)$	$\Pi + \Delta + \Phi$	$\ldots(3a'')(12a')^2(13a')$	$^3A''(sf)$	$A'' + 2A'$	Bent
			$\ldots(3a'')^2(12a')(13a')$	$^3A'(sf)$	$A' + 2A''$	Bent
$\ldots(3\pi)^4$	$^1\Sigma^+$	Σ^+	$\ldots(3a'')^2(12a')^2$	$^1A'$	A'	Linear

$C_{\infty v}$, $\Gamma_{(triplet)}$: $\Sigma^- + \Pi$

C_s, $\Gamma_{(triplet)}$: $A' + 2A''$

*(f_{LIN}): Transition is electric dipolar forbidden in linear conformation.

**(sf): Spin forbidden transition.

render this approximation invalid. This effect is generally treated by first order perturbation methods. The vibronic terms V_{eN} in the electronic Hamiltonian H_e of a molecular system are, in a higher approximation than that of Born and Oppenheimer, variable functions of the nuclear coordinates. Where such terms are included, H_e is given by

$$H_e = (H_e)_o + \sum_u \left(\frac{\partial H}{\partial Q_u}\right)_o Q_u + \ldots \text{ higher terms} \qquad [3.1]$$

where Q_u are the normal coordinates of the u normal vibrations, and the subscript zero refers to the equilibrium conformation in the ground state of the molecule. The first-order correction to the electronic Hamiltonian

$$H^1 = \sum_u \left(\frac{\partial H_e}{\partial Q_u}\right)_o Q_u \qquad [3.2]$$

perturbs the set ψ_e^o, which are the electronic eigenfunctions of H_e, in the Born-Oppenheimer Approximation, evaluated at $Q_u = 0$. The mixing, through this perturbation, of the eigenfunctions of any two electronic states i and j is inversely proportional to the square of the difference of the zeroth-order energies of these states $(E_j^o - E_i^o)$. Two cases of vibronic coupling are discussed briefly here. These are: (1) Type (A) or Renner Coupling, and (2) Type (B) or Herzberg-Teller Coupling. Both are considered to be due to the same phenomenon, i.e., dependence of the electronic eigenfunctions upon nuclear coordinates.

3.2.1. Type (A) Coupling: Renner Effect

The possibility of degenerate electronic states occurs in molecules classified under the $C_{\infty v}$ point group. Where the axial component of electronic angular momentum, $\Lambda\hbar$, is non-zero, two electronic states result, which are, in zeroth-order approximation, degenerate. However, if the molecule is distorted

such that the symmetry of the equilibrium nuclear conformation is destroyed, these electronic states are no longer degenerate by reason of symmetry. The two eigenfunctions for the distorted molecule correspond to different electron distributions and the potential surfaces representing these states are, in general, different functions of the distortion. For a linear ABC-type molecule in free space, such a distortion occurs during the asymmetric bending vibration, ν_2. This has vibrational angular momentum associated with it, and the electronic and vibrational motions may interact. The vibrational energy levels in the two states may be strongly perturbed by the interaction, and a complex spectrum results. This interaction, first suggested by Teller[40,41] was subsequently formulated by Renner[42].

The separation of the potential surfaces is a function of the strength of vibronic (Renner) coupling. Three model cases have been described in the literature, for which potential surface diagrams are shown schematically in Fig. 3.4. These cases are:

(a) Weak Renner Effect. The minima of both potential surfaces, denoted $U^+(r_b)$ and $U^-(r_b)$, where r_b is the coordinate of bending in a plane containing the molecule, occur at $r_b = 0$. Both electronic states are stable in the linear conformation. Excitation of the bending vibration, ν_2, results in a small separation of the potential surfaces of the electronic states. Vibronic energy expressions have been derived by Renner[42] for the Π electronic states and by Mörer and Travis[43] for Δ states.

(b) Intermediate Renner Coupling. In this case, an energy minimum is achieved by angular distortion of the molecule from the linear conformation. $U^+(r_b)$ and $U^-(r_b)$ represent separate non-degenerate electronic states for all $r_b \neq 0$. The minima in these potential surfaces correspond to $r_b = 0$,

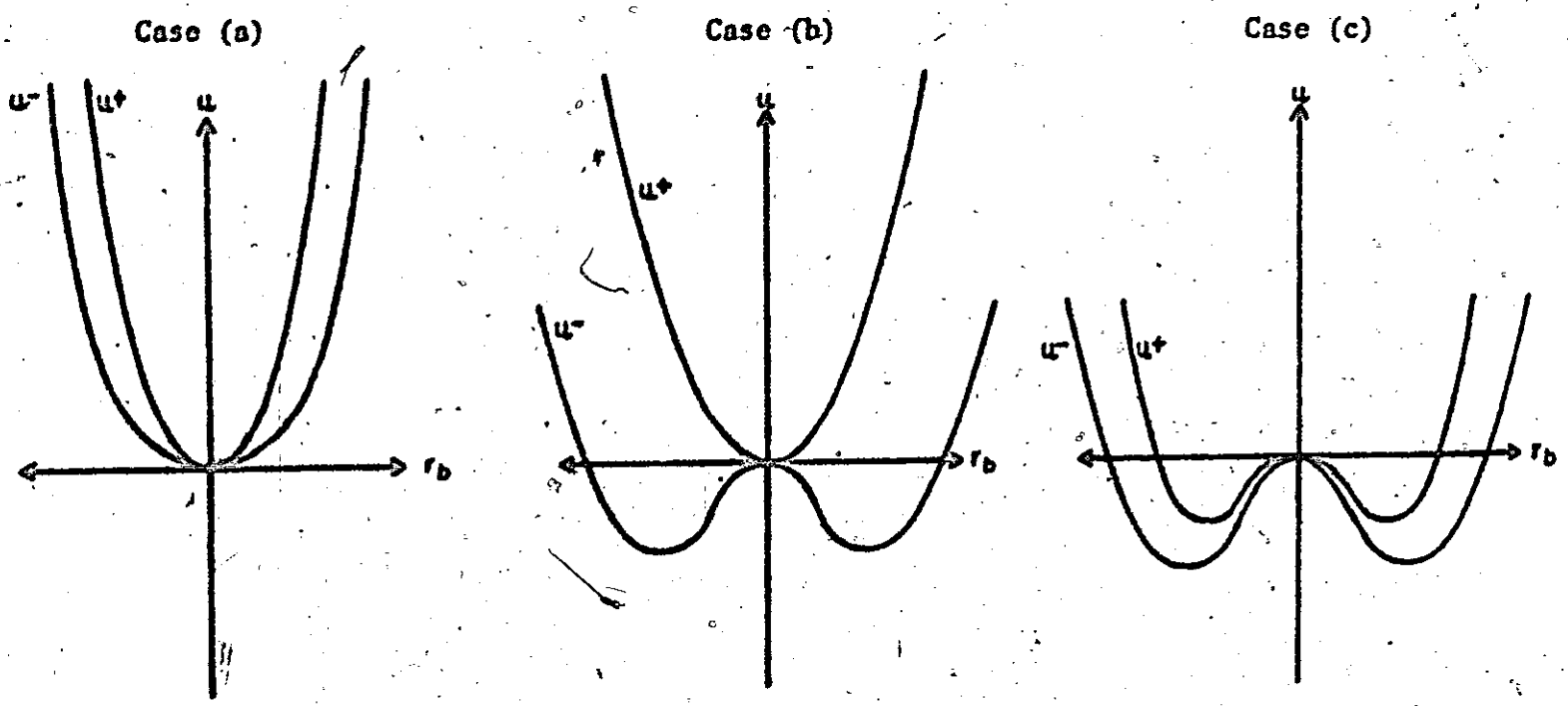

Fig. 3.4. Potential curves for weak (a), intermediate (b), and strong (c) Renner Effect. Potential energy $U(r_b)$ is plotted in the ordinate. r_b is the bending coordinate.

for $U^+(r_b)$ and $r_b \neq 0$ for $U^-(r_b)$. Since these potential surfaces are in contact, the molecule may (classically) convert from one surface to the other, and only levels of vibronic symmetry Σ^+ and Σ^- may be definitely assigned to $U^+(r_b)$ and $U^-(r_b)$, respectively. The sign of the Renner parameter determines the relative energies of the electronic states represented by $U^+(r_b)$ and $U^-(r_b)$. A theoretical treatment of case (b) has been given by Pople and Longuet-Higgins[44] for a $^1\Pi$ state.

(c) Strong Renner Coupling. In this case, the minima in both potential surfaces occur at $r_b \neq 0$. Case (c) coupling has been considered by Dixon[45,46,47,48].

Magnitude of the Renner Coupling. The Renner coupling constant (ϵ for a Π and n/ω_2 for a Δ electronic state) indicates the magnitude of the Renner coupling. To date, no attempt has been made to calculate these parameters, and they are normally determined from an analysis of experimental data. However, as suggested by Renner[42], a qualitative estimate may be obtained from a consideration of the symmetries of close-lying electronic states.

In a sixteen valence-electron triatomic molecule of $C_{\infty v}$ symmetry, the electronic states $^1\Sigma^+$, $^1\Sigma^-$ and $^1\Delta$ result from the same $(\pi)^3(\pi)$ configuration. Excitation of the degenerate bending vibration momentarily distorts these states to the bent conformation, in which their vibronic symmetries are given by the correlation:

$C_{\infty v}$		C_s
$^1\Sigma^+$	→	$^1A'$
$^1\Sigma^-$	→	$^1A''$
$^1\Delta$	→	$^1A' + {}^1A''$

Provided that the energy separations of these states are not large, those of

the same symmetry may interact to repel each other, i.e., there is Renner coupling in the Δ state, and the coupling may be considered to arise via the interaction with close-lying states of the same symmetry. An illustration of this approach is apparent in the $\tilde{A}$ ($^1A''$) ← $\tilde{X}$ ($^1\Sigma^+$) and $\tilde{B}$ ($^1A''$) ← $\tilde{X}$ ($^1\Sigma^+$) transitions of HCN, observed in absorption by Herzberg and Innes[49]. The electronic configuration of the ground ($\tilde{X}$) state is $(\sigma)^2(\pi)^4$ and the $\tilde{A}$ and $\tilde{B}$ excited states have been shown to result from the electron promotion $(\sigma)^2(\pi)^3(\pi) \leftarrow (\sigma)^2(\pi)^4$. The $\tilde{A}$ (A'') electronic state has been assigned as one component of a Renner-split $^1\Delta$ state and the $\tilde{B}$ state as $^1A''$, which correlates with the $^1\Sigma^-$ state of the linear conformation. The analysis of the spectrum indicates that the molecule is strongly bent, in both the $\tilde{A}$ and $\tilde{B}$ states, the energy separation of whose electronic origin bands is ~2500 cm^{-1}.

3.2.2. Type (B) or Herzberg-Teller Coupling

Vibronic interaction of this type may mix zeroth-order electronic eigenfunctions $\psi_e(r,Q_o)$ when either totally or non-totally symmetric vibrations are excited. A detailed treatment of type (B) coupling has been given by Hochstrasser[6]. Only the results of importance of this thesis will be stated here.

If the eigenfunctions, $\psi_i(r,Q_o)$ and $\psi_j(r,Q_o)$, of close-lying electronic states i and j, are mixed through excitation of a normal vibration μ in i, a band of vibronic energy

$$E = E_{oo}^{io} + h\nu_\mu^{(i)}$$

may appear in the spectrum corresponding to the transition i ← 0. E_{oo}^{io} is the purely electronic energy of the transition i ← 0, and $h\nu_\mu^{(i)}$ is the energy of a quantum of the μ^{th} vibration in the i^{th} electronic state. The conditions

such that the energy E appears in the spectrum are:

(i) the electronic transition $j \leftarrow 0$ is electric dipolar allowed;

and (ii) $\Gamma(Q_\mu^i) = \Gamma[\psi_i(r,Q_o)] \times \Gamma[\psi_j(r,Q_o)]$

where $\Gamma(Q_\mu^i)$, the irreducible representation of the normal coordinate Q_μ of the μ^{th} normal vibration in i, may be totally or non-totally symmetric. The electronic transition $i \leftarrow 0$, which may be electric dipolar allowed or forbidden, is then said to "borrow" intensity from the transition $j \leftarrow 0$. The intensity of the vibronic component of energy E is inversely proportional to the magnitude of the quantity

$$(E_j^o - E_i^o)$$

where E_k^o is the zeroth-order energy of the state k. The transition between the vibronic states $\psi_{i\mu}$ and ψ_{oo} has the polarization of the vector transforming as $\Gamma(Q_\mu^i)$.

When the transition $i \leftarrow 0$ is electronically allowed, the perturbation can cause the appearance of relatively weak additional bands, involving single-quantum excitations of non-totally symmetric vibrations in the spectrum. When the transition $i \leftarrow 0$ is forbidden, only the bands resulting from the perturbation appear. These may act, in both cases, as false or pseudo-origins for a spectrum involving excitation also of various quanta of totally symmetric vibrations. The perturbing state j is another excited electronic state of the molecule. When the zeroth-order ground state eigenfunction ψ_1^o is distorted by excitation of an antisymmetric vibration in that state, additional bands may appear in the spectrum through operation of the same perturbation mechanism[49].

3.3. Rydberg Transitions

3.3.1. General

Molecular orbitals are formed, in the LCAO/MO approximation, from valence shell atomic orbitals of the atoms of the molecule. Electronic transitions in which the electronic configurations of the participating electronic states may be described in terms of these M.O.'s are called intravalence shell transitions. In the higher energy region of the spectrum, bands may be observed which correspond to transitions to excited molecular orbitals in which the principal quantum number (n) of the atomic orbitals is greater than the value (m) in the valence shell by an integral quantity,

$$\text{i.e.,}\quad n = m+1,\ m+2,\ m+3,\ldots\ldots,\infty. \qquad [3.3]$$

n then defines a series of extravalance shell or Rydberg transitions, the electronic origin energies of which are given approximately by

$$\sigma_n = \sigma_\infty - Z_c^2 R/(n-\delta)^2 = \sigma_\infty - T_n \qquad [3.4]$$

Here: σ_n is the wavenumber of the origin band of the spectrum corresponding to the transition to the extravalence shell orbital of index number n,

σ_∞ is the wavenumber of the series limit. This corresponds to the ionization energy of an electron from a valence shell M.O.,

R is the Rydberg constant for infinite mass (109,737.4 cm^{-1})

Z_c is the charge on the core (Z_c = 1 for a neutral atom or molecule),

δ is the quantum defect,

and the term values, T_n, are the energy differences between the ionization potential and the electronic origins of the members of a series.

Equation [3.4] was originally derived for atoms where the field experienced by the Rydberg electron is close to spherically-symmetric. For an electron in a Rydberg molecular orbital, the core field deviates somewhat from this symmetry, and the fit of the spectral energies to equation [3.4] improves as n, and consequently the size of the Rydberg M.O., increases. Where the series limit is not observed, the adiabatic ionization potentials may be obtained approximately by extrapolation of the observed T_n to $T_n = 0$. The energy of the first ionization potential of the molecule corresponds to the energy of formation of the molecular ion, usually in its ground electronic state.

Molecular Rydberg orbitals are classified under the molecular point group symmetry. They are labelled $n\ell\Gamma_i$, where n and ℓ are the principal and orbital angular momentum quantum numbers, respectively, of the orbital in the atomic description, and Γ_i is the irreducible representation (I.R.) under the molecular point group symmetry. The I.R.'s of s, p and d atomic orbitals under the C_s and $C_{\infty v}$ point groups are given in Table 3.2. The zeroth-order degeneracies of the p, the d and the f atomic orbitals are removed under the reduced symmetry of the molecule[50]. Accordingly, atomic orbitals of the same principal quantum number form molecular Rydberg orbitals which differ in energy and several series converging to the same ionization limit may be observed. These differences decrease for the higher energy members of each series since the potential field becomes closer to being spherically-symmetric. For linear ABC-type molecules, some of these series are:

$$ns\sigma,\ np\sigma,\ np\pi,\ nd\sigma,\ nd\pi \text{ and } nd\delta.$$

Where the spin-orbit coupling is small, the selection rules governing Rydberg

transitions are those outlined in Chapter I. Since these transitions are atomic-like in nature the additional approximate selection rule $\Delta\ell = \pm 1$ must be included, where ℓ is the (atomic) orbital angular momentum of the Rydberg electron.

In molecular Rydberg transitions involving weakly-bonding or non-bonding electrons largely localized on one atom, the following empirical correlations are found between atomic and molecular series:

(1) σ_∞ is often changed considerably from atom to molecule, the change being usually in the direction of higher energy.

(2) The term values T_n and the quantum defect δ vary only slightly from atom to molecule[51].

3.3.2. δ-Values

δ, the quantum defect, has been used to characterize the various Rydberg series of atoms and molecules[52]. For molecules containing only first-row atoms, δ is small (<0.1) for states derived from nd Rydberg electrons, somewhat larger (0.3 - 0.5) for np electrons and largest (0.9 - 1.2) for ns electrons. The effective quantum number n^*, given by

$$n^* = n - \delta$$

is then non-integral and ℓ-dependent. The magnitude of δ reflects the deviation of the core potential from a coulomb field. This deviation arises from polarization of the inner valence electrons by the Rydberg electron, and from the varying degrees of penetration of the Rydberg electron into this core[53]. Mulliken[54] has interpreted the value of δ as the magnitude of the inward phase shift, relative to hydrogen, of the nodes and loops of the radial part of the eigenfunction of the Rydberg electron.

TABLE 3.2

THE IRREDUCIBLE REPRESENTATIONS OF SOME ATOMIC ORBITALS UNDER THE C_s AND $C_{\infty v}$ POINT GROUPS

Atomic Orbital	C_s	$C_{\infty v}$
s	a'	σ
p_x	a''	π
p_y	a'	π
p_z	a'	σ
d_{z^2}	a'	σ
d_{yz}	a'	π
d_{xz}	a''	π
$d_{x^2-y^2}$	a'	δ
d_{xy}	a''	δ

In molecular Rydberg series, some complications arise in the determination of the values of both δ and T_n. These are, briefly:

(1) δ decreases rapidly with increase in ℓ, becoming negligible for $\ell \geq 3$.

(2) There is a small dependence of δ on n. Some empirical formulae describing this dependence have been given by Condon and Shortley[53].

(3) At small n values, the quantum number λ of the axial component of orbital angular momentum of the Rydberg electron is well defined. Where this is strongly coupled to the molecular axis, several Rydberg levels corresponding to the same value of n and ℓ, but distinguished by λ, occur. Examples are given in Section 3.3.1. These levels are, in general, non-degenerate.

(4) At large n values, the energy separation between successive members of a Rydberg series becomes equal to or less than the energies of nuclear motion. Coupling of nuclear and electronic motion occurs, leading to a breakdown of the Born-Oppenheimer approximation. ℓ, but not λ, is well defined in the limit. This phenomenon, commonly called "ℓ uncoupling", has been discussed by Mulliken[54] and Herzberg[55].

(5) Several Rydberg states, which differ appreciably in energy, may result from the same electron configuration. Where spin-orbit coupling is large, the normal selection rules (Chapter I, Section 1.3) are violated and transitions to several of these states may become allowed. T_n must then be approximated by the centroid of the origin energies of these transitions.

3.3.3. Spin-Orbit Coupling

Coupling of the spin and orbital angular momenta occurs in molecules and the coupling mechanisms are analogous to those discussed for atoms[55,56].

Weak spin-orbit or (Λ,S) coupling in molecules is analogous to Russell-Saunders or (L,S) coupling in atoms, and strong spin-orbit or (Ω_c,ω) coupling in molecules is analogous to (j,j) coupling atoms. The transition from weak to strong spin-orbit coupling in the Rydberg series of states associated with the electron configurations (i) $\ldots(\pi)^3_{core}(n\sigma)_{Ryd}$ and (ii) $\ldots(\pi)^3_{core}(n\pi)_{Ryd}$ is of importance in this work. In OCS and OCSe, all of the states resulting from these configurations are expected to be stable in the linear conformation (see Fig. 3.2).

(i) $(\pi)^3_{core}(n\sigma)_{Ryd}$. The states $^1\Pi$ and $^3\Pi$ result from this electronic configuration. However, weak coupling of Λ, the quantum number of the axial component of the total orbital angular momentum, and Σ, the quantum number of the axial component of the total spin angular momentum, results in a splitting of the energies of the three spin-orbit components of the triplet state. Their energies are then given by

$$T_o = T_o + A'\Lambda\Sigma \qquad [3.5]$$

where T_e is the energy (in cm^{-1}), including the effects of spin-orbit coupling, of a component state,

T_o is the energy of the state in the absence of spin-orbit coupling, and

A' is the spin orbit coupling parameter.

The magnitude of A' increases rapidly with the atomic number of the atoms forming the molecule.

The energy splitting (in cm^{-1}) of the $^1\Pi$ and $^3\Pi$ states, here denoted X, is due to inter-electron repulsion. Generally, in the weak coupling case, $|X| >> |A'|$. These splittings are illustrated schematically in the figure below.

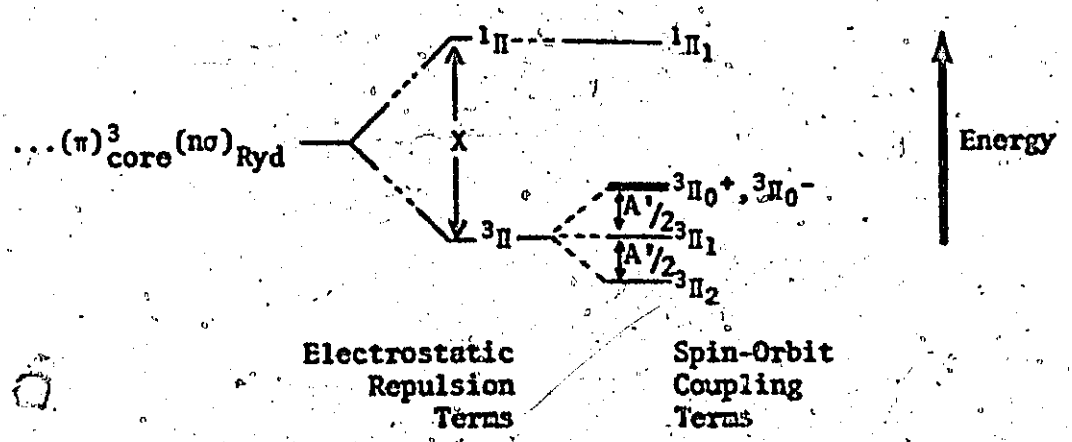

The subscripts on the symmetry species for the electronic states are values of the quantum numbers Ω for the axial component of the total angular momentum about the inter-nuclear axis, $\Omega\hbar$. Ω is given by

$$\Omega = |\Lambda + \Sigma| \qquad [3.6]$$

In the case of strong spin-orbit coupling, the spin and orbital angular momenta of the core and Rydberg electrons are separately coupled. The spin and orbital angular momenta of the valence core, here described by the electron configuration $\ldots(\pi)^3_{core}$, are strongly coupled in (Λ,S) coupling and give an axial component of total angular momentum about the internuclear axis $\Omega_c\hbar$. The total angular momentum of the Rydberg electron, $\sigma\hbar$, is then coupled to $\Omega_c\hbar$. The electron configuration and resulting states for the molecular core, where $\Omega_c = 1/2, 3/2$, are

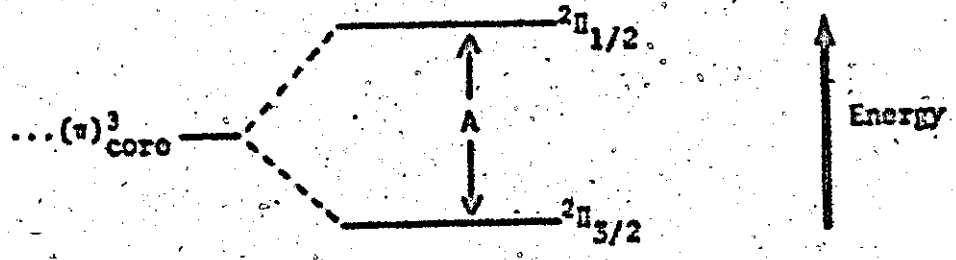

Core Spin-Orbit Coupling

From equation [3.5], the energy separation of the $^2\Pi_{1/2}$ and $^2\Pi_{3/2}$ states is equal to A, the spin-orbit coupling constant for the $(\pi)^3$ core electron configuration of the monopositive ion. Since the π valence M.O. is more than half-filled, the $^2\Pi_{3/2}$ state lies at lower energy.

The states resulting from (Ω_c,ω) coupling are classified according to their value of Ω, which is a well-defined quantum number at any strength of spin-orbit coupling. Two states result for each Ω-value[57], which are, in zeroth-order approximation, degenerate. When the finer interactions of the electrons are taken into account, the degeneracy of each pair with $\Omega > 0$ remains, but each pair with $\Omega \geq 0$ is split into non-degenerate $\Sigma^+(0^+)$ and $\Sigma^-(0^-)$ states, whose eigenfunctions are symmetric and antisymmetric respectively, with respect to inversion in a plane containing the molecule.

The states resulting from the weak and strong spin-orbit coupling cases may then be correlated according to Ω. Intermediate cases correspond to variations in the strength of the coupling of the motions of the Rydberg electron to the internuclear axis. This correlation is shown schematically in Fig. 3.5.

Similarly, a correlation diagram for the electron configuration $\ldots(\pi)^3_{core}(n\pi)_{Ryd}$ may be drawn between these limiting coupling cases. This is shown schematically in Fig. 3.6. It must be emphasized that the energy ordering, in (Λ,S) coupling, of the states resulting from this configuration is not known. The L.H.S. ordering shown is assumed and the correlation by Ω-value are made on the basis of the non-crossing rule[58].

In (Ω_c,ω) coupling, Ω is the only "good" quantum number and the selection rules for electronic transitions are:

$$\Delta\Omega = 0, \pm 1 \quad \text{and} \quad 0^+ \not\leftrightarrow 0^- .$$

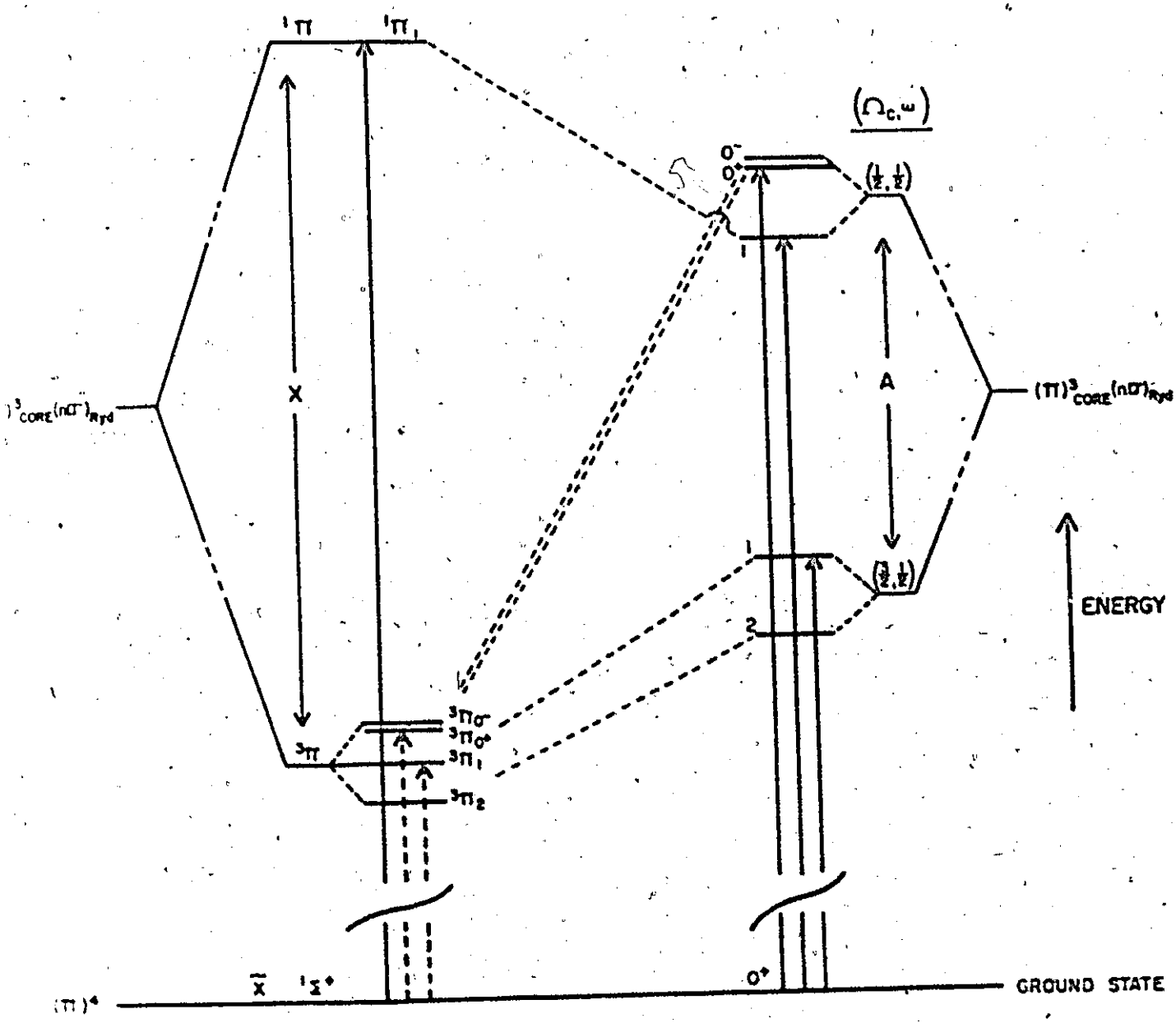

Fig. 3.5. Schematic correlation between (Λ,S) and (Ω_c,ω) coupling for the $\ldots(\pi)^3_{core}(\sigma)_{Ryd.}$ configuration.

In the case $(\pi)^3_{core}(n\sigma)_{Ryd}$, the transition $^1\Pi_1 \leftarrow \tilde{X}^1\Sigma^+$ only is allowed in (Λ,S) coupling. As the strength of spin-orbit coupling increases, intra-configuration mixing of the eigenfunctions of the $^1\Pi_1$ and $^3\Pi_1$ states occurs[59]. The "B_n" transition $^3\Pi_1(1) \leftarrow \tilde{X}^1\Sigma^+(0^+)$ then "borrows" intensity from the "C_n" transition $^1\Pi_1(1) \leftarrow \tilde{X}^1\Sigma^+(0^+)$. In the limit of "ideal" (Ω_c,ω) coupling, these transitions have equal intensity, and their electronic origin energies are separated approximately by A[59]. Because the strength of the spin-orbit coupling increases rapidly with increasing value of n, the spectra of Rydberg series corresponding to the electron promotion $\ldots(\pi)^3_{core}(n\sigma)_{Ryd} \leftarrow (\pi)^4$ show three main effects:

(1) The ratio of the intensities of the "B_n" and "C_n" transitions, $I_{"B_n"}/I_{"C_n"}$, increases with increasing n to the limiting value of 1.

(2) The separation of their electronic origin energies (in cm^{-1}), $(\nu_{"C_n"} - \nu_{"B_n"})$, is a positive quantity, intermediate in magnitude between X and A, and tends to limit value A as the coupling strength increases.

(3) The intensity of the $^3\Pi_{0^+} \leftarrow \tilde{X}^1\Sigma^+(0^+)$ transition is low, since intra-configuration mixing can occur only for states of the same Ω-value[59].

In the case $(\pi)^3_{core}(n\pi)_{Ryd}$, only the transition $^1\Sigma^+(0^+) \leftarrow \tilde{X}^1\Sigma^+(0^+)$ is allowed for all coupling strengths. All other states, in (Ω_c,ω) coupling, of Ω-value 0^+ or 1, correlate with triplet states in (Λ,S) coupling. The intensities of transitions to these states from the ground electronic state are expected to be low except in the case where the aforementioned "borrowing" mechanism operates. This may lead, in coupling cases close to the (Ω_c,ω) limit, to enhanced intensity of the $^3\Sigma^-(0^+) \leftarrow \tilde{X}^1\Sigma^+(0^+)$ transition, as the two 0^+ states correspond to mixtures of the $^3\Sigma^-(0^+$ components) and $^1\Sigma^+$ states of

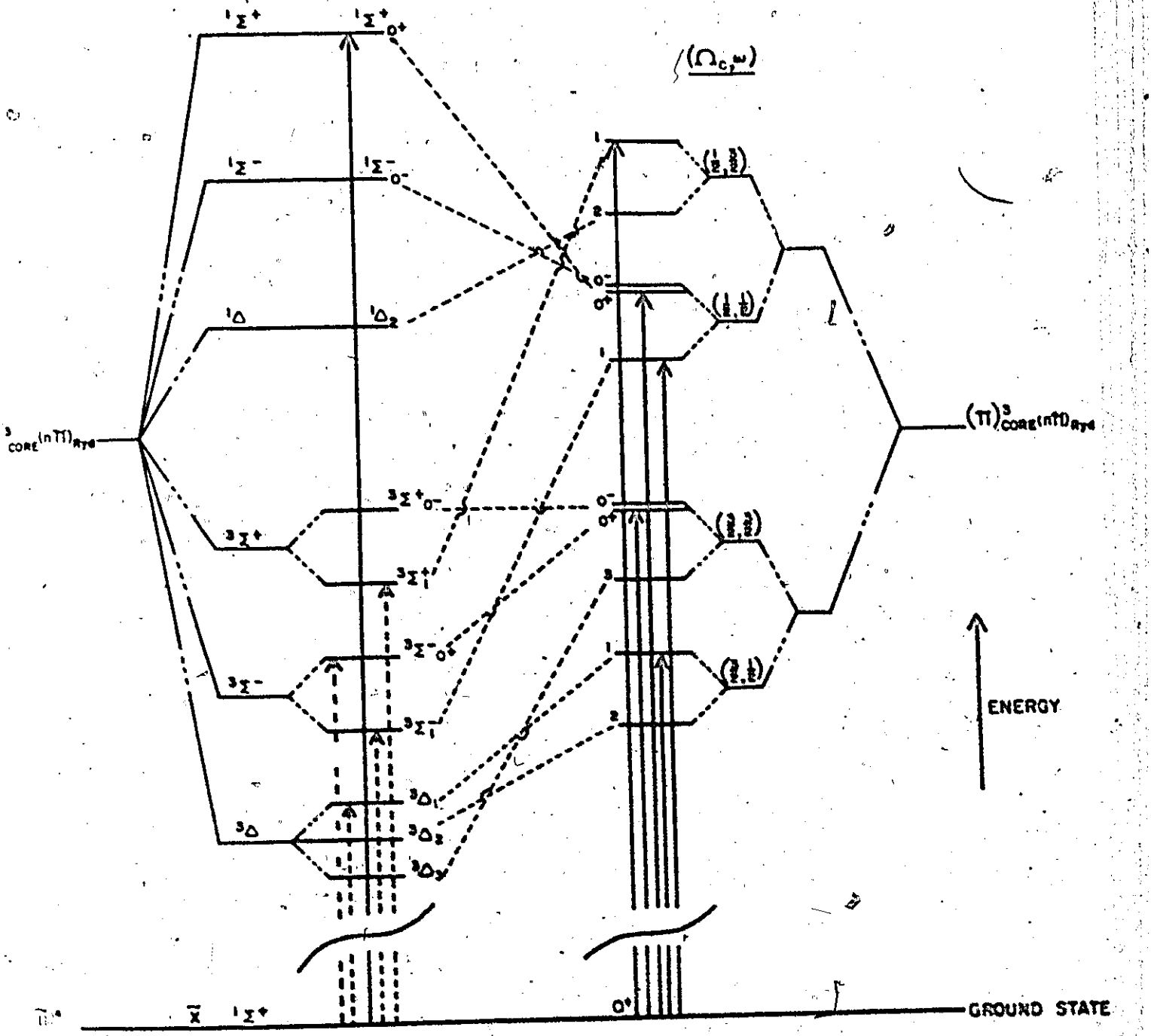

Fig. 3.6. Schematic correlation between (Λ,S) and (Ω_c,ω) coupling for the $\ldots(\pi)^3_{core}(\pi)_{Ryd.}$ configuration.

(A,S) coupling.

3.4. Oscillator Strengths of Electronic Transitions

A method of measuring the intensities of electronic transitions has been given by Mulliken and Rieke[60].

The oscillator strength

$$f^{io} = \frac{mc^2}{\pi e^2 N_o} f_{io} \, k_\nu d_\nu = 4.3 \times 10^{-9} \int \epsilon_\nu d_\nu \qquad [3.7]$$

defines the intensity of a transition between the electronic states o and i induced by the interaction of the molecule with electromagnetic radiation, where:

m and e are the electronic mass and charge, respectively,

N_o is the number of molecules, per unit volume, in the state o,

k_ν and ϵ_ν are the absorption and extinction coefficients, respectively,

and f_{io} is a quantity proportional to the square of the absolute value of the electronic transition moment[61].

Mulliken and Rieke have shown that, if the intensity envelope of the complete spectral system is triangular in shape, a good approximation to $\int \epsilon_\nu d_\nu$ is $\Delta\nu_{1/2}$. This latter quantity is the width (in cm^{-1}) of the intensity envelope of the whole spectral system at an intensity value equal to half the intensity maximum.

The strongest transitions observed in molecular systems are those allowed transitions in which an electron is promoted to a molecular Rydberg orbital. The oscillator strength of the first member of such a Rydberg series is of the order of unity. Since the transition probability is inversely proportional to the cube of the transition frequency[61], the intensity of

succeeding members falls off. Allowed and forbidden intravalence shell transitions generally have oscillator strengths in the ranges 10^{-1} - 10^{-3} and 10^{-4} - 10^{-6}, respectively, although perturbations such as vibronic and spin-orbit coupling may affect these values.

3.5. Vibrational Isotope Effect

Molecules of identical chemical composition but which contain atoms of different atomic masses have identical electronic structures and the potential function under the influence of which the nuclei vibrate is the same to a very high degree of approximation. Because of the difference in masses the vibrational eigenvalues, and consequently the vibrational frequencies, are changed. The magnitudes of vibrational isotope effects may be used to identify the various normal vibrations.

Isotope calculations are based on the harmonic oscillator approximation and therefore hold rigorously only for zeroth-order fundamental frequencies ω_j. However, since the anharmonic constants x_ik are small, the observed fundamental frequencies ν_j may be used in place of ω_j to obtain a reasonable approximation to the vibrational isotope shifts.

Two methods have been used to calculate the vibrational isotope shifts for the isotopic pair $OCSe^{80}$ and $OCSe^{78}$. The first is due to Teller and Redlich[62], who showed that, for an isotopic pair, the product of the $\omega(i)/\omega$ values for the vibrations of a given symmetry type is independent of the potential constants and depends only on the masses of the atoms and the geometrical structure of the molecule. The general formula for any isotopic pair of molecules is given by

$$\frac{\omega_1^{(i)}}{\omega_1}\cdot\frac{\omega_2^{(i)}}{\omega_2}\cdots\frac{\omega_f^{(i)}}{\omega_f}=\sqrt{\left(\frac{m_1}{m_1^{(i)}}\right)^{\alpha}\left(\frac{m_2}{m_2^{(i)}}\right)^{\beta}\cdots\left(\frac{M^{(i)}}{M}\right)^{t}\left(\frac{I_x^{(i)}}{I_x}\right)^{\delta x}\left(\frac{I_y^{(i)}}{I_y}\right)^{\delta y}\left(\frac{I_z^{(i)}}{I_z}\right)^{\delta z}}$$

where: the superscript i refers to one of the isotopic pair,

$\omega_1, \omega_2, \ldots, \omega_f$ are the zeroth-order frequencies of the f genuine vibrations of the symmetry type considered,

$m_1, m_2, \ldots$ are the masses of the representative atoms of the various sets. Each set consists of the atoms that are transformed into one another by the various symmetry operations of the molecular point group,

$\alpha, \beta \ldots$ are the numbers of vibrations each set contributes to the symmetry type considered,

M is the total mass of the molecule,

t is the number of translations of the symmetry type considered,

I_x, I_y and I_z are the moments of inertia of the molecule about the x, y and z axes through the centre of mass, and

δx, δy and δz are 1 or 0, depending on whether or not the rotation about the x, y or z axes, respectively, is a non-genuine vibration of the symmetry type considered. With respect to $\alpha, \beta, t, \delta x, \delta y, \delta z$, degenerate vibrations are counted only once.

A calculation of the vibrational potential energy distribution, as shown in Appendix A.2, shows the degree of localization of any normal vibration of a molecule. If a particular normal vibration μ can be shown to involve mainly that part of the molecule which does not contain the "isotopic" atom, its frequency ω_μ is largely unaffected by isotopic substitution and the factors $\omega_\mu^{(i)}/\omega_\mu$ is almost unity.

The second method employed in the calculation of vibrational isotope shifts is due to Adel[63] for end-atom isotope effect in a triatomic molecule. Here, the known ground state parameters of the molecules (c.f., Table

1.2) were used in such calculations. Provided that the changes in vibrational frequency, force constant, and geometry are small on electronic excitation, the results are a reasonable approximation to the excited state vibrational isotope shifts.

CHAPTER IV

MODEL POTENTIAL CALCULATIONS ON THE RYDBERG STATES OF LINEAR ABC-TYPE MOLECULES*

4.1. General

Recent advances in the theory of Rydberg transitions[50-54,60-71] have prompted renewed interest in the analysis and assignment of Rydberg transitions of polyatomic molecules. New ways of calculating the term values, T_n, for the members of various Rydberg series of diatomic and polyatomic molecules have been investigated. In these calculations, the finer interactions of the motions of the core and Rydberg electrons are largely ignored.

In a Rydberg transition, the electron is excited to an orbital large in size relative to a singly-charged core. Mulliken[54] has shown that, if the potential field experienced by the Rydberg electron is close to a spherically symmetric coulomb field, the eigenfunctions of this electron, ψ_{Ryd},

(i) are a solution of the one-electron Schrödinger equation for the N^{th} (Rydberg) electron in the average field of the other N-1 electrons, and

(ii) have the general form of the hydrogen atom solutions to the Schrödinger equation, i.e.,

$$\psi_{Ryd} = Y_{\ell m}(\theta,\phi)R_{n\ell}(r) \qquad [4.1]$$

where $Y_{\ell m}(\theta,\phi)$ are spherical harmonics, and

---

*The approach described here was developed by P. R. Greening[64] for calculations on the Rydberg states of linear AB_2-type molecules.

$R_{n\ell}(r)$ are hydrogen-like radial factors (c.f. Chapter III, Section 3.3.2).

The total electronic eigenfunction of the system, ψ, in this approximation, is given by

$$\psi = \psi_{Core}^{(1,\ldots,N-1)} \psi_{Ryd}^{(N)} \qquad [4.2]$$

where ψ_{Core} is the core wavefunction in the average field of the Rydberg electron.

In this independent particle approximation, the ψ_{Ryd} must be orthogonal to the core solutions of the one-electron Schrodinger equation with the Hamiltonian H, i.e., where

$$H \psi_{Ryd} = \epsilon_{Ryd} \psi_{Ryd} \qquad [4.3]$$

and

$$H \psi_{core} = \epsilon_{core} \psi_{core}, \qquad [4.4]$$

$$\langle \psi_{Ryd}, \psi_{core} \rangle = 0. \qquad [4.5]$$

If equation [4.5] is not satisfied, then trial solutions ψ_{Ryd} may variationally "collapse"[72] into the core.

Accurate core eigenfunctions are difficult to obtain, especially for open-shell core electron configurations. However, this difficulty, and the constraint of equation [4.5] on the eigenvalue equation, may be replaced in model potential theory[72] by adding a suitable model potential, V_ℓ, to H and solving the new eigenvalue equation

$$(H + V_\ell)\phi_{Ryd} = \epsilon_{Ryd} \phi_{Ryd} \qquad [4.6]$$

where the ϕ_{Ryd} are not subject to orthogonality constraints, but the eigen-

value, ϵ_{Ryd}, is unchanged[72]. V_ℓ represents the potential field, due to the nuclei and core electrons, experienced by the Rydberg electron. To account for equation [3.4], this potential must vary as -1/r at large r. In molecular calculations, V_ℓ must have the symmetry of the molecular framework. Equation [4.6] represents a massive simplification in the approach to the calculation of Rydberg state term values over the solution of the Schrödinger equation for the N-electron system. However, by a suitable choice of V_ℓ, some physical insight into the problems of the calculation, and a better understanding of the limits of the model used, may be obtained.

The model potential calculation described here is in two parts. These are:

(i) semi-empirical calculations of Rydberg state term values for various atoms. The parameters in the model potential are varied to obtain a good fit of the experimental and calculated term values. This procedure is essentially a quantum defect (δ) fitting device; and

(ii) calculations on molecules, where the molecular model potential is approximated to a linear superposition of the best-fit model potentials of the component atoms.

This approach is somewhat similar to that described by Botts and McKoy[69].

4.2. Atomic Calibration

The radial part of the Schrödinger equation for the hydrogen atom has the form[73]

$$\frac{1}{2r^2}\frac{d}{dr}\left(r^2\frac{dR}{dr}\right) + \left[E + \frac{1}{r} - \frac{\ell(\ell+1)}{2r^2}\right]R = 0 \qquad [4.7]$$

where the R_n (r) are the radial parts of the hydrogen eigenfunctions, and E_n are the energy eigenvalues. Substitution of

$$P_{(r)} = r\,R_{(r)}$$

yields the equation

$$-\frac{1}{2}\frac{d^2P_{(r)}}{dr^2} + \left[\frac{\ell(\ell+1)}{2r^2} - \frac{1}{r}\right]P_{(r)} = E\,P_{(r)} \qquad [4.8]$$

Equation [4.8] may be rewritten as

$$HP_{(r)} = EP_{(r)}$$

where

$$H = \left[-\frac{1}{2}\frac{d^2}{dr^2} + \frac{\ell(\ell+1)}{2r^2} - \frac{1}{r}\right] \qquad [4.9]$$

Solutions to equation [4.8] for the hydrogen atom are

$$P_{n\ell}(r) = \sqrt{\left\{\frac{(n-\ell-1)!\,Z}{n^2[(n+\ell)!]^3}\right\}}\left(\frac{2r}{n}\right)^{\ell+1} e^{-r/n}\, L_{n+\ell}^{2\ell+1}\left(\frac{2r}{n}\right) \qquad [4.10]$$

where the $L_{n+\ell}^{2\ell+1}(2r/n)$ are the associated laguerre polynomials[74]. The E_n are then given by

$$E_n = \int_0^\infty P_n(r)\, H\, P_n(r)\, dr = -\frac{1}{2n^2} \qquad [4.11]$$

and the term values (in cm^{-1}) of the hydrogen spectrum written as

$$T_n = R/n^2 \qquad [4.6]$$

R is the Rydberg constant = 109737 cm^{-1}.

For many-electron atoms, the term values of a Rydberg series may be described in good approximation by equation [4.12] if n, the principal

quantum number in the hydrogen description, is allowed non-integral values. The T_n are then written as

$$T_n = R/n^{*2} \qquad [4.13]$$

where n*, the effective quantum number, is given by

$$n^* = (n - \delta) \qquad [4.14]$$

The quantities n*, n and δ have already been discussed. The one-electron Schrödinger equation for a Rydberg electron in such a system may be written as

$$-\frac{1}{2}\frac{d^2G(r)}{dr^2} + \left[\frac{\ell(\ell+1)}{2r^2} + V_\ell(r)\right]G(r) = \varepsilon\, G(r) \qquad [4.15]$$

or, by use of equation [4.3], as

$$[H + 1/r + V_\ell(r)]\; G(r) = \varepsilon\, G(r) \qquad [4.16]$$

Here, $V_\ell(r)$ is some model potential which describes the field experienced by a Rydberg electron in a many-electron atom. It is here assumed that G(r) can be approximated as a linear combination of hydrogen functions, i.e.,

$$G_i(r) = \sum_n C_{ni}\, P_n(r) \qquad [4.17]$$

The purpose of this approximation is to retain the hydrogen-like character of all Rydberg orbitals. By application of the usual variational procedure[75] of setting up the secular equation, elements of the form

$$H_{nm} = \int_0^\infty P_n(r)[H + 1/r + V_\ell(r)]\, P_m(r)\, dr$$

$$= \int_0^\infty P_n(r)\, H\, P_m(r)\, dr + \int_0^\infty P_n(r)[1/r + V_\ell(r)]P_m(r)\, dr \qquad [4.18]$$

are found. The first integral in equation [4.18] is the energy expression for the hydrogen atom. Hence

$$H_{nm} = E_n + I_n$$

where

$$I_n = \int_0^\infty P_n(r) \left[\frac{1}{r} + V_\ell(r)\right] P_m(r)\, dr \qquad [4.19]$$

In the evaluation of the I_n, the form of the model potential chosen is that first applied by I. V. Abarenkov and V. Heine[71] to calculations of Rydberg state term values for atoms and molecules. $V_\ell(r)$ is approximated as the sum of two quantities:

(1) a constant potential, A, inside a core of radius r_0; and

(2) a coulombic potential, $-Z/r$, in the region $r_0 \to \infty$. Here, Z is the effective charge of the atom.

This model potential is represented schematically in the figure below. Clearly, this potential distribution is not a representation of the true potential for all points in space. However, the boundary condition that the potential approach $-\frac{1}{r}$ at large r is satisfied, and the constant core potential A represents an average value in a region in which the true potential must have a complicated form.

$$V_\ell(r) = A \qquad (r < r_0)$$

$$V_\ell(r) = -Z/r \quad (r \geq r_0)$$

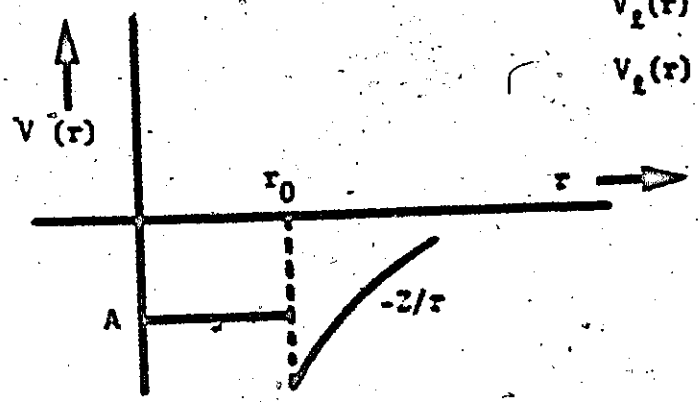

The potential field, due to the core electrons and nuclei, experienced by a Rydberg electron in the core region is, physically, a continuous function of r. In the mathematical model, A represents the average of this field. Accordingly, it is not essential in these calculations to match the values of the core and coulomb potentials at r_0. Equation [4.18] then yields

$$I_n = \int_0^{r_0} P_n(r)\left[\frac{1}{r} + A\right) P_m(r)\, dr + \int_{r_0}^{\infty} P_n(r)(1/r - 1/r)\, P_m(r)\, dr$$

$$= \int_0^{\infty} P_n(r)\ [1/r + A]\ P_m(r)\, dr$$

Substitution in equation [4.10] yields, for s-functions ($\ell = 0$)

$$H_{nm} = E_n + \left[\frac{16(n-1)!(m-1)!}{n^4m^4(n!)^3(m!)^3}\right]^{1/2} \int_0^{r_0} r^{2\ell} e^{-r(m+n)/mn} L_n^1\left(\frac{2r}{n}\right) L_m^1\left(\frac{2r}{m}\right)\left[\frac{1}{r} + A\right]dr \quad [4.20]$$

The associated laguere polynomials are described by the relations

$$L_{n+\ell}^{2\ell+1}(x) = B_0 + B_1 x + \ldots\ldots B_{n-\ell-1} x^{n-\ell-1}$$

i.e.,

$$L_n^1(x) = \sum_{r=0}^{n-1} B_{nr} x^r \quad [4.21]$$

where the B_{nr} are given by standard expressions[75]. Substitution of equation [4.21] into [4.14] yields

$$H_{nm} = E_n + \left[\frac{16(n-1)!(m-1)!}{n^4m^4(n!)^3(m!)^3}\right]^{1/2} \sum_{s=0}^{n-1} \sum_{t=0}^{m-1} B_{ns} B_{nt} \int_0^{r_0} r^{s+t+2\ell} e^{-[r(m+n)/mn]} \left[\frac{1}{r} + A\right]dr \quad [4.22]$$

The integral in equation [4.22] is of the form

$$I_n = \int_0^{r_0} x^n e^{-ax} dx$$

which can be integrated by parts to yield

$$I_n = \frac{n!}{\alpha^{n+1}} \left[1 - e^{-\alpha r_0} \sum_{k=0}^{n} \frac{(\alpha r_0)^{n-k}}{(n-k)!} \right]$$

Calculations were carried out with the aid of a CDC 6400 computer. The sets of basis functions 1s,...,10s and 2p,...,9p were used. The eigenfunctions obtained as variational method solutions to equation [4.10] formed an orthonormal set. A and r_0 were treated as parameters and were adjusted to obtain a good fit of the calculated and observed term values for the ns and np Rydberg series in carbon, oxygen, sulfur and selenium. Some of these results are listed below. All quantities are given in atomic units (a.u.)

OXYGEN s-SERIES $r_0 = 2.5 \pm 0.05$ $A = 0.02 \pm 0.005$

n	2	3	4	5	6	
T_n* (obs.)	0.15048	0.06199	0.03381	0.02127	0.01461	(76)
T_n (calc.)	0.15075	0.06192	0.03365	0.02113	0.01450	

SULFUR s-SERIES $r_0 = 2.5 \pm 0.05$ $A = 0.52 \pm 0.005$

n	2	3	4	5	6	
T_n* (obs.)	0.12858	0.05560	0.03115	0.01992	0.01384	(76)
T_n (calc.)	0.12866	0.05544	0.03102	0.01984	0.01378	

OXYGEN p-SERIES $r_0 = 2.5 \pm 0.05$ $A = -0.19 \pm 0.005$

n	2	3	4	5	6	
T_n** (obs.)	0.09659	0.04626	0.02718	0.01788	-	(76)
T_n (calc.)	0.09763	0.04457	0.02562	0.01667	0.01171	

*Average of ^3S component term values.

**Average of ^3P component term values.

SELENIUM p-SERIES r_0 = 3.2±0.05 A = 0.09±0.005

n	2	3	4	5	6	
T_n^{**}(obs.)	0.08190	0.04119	0.02558	0.016031	0.01163	(76)
T_n (calc.)	0.08397	0.03981	0.02353	0.01562	0.01115	

The set (A,r_0), which gives a best fit of T_n(calc.) to T_n(obs.) for all n of a given series, is not found to be unique. Rather, a wide range of (A,r_0)-values may be used to generate T_n(calc.) values which are within 5% of T_n(obs.). This range is illustrated schematically in the figure below.

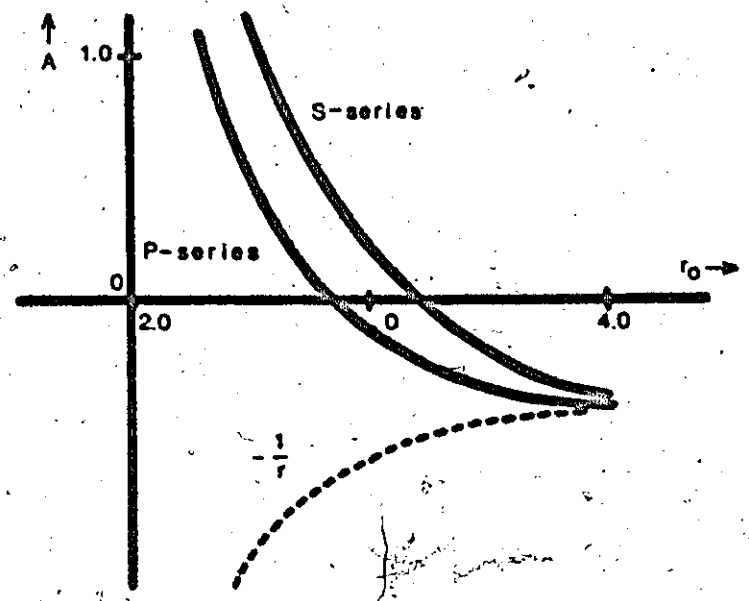

Plot of A vs r_0 (a.u.) for best fit.

In order to retain some physical significance for the parameters, all values of r used are in the range of known ionic core radii, i.e., 2-4 a.u. In this region, dA/dr is closest to unity and the calculated energies are insensitive to small changes in these parameters, thus facilitating the fit to the experimental data.

The lowest energy eigenvalue eigenfunctions of the calculated series are denoted "2s" and "2p" for all atoms as the largest coefficients C_i in the eigenfunctions are those of the hydrogen 2s and 2p A.O.'s, respectively. By

use of a model potential, solutions of the one-electron Schrödinger equation yield only model wavefunctions. The distinction must be made between these "2s" (or "2p") eigenfunctions generated from a linear combination of hydrogenic eigenfunctions in a non-coulombic field, and Slater-type 2s (or 2p) functions, which are derived from the true self-consistent effective potential. The value of r for which the radial probability density is a maximum illustrates this distinction. This value is ∿5 a.u. for the former eigenfunction and ∿3 a.u. for a Slater-type 2s function.

4.3. Calculation of Molecular Term Values

The theory can now be applied to the linear ABC-type molecules OCS and OCSe. The model one-electron Hamiltonian, in the Born-Oppenheimer approximation, for the Rydberg-electron in molecules, has the form

$$H_M = -\frac{1}{2}\nabla^2 + V_{Mol}$$

where the ∇^2 are kinetic energy operators in the coordinate system chosen and V_{Mol} is some suitable model potential. A form of V_{Mol}, suggested by S. A. Rice et. al.[70] is a sum of atomic potentials described by the parameters calculated in the atomic calculation,

i.e.,
$$V_{Mol} = \sum_{i}^{atoms} V_i \qquad [4.23]$$

Each atom i has its own core region, which is taken to be a sphere of radius r_i^o centred on the ith nucleus. V_i is then of the form

$$V_i = -\delta Z_i/r_i \qquad (r_i \geq r_0)$$
$$V_i = A_i \qquad (r_i \leq r_0) \qquad [4.24]$$

where δZ_i is the partial (nuclear) charge associated with atom i. If the molecular core has net charge Z_c, then

$$Z_c = \sum_{i}^{\text{atoms}} \delta Z_i \qquad [4.25]$$

For the series OCS and OCSe, the following assumptions are made:

(i) The value of r_0 for the carbon atom, r_C, remains unchanged in the series.

(ii) $r_C = r_{OX}$, the value of r_0 for the oxygen atom.

(iii) For ABC-type molecules, OCS and OCSe, $r_{OX} = r_C = r_{C-O}$, the C-O bond length (a.u.) and $r_{S,Se} = r_{S,Se-C}$, the S,Se-C bond length (a.u.).

Ground electronic state bond lengths were used in these calculations. The bond lengths are found to be little changed in the Rydberg states of OCS[77].

Assumption (i) can be justified from known molecular charge distributions. Bader and Beddall[79] have shown that charge populations in such CO fragments undergo only small changes as the bonding environment is changed. Accordingly, only a small change in r_C is expected in the pair OCS, OCSe. Assumption (iii) gives an r_0-value in the range 2-4 a.u., which is used in the atomic calculations above. These assumptions are supported by evidence from electron density diagrams for the molecules CO_2 and OCS[78]. These diagrams are based on wavefunctions calculated by McLean and Yoshimine[32] for these molecules. Weeks and Rice[72] have suggested that the model potential radius, r_0, should be chosen to be roughly equal to the core radius and should contain ~95% of the core electron density. Simple volume-charge distribution calculations for these diagrams indicate values, for each of the constituent atoms, of "radii", within which 95% of the electron density is confined. These are in the range of 2.4-2.5 a.u. for r_C

and r_0, in both OCO and OCS, and ~2.9 a.u. for r_S. When the Rydberg electron is removed from the valence core, these values should decrease only slightly. The r values chosen in the model potential for these calculations enclose most of the core electron density and reproduce closely the symmetry of the electron distribution. Assumptions (i), (ii) and (iii) are therefore considered both reasonable and intuitively appealing. The form of the molecular model potential used is represented schematically in the figure below.

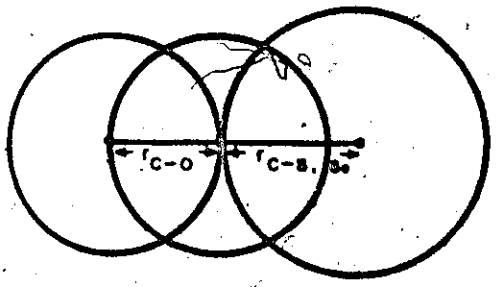

OCS: $r_{C-O} = r_C = r_{OX} = 2.19$ a.u.
$r_{C-S} = r_S = 2.94$ a.u.

OCSe: $r_{C-O} = r_C = r_{OX} = 2.19$ a.u.
$r_{C-Se} = r_{Se} = 3.23$ a.u.

The parameters used in these calculations were:

O:	A(s) = 0.11	A(p) = -0.025
C:	A(s) = 1.1	A(p) = -0.15
S:	A(s) = 0.085	A(p) = 0.052
Se:	A(s) = -0.01	A(p) = 0.09

For a one-centre expansion of functions about an atom i of the ABC-type molecule, the Schrödinger equation can be written as

$$[H^{(i)} + 1/r_i + \sum_{a,b,..,j}^{atoms} V(r_j)]\,\phi(r_i) = \epsilon\phi(r_i) \qquad [4.26]$$

This leads to matrix elements of the form

$$H_{nm}^{(i)} = \int_0^\infty \phi_n(r_i)[H^{(i)} + 1/r_i + \sum_j^{atoms} V(r_j)]\phi_m(r_i)d\tau_i \qquad [4.27]$$

Upon substitution for $V(r_j)$ for $i = j$ and $i \neq j$, equation [4.27] becomes

$$H_{nm}^{(i)} = \int_0^\infty \phi_n(r_i) H^{(i)} \phi_m(r_i) d\tau_i + \int_0^\infty \phi_n(r_i) [\frac{1}{r_i} + V(r_i)] \phi_m(r_i) d\tau_i$$

$$+ \sum_{j \neq i}^{\text{atoms}} \int_0^\infty \phi_n(r_i)\ V(r_j)\ \phi_m(r_i)\ d\tau_i \qquad [4.28]$$

By analogy with equations [4.16] - [4.19] (incl.), equation [4.28] may be written

$$H_{nm}^{(i)} = E_n(n=m) + \int_0^\infty \phi_n(r_i) [\frac{1}{r_i} + V(r_i)]\ \phi_m(r_i) d\tau_i$$

$$+ \sum_{j \neq i}^{\text{atoms}} \int_0^\infty \phi_n(r_i)\ V(r_j)\ \phi_m d\tau_i \qquad [4.29]$$

Upon substitution of the model potential described by equations [4.24] and [4.25] the first integral of equation [4.29] is given as

$$\int_0^\infty \phi_n(r_i) [\frac{1}{r_i} + V(r_i)] \phi_m(r_i) d\tau_i = \int_0^{r_{i_o}} \phi_n(r_i) [\frac{1}{r_i} + A_i] \phi_m(r_i) d\tau_i$$

$$+ \int_{r_{i_o}}^\infty \phi_n(r_i) [\frac{1}{r_i} - \frac{\delta Z_i}{r_i}] \phi_m(r_i) d\tau_i \qquad [4.30]$$

which is readily evaluated as before. The second integral of equation [4.29], denoted as I_{nm}, may be written in the general form

$$I_{nm} = \int_0^\infty \phi_n(r_i) V(r_j) \phi_m r_i d\tau_i = \int_0^\infty \phi_n^a\ V^b\ \phi_n^a\ d\tau_a \qquad [4.31]$$

a and b refer to nuclei, not necessarily adjacent. Where s and p functions, denoted by ϕ_{ns} and ϕ_{np}, respectively, are used in the calculation, three types of integrals are obtained from equation [4.31]. These are:

$$I^{ss}_{nm} = \int_0^\infty \phi^a_{ns}\, V^b\, \phi^a_{ms}\, d\tau_a \qquad [4.32]$$

$$I^{sp}_{nm} = \int_0^\infty \phi^a_{ns}\, V^b\, \phi^a_{mp}\, d\tau_a \qquad [4.33]$$

$$I^{pp}_{nm} = \int_0^\infty \phi^a_{np}\, V^b\, \phi^a_{mp}\, d\tau_a \qquad [4.34]$$

The method of evaluation of these integrals is given by Greening [64].

Two other variables are obvious in the proceeding discussion:

(i) For a linear ABC-type molecule, the functions can be expanded about any of three nuclear centres. Trial calculations on OCS and OCSe indicated that the term values were moderately insensitive (±8%) to choices of nucleus for this one-centre expansion. As discussed in Chapter III, Section 3.3.2, in molecules containing large end-atoms, the molecular T_n(obs.) and δ-values are little changed from those of the largest atom. These observations suggest that the Rydberg electron density in such molecules is largely localized on these atoms. Accordingly, in the final calculations for the molecules OCS and OCSe, the functions were centred on the sulfur and selenium atoms, respectively.

(ii) The charge distribution δZ_i was taken, in the final calculations, to be +1/2 e each for S/Se and O in OCS/Se. This non-delocalized distribution is considered reasonable, as the sum of the squares of the coefficients for S and O A.O.'s are largest in the (calculated) highest-filled 3π M.O. of OCS [32]. Other distributions were used also, but the results were insensitive to changes in the distributions.

Term values calculated for OCS and OCSe are given in Tables 4.1 and 4.2, respectively.

TABLE 4.1

MODEL POTENTIAL METHOD TERM VALUES FOR OCS

	ns σ	no s-p mixing[a]						ns σ s-p mixing[b]	
	C-centred	S-centred				O-centred		S-centred	
	$(\frac{1}{2}, 0, \frac{1}{2})$[c]	$(\frac{1}{2}, 0, \frac{1}{2})$		$(\frac{2}{3}, 0, \frac{1}{3})$		$(\frac{1}{3}, \frac{1}{3}, \frac{1}{3})$		$(\frac{1}{3}, \frac{1}{3}, \frac{1}{3})$	
n	T_n (au)	T_n (au)	T_n (cm^{-1})	T_n (au)	T_n (cm^{-1})	T_n (au)	T_n (cm^{-1})	T_n (au)	T_n (cm^{-1})
2	.104936	.093532	20527	.095495	20959	.099547	21848	.105884	23239
3	.047539	.043774	9607	.044394	9743	.046630	10234	.047072	10331
4	.027156	.025381	5571	.025658	5631	.026877	5899	.026782	5878
5	.017558	.016571	3637	.016716	3669	.017443	3828	.017386	3816
6	.012270	.011671	2562	.011753	2580	.012212	2680	.012255	2690
7	.009041	.008662	1901	.008710	1912	.009009	1977	.009140	2006
8	.006917	.006677	1465	.006705	1472	.006899	1514	.007093	1557
9	.005430	.005291	1161	.005305	1164	.005421	1190	.005312	1166

TABLE 4.1 (cont'd.)

	ns σ s-p mixing		np σ s-p mixing				np π			
	S-centred				S-centred				S-centred	
	$(\frac{1}{2}, 0, \frac{1}{2})$		$(\frac{1}{3}, \frac{1}{3}, \frac{1}{3})$		$(\frac{1}{2}, 0, \frac{1}{2})$		$(\frac{1}{3}, \frac{1}{3}, \frac{1}{3})$		$(\frac{1}{2}, 0, \frac{1}{2})$	
n	T_n (au)	$T_n(cm^{-1})$*	T_n (au)	$T_n(cm^{-1})$	T_n (au)	$T_n(cm^{-1})$*	T_n (au)	$T_n(cm^{-1})$	T_n (au)	$T_n(cm^{-1})$*
2	.110678	24291	.085788	18829	.074748	16405	.080996	17777	.079224	17389
3	.049604	10886	.040632	8918	.036741	8064	.039604	8693	.039043	8569
4	.028003	6146	.023849	5234	.022021	4833	.023551	5169	.023323	5119
5	.018042	3960	.015664	3438	.014670	3220	.015653	3436	.015546	3412
6	.012641	2774	.011034	2422	.010448	2293	.011173	2452	.011118	2440
7	.009381	2059	.008148	1788	.007791	1710	.008381	1840	.008351	1833
8	.007258	1593	.006225	1366	.006008	1319	.006517	1430	.006500	1427
9	.005772	1267	-	-	.004727	1037	.005201	1141	.005237	1149
	$\delta^t_{average}$ = 0.21				$\delta^t_{average}$ = 0.68				$\delta^t_{average}$ = 0.65	

*These values used as T_n(calc.) in Chapter 5.

[a]When s-A.O.'s only are used in the calculation.

[b]When s and p-A.O.'s are used.

[c]Charge distribution (δZ_{Se}, δZ_C, δZ_O).

[t]When the relationship $T_n = R/(n+\delta)^2$ is used.

cf. equations [4.32]-[4.34].

TABLE 4.2

MODEL POTENTIAL METHOD TERM VALUES FOR OCSe

	ns σ no s-p mixing[a]				ns σ s-p mixing[b]			
	C-centred		Se-centred		Se-centred			
	$(\frac{1}{2}, 0, \frac{1}{2})$[c]		$(\frac{1}{2}, 0, \frac{1}{2})$		$(\frac{1}{3}, \frac{1}{3}, \frac{1}{3})$		$(\frac{1}{2}, 0, \frac{1}{2})$	
n	T_n (au)	$T_n(cm^{-1})$	T_n (au)	$T_n(cm^{-1})$	T_n (au)	$T_n(cm^{-1})$	T_n (au)	$T_n^*(cm^{-1})$
2	.107859	23672	.093234	20463	.106343	23340	.109714	24080
3	.049084	10772	.044270	9716	.048005	10536	.049906	10953
4	.028036	6153	.025765	5655	.027445	6024	.028413	~~6236~~
5	.018119	3977	.016825	3693	.017860	3920	.018424	4044
6	.012657	2778	.011835	2598	.012623	2770	.012981	2849
7	.009324	2046	.008767	1924	.009449	2074	.009677	2124
8	.007132	1565	.006743	1480	.007360	1616	.007432	1631
9	.005591	1227	.005328	1169	.005294	1162	.005717	1255
							$\delta_{average}$ = 0.87	

TABLE 4.2 (cont'd.)

	np σ s-p mixing				np π			
	Se-centred				Se-centred			
	$(\frac{1}{3}, \frac{1}{3}, \frac{1}{3})$		$(\frac{1}{2}, 0, \frac{1}{2})$		$(\frac{1}{3}, \frac{1}{3}, \frac{1}{3})$		$(\frac{1}{2}, 0, \frac{1}{2})$	
n	T_n(au)	$T_n(cm^{-1})$	T_n (au)	$T_n^*(cm^{-1})$	T_n (au)	$T_n(cm^{-1})$	T_n (au)	$T_n^*(cm^{-1})$
2	.082611	18131	.072643	15943	.077915	17100	.076466	16782
3	.039520	8674	.035947	7890	.038610	8474	.038165	8376
4	.023329	5120	.021584	4737	.023148	5080	.022970	5041
5	.015363	3371	.014361	3152	.015463	3394	.015380	3375
6	.010820	2375	.010203	2239	.011075	2431	.011032	2421
7	.007972	1750	.007664	1682	.008327	1828	.008303	1822
8	.006051	1328	.006141	1348	.006490	1424	.006477	1422
9	-	-	.004512	990	.005154	1131	.005148	1130
			$\delta^t_{average}$ = 0.62				$\delta^t_{average}$ = 0.70	

*These values used as T_n(calc.) in Chapter 5.

[a] When s-A.O.'s only are used in the calculation
[b] When s and p A.O.'s are used
[c] Charge distribution (δZ_{Se}, δZ_C, δZ_O).
[t] When the relationship $T_n = R/(n+\delta)^2$ is used.

} c.f. equations [4.32] - [4.34].

These results are used in the analysis of the spectra of OCS and OCSe reported in Chapter V. The assumption is made that the model potential chosen for these calculations adequately represents the potential field experienced by a Rydberg electron outside the $\ldots(\pi)^3$ core electron configuration of these molecules.

The values calculated are term values. Approximate values of transition energies (T_o) for Rydberg state ← ground state transitions may be obtained (cf. equation [3.1]) if the ionization potential (I.P.) of the molecule is known.

The calculated values of $T_{2s\sigma}$(OCS) and $T_{2s\sigma}$(OCSe) are almost equal (~24000 cm^{-1}). So also are the calculated values $T_{2p\sigma}$(OCS,Se) (~16000 cm^{-1}) and $T_{2p\pi}$(OCS,Se) (~17000 cm^{-1}). The first members of corresponding Rydberg transitions of these molecules should, to a good approximation, be separated in energy by the value of the quantity I.P.(OCS) - I.P.(OCSe). This predicted "phase shift" of the energies of analogous transitions in OCS and OCSe is supported by the experimental results for those molecules reported in Chapter V.

Robin[80] has given an analysis of experimentally-determined term values in the Rydberg spectra of a wide variety of molecules viz. oxides, amines, olefins, ketones and parafins. For each of these molecules, the term values for the first s, p and d series members are within the ranges 24000-40000 cm^{-1}, 17000-22000 cm^{-1} and 12000-14000 cm^{-1}, respectively. For molecules of low molecular weight, the term values tend to the lower range limits. The results of the model potential method calculations show excellent agreement with these lower values.

CHAPTER V

DESCRIPTIONS AND ANALYSES OF THE OBSERVED SPECTRA

This chapter is sub-divided into three sections, viz.

5.A. Observed Absorption Spectrum of OCSe

5.B. Observed Absorption Spectrum of OCS

5.C. Observed Absorption Spectrum of CS_2

Though the analysis of the electronic spectrum of OCSe constitutes the main subject material of this work, the details of the spectra of OCS and CS_2 are included to support this analysis.

It is assumed (i) that all of the observed electronic spectra result from electronic excitation from the ground electronic state and (ii) that the transitions are electric dipolar. The large ($>10^{-4}$) oscillator strengths measured for these transitions and observations, in the spectra, of frequency intervals corresponding to excitation of ground state vibrational motions, support these assumptions.

5.A. Observed Absorption Spectrum of OCSe

5.A.1. The Infrared Spectrum of OCSe

The molecule OCSe has been shown, by microwave work[16], to be linear in the ground ($\tilde{X}\ ^1\Sigma^+$) electronic state. The (classical) descriptions and the symmetries of the four normal vibrations of linear OCSe are given below.

Normal Vibration	Description	Symmetry
ν_1	stretch	σ
ν_2 (doubly degenerate)	bending	π
ν_3	stretch	σ

TABLE 5.1

FREQUENCIES OF OBSERVED INFRARED BANDS OF OCSe

Molecule	Frequency* (cm^{-1})	Type	Intensity**	Assignment
$OCSe^{nat}$	465	$\perp$	vw	ν_2
	644†	$\parallel$	w	ν_3
	928	$\parallel$	vw	$2\nu_2$
	2027	$\parallel$	vs	ν_1
	2666	$\parallel$	w	$\nu_1 + \nu_3$
$OCSe^{80}$	2026.3††	$\parallel$	vs	ν_1
$OCSe^{78}$	2670	$\parallel$	w	$\nu_1 + \nu_3$
	2026.5††	$\parallel$	vs	ν_1

*All frequencies in vacuum wavenumber units (cm^{-1}).

**w = weak, s = strong.

†Partially obscured by a band of the impurity CO_2 at 647.6 cm^{-1}.

††Accuracy ±0.5 cm^{-1}.

TABLE 5.2

VIBRATIONAL POTENTIAL ENERGY DISTRIBUTION FOR THE GROUND STATE OF OCSe

Normal Mode	k_{12} (SeC)*	k_{23} (CO)
ν_1	0.146	0.854
ν_3	0.854	0.146

TABLE 5.3

GROUND STATE VIBRATIONAL ISOTOPE SHIFT CALCULATIONS FOR OCSe

Normal Mode	Isotope Shift ($\nu_{78} - \nu_{80}$) cm^{-1}	
	Product Rule	Adel
ν_1	0.0**	0.3
ν_2	0.1	0.5
ν_3	2.1**	3.5

*See Appendix A.2.

**See text.

The frequencies of measured bands in the infrared spectra of $OCSe^{nat}$, $OCSe^{80}$ and $OCSe^{78}$ are given in Table 5.1. These frequencies are presumed to correspond to vibrational transitions from the zeroth vibrational level of the $\tilde{X}\ ^1\Sigma^+$ state. The selection rules governing vibrational transitions and term value formulae have been given by Herzberg[81]. Bands are classified as parallel (||) or perpendicular ($\perp$) according to whether the non-zero component of the vibrational transition moment is in the direction of the molecular (Z) axis or at a right angle to this. The frequencies measured in this work differ slightly from those previously reported (c.f. Table 1.2). No rotational fine structure could be resolved in any of these bands.

5.A.2. Vibrational Potential Energy Distribution and Isotope Shift

The vibrational potential energy distribution in the ground state of OCSe has been calculated as described in Appendix A.2. The results (c.f. Table 5.2) show that the ν_1 and ν_3 vibrational motions are almost completely (~85%) localized in the CO and CSe fragments, respectively. The vibrational isotope shifts for ν_1, ν_2 and ν_3 may then be calculated according to the Redlich-Teller product rule (c.f. Chapter 3, Section 3.5.) if $\omega_1^{(i)}/\omega_1$ is assumed to be unity. Table 5.3 lists these results, together with those calculated by the method of Adel. Both methods show that the isotope shift for ν_3 is distinctively larger than those for ν_1 and ν_2. Little change in these shifts, calculated for the ground state, is expected for excited electronic states.

5.A.3. Description and Analysis of the 2700 Å - 2200 Å Absorption System of OCSe

5.A.3.1. Description

In the spectral region 5000 Å - 2800 Å, no absorption by OCSe could

be observed at pressure-path lengths of 0.02 m-atm. However, a weak absorption system occurs in the region 2700 Å - 2200 Å, a spectrophotometer (Cary 14) trace of which is shown in Fig. 5.1.

Under higher resolution (Bausch and Lomb and Hilger Watts spectrographs), this absorption system showed the features:

(i) two moderately strong series of diffuse bands, and

(ii) two weak series of diffuse bands.

No decrease in the diffuseness of these bands could be observed when

(i) the system was photographed under the high resolution of the Ebert instrument; or

(ii) $OCSe^{80}$ was used in place of $OCSe^{nat}$.

It was therefore concluded that the bands of this system are genuinely diffuse. As all of the observed bands appear equally diffuse, the mechanism responsible is probably that of predissociation by electronic transition (Case I predissociation). These bands have been reported as diffuse under high resolution by Bavia, Di Lonardo, Galloni and Trombetti[12], and in the flash photolysis of solid-phase (77°K) OCSe at $\lambda > 2200$ Å, dissociation of OCSe to the products

$$CO\ (^1\Sigma^+) \quad + \quad Se\ (^1D_g) \qquad \text{is reported.}$$

Also, the bands of the analogous absorption system of OCS (2650 Å - 2000 Å) have been reported as diffuse[82] [photodissociation of gas-phase OCS at $\lambda > 2200$ Å is reported to yield the products $CO\ (^1\Sigma^+) + S\ (^1D_g)$][11].

The vacuum frequencies, relative intensities and assignments of these bands of $OCSe^{nat}$ are given in Table 5.4. The analysis is incomplete, as no electronic origin could be assigned. However, the bands were assigned to four progressions viz. A, B, C and D, and numbered consecutively as members

TABLE 5.4

MEASURED BANDS OF $OCSe^{nat}$

IN THE 37600 cm^{-1} (2659.5 Å) - 42700 cm^{-1} (2341.9 Å) REGION

Band Frequency* (cm^{-1})	Relative Intensity**	Assignment[a]	
		Progression	Number
< 37647.8	Several diffuse features too weak for measurement.		
	< 0.5		
37648	1.00	A	n
37949	1.15	B	m
37084	vw	unassigned	
38117	1.25	A	n+1
38414	1.44	B	m+1
38528	vw	unassigned	
38573	1.51	A	n+2
38780	w	C	p
38844	1.70	B	m+2
39034	1.78	A	n+3
39227	w	C	p+1
39304	1.88	B	m+3
(39400)[b]	w	D	Q
39493	1.98	A	n+4
39725	2.08	B	m+4
39862	w	D	Q+1
39953	2.13	A	n+5
40040	w	C	p+3
40162	2.21	B	m+5

Band Frequency* (cm^{-1})	Relative Intensity**	Assignment[a]	
		Progression	Number
40290	w	D	Q+2
40374	2.21	A	n+6
40405	vw	unassigned	
40510	w	C	p+4
40598	2.24	B	m+6
40720	w	D	Q+3
40806	2.25	A	n+7
41038	2.24	B	m+7
41167	w	D	Q+4
41237	2.21	A	n+8
41398	w	C	p+6
41472	2.15	B	m+8
41567	w	D	Q+5
41649	2.15	A	n+9
41804	w	C	p+7
41875	2.10	B	m+9
42076	2.10	A	n+10
42272	1.98	B	m+10
42469	1.98	A	n+11
42667	1.70	B	m+11

*Vacuum wavenumber units (cm^{-1}). Estimated accuracy ±15 cm^{-1}.

**a Log I absorption. This quantity is arbitrarily set to unity for the band at 37647.8 cm^{-1}.

[a]See text.

[b]Overlapped by 2537 Å Hg emission line.

Fig. 5.1. Low resolution absorption spectrum of OCSe in the 2100 Å - 2900 Å region.

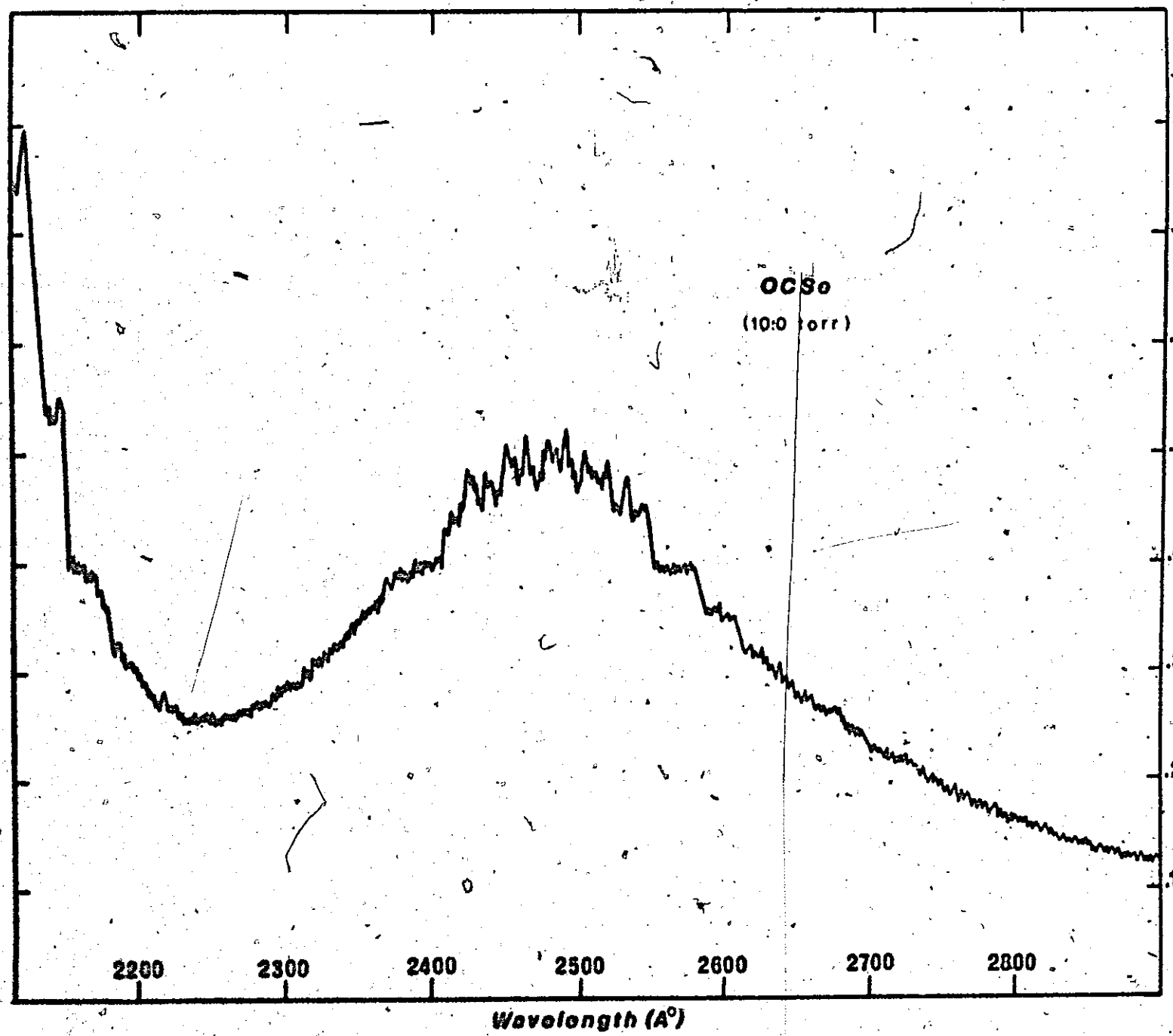

FIG 5.2 Spectrogram of a Portion of the 2100 Å - 2700 Å Absorption System of OCSe. (The emission line is that of Hg at 2537 Å)

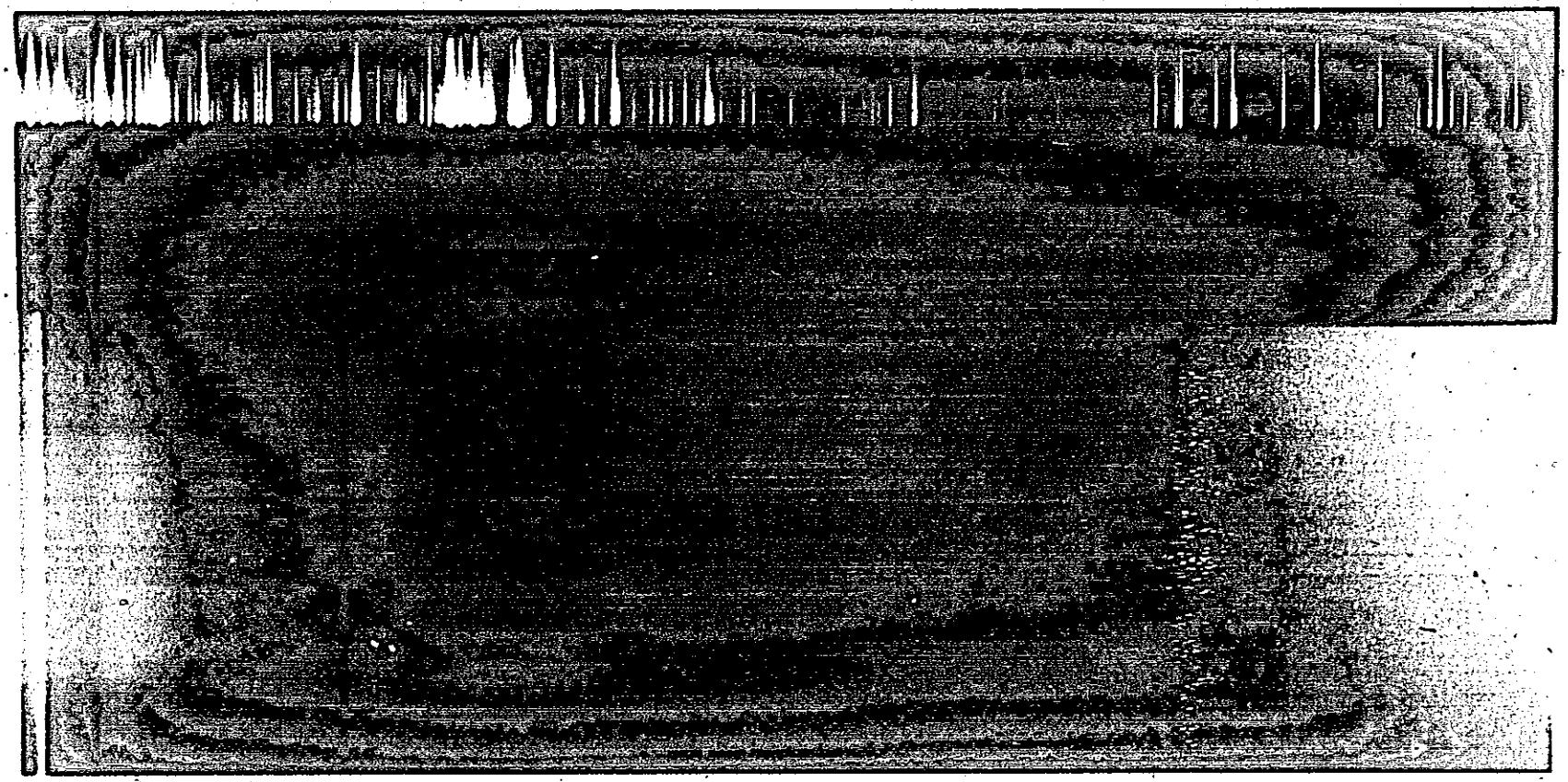

of these progressions. A low resolution spectrogram of a portion of this spectrum is shown in Fig. 5.2.

The strongest bands of the absorption belong to the A and B progressions. The intensity of the r^{th} member of the A progression $I_A^r > I_B^{r-1}$ ($r_{A,B} = n, m, \ldots, n+11, m+11$). The intensity maximum in both the A and B progressions occurs at approximately the same frequency and, in all four progressions, the frequency interval between successive bands was ~450 cm^{-1}. Under low resolution (Cary 14), the results of temperature-dependence studies of absorption intensities were inconclusive; the effect of the increase in temperature on the spectrum was to greatly reduce the sharpness of the observed bands. No temperature-dependence studies were attempted when the absorption was photographed under higher resolution.

5.A.3.2. Analysis

The measured oscillator strength of the absorption (here assumed to correspond to a single electronic transition) is $f \sim 3\times10^{-3}$. This value would seem to preclude a triplet-singlet transition, rendered allowed through spin-orbit coupling, as being responsible for the absorption. The similar f-value (2×10^{-3})[33] of the analogous absorption system (2650 Å - 2000 Å) of the lighter isoelectronic molecule OCS supports the analysis of the system in terms of a singlet-singlet transition.

The singlet states resulting from the electron configuration $\ldots(3\pi)^3(4\pi)$ of linear OCSe are:

$$^1\Delta,\ ^1\Sigma^-\ \text{and}\ ^1\Sigma^+ .$$

The electronic transition $^1\Sigma^+ \leftarrow \tilde{X}\ ^1\Sigma^+$ only is electric dipolar allowed in linear confirmation. According to the Walsh diagram (Fig. 3.2) and the state

energy calculation for the isoelectronic molecule NCS^- (Fig. 3.3), the molecule OCSe should be bent in the electronic states $^1A'$ ($^1\Delta$), $^1A''$ ($^1\Delta$) and $^1A''$ ($^1\Sigma^-$). From the NCS^- calculation, the energy ordering of these states is

$$T_o\{^1A'(^1\Delta'')\} < T_o\{^1A''(^1\Sigma^-)\} < T_o\{^1A''(^1\Delta)\}$$

Some arguments are now presented for an alternative energy ordering of these states. These are:

(i) If the ordering (Hund's Rule) in the linear conformation is

$$T_o\ (^1\Delta) < T_o\ (^1\Sigma^-)\ ,$$

the calculated ordering implies a violation of the "diatomic" non-crossing rule[83] for the two $^1A''$ states. Such violations are rare for polyatomic molecules[84, 85].

(ii) In the lowest energy absorption system of CO_2 (1750 Å - 1400 Å), the excited state in the transition involved in the absorption has been identified[86, 87] as $^1B_2$ ($^1\Delta_u$) (OĈO = 122°).

(iii) In CS_2, the lowest energy absorption systems, observed in the regions 4300 Å - 3300 Å (T_o - 3.25 ev) and 3400 Å - 2900 Å (T_o - 3.7 ev), have been assigned to correspond to the transitions $^3A_2$ ($^2\Delta_u$) ← $\tilde{X}\ ^1\Sigma_g^+$ [88] (f - 2×10^{-4})[33] and $^1A_2$ ($^1\Delta_u$), $^1B_2$ ($^1\Delta_u$) ← $\tilde{X}\ ^1\Sigma_g^+$ [89] (f - 2.7×10^{-4})[33], respectively.

(iv) The $^1A''$ ($^1\Sigma^-$) state is, from (i), (ii) and (iii), expected to be at a higher energy, relative to that of the ground state, than either of the bent conformation components of the $^1\Delta$ state. The $^1A'$ ($^1\Delta$) and $^1A''$ ($^1\Delta$) states are (Renner) components of the $^1\Delta$ state, and their potential surfaces may be represented as in Fig.

3.3. The Renner coupling in the $^1\Delta$ state is, in this case, expected to be strong and the $^1A''$ ($^1\Delta$) state is expected to be the lower-energy component (c.f. Chapter 3, Section 3.2.1.).

The energy ordering of these states, viz.

$$T_o\{^1A''(^1\Delta)\} < T_o\{^1A'(^1\Delta)\}, T_o\{^1A''(^1\Sigma^-)\},$$

is then considered reasonable.

A tentative assignment is now proposed. The excited electronic state involved in the transition responsible for the 2700 Å - 2200 Å absorption system of OCSe is most likely $^1A''$, derived from $^1\Delta$ of the linear conformation. The transition is bent-linear and, by application of the Franck-Condon Principle, activity of ν_2', the excited state bending vibrational motion, is expected. The frequency intervals of ~450 cm^{-1} are therefore assigned as quanta of ν_2'. The alternative assignment, i.e., ν_3' ~ 450 cm^{-1}, requires a decrease of ~30% from the ground ($\tilde{X}$) state ν_3'' frequency (644 cm^{-1}). The ν_3' frequency has been determined in this work to be consistently in the range 500-580 cm^{-1} for higher energy excited states of OCSe.

The rapid decrease in the intensities of bands observed to lower frequencies than 37648 cm^{-1} suggests an electronic origin in this region, as a fairly regular increase in intensity is observed for bands to higher frequencies than this. Bavia, Di Lonardo, Galloni and Trombetti observed some bands of the A and B progressions, and assigned the band of the A progression at ~39034 cm^{-1} as the origin (0_0^0) band of the transition $^1A'$ ($^1\Delta$) or $^1A''$ ($^1\Delta$) $\leftarrow \tilde{X}\ ^1\Sigma^+$. These authors assigned the members of the B progression as $2_0^j\ 3_1^0$, and the band at 38844 cm^{-1} was assigned as the "hot"

band false origin (3_1^0) of the B progression. The results of the present investigation indicate an electronic origin at lower frequencies (<38000 cm^{-1}). However, the vibronic assignment of the members of the A and B progressions as 2_0^k and $2_0^k 3_1^0$, respectively, of the one electronic transition is considered reasonable on the basis of the following evidence:

(i) The appearance of the bands of both progressions is similar.

(ii) The intensity maximum in both progressions occurs in the same region [40806 cm^{-1} (A) and 40598 cm^{-1} (B)].

(iii) The energy separation, $\nu^A_{n+i} - \nu^B_{m+i-1}$ (i = 1,...,10), is close to ν_3'' (644 cm^{-1}).

(iv) If the transition is to an excited state in which the molecule is bent, the intensities of vibronic transitions involving excitation of ν_1', the excited state (essentially) C-O stretching motion, are expected to be low. Also, if ν_1' were excited in progression A or B; the energies of the (A and B) members of maximum intensity should be different by an amount roughly corresponding to the ν_1' frequency. The observed difference (~200 cm^{-1}) is considered too small to allow an assignment involving ν_1' (ν_1'' = 2027 cm^{-1}).

(v) The frequency intervals in both the A and B progressions decrease from ~460 cm^{-1} to ~390 cm^{-1} towards higher frequencies. These intervals are similar, within measurement accuracy limits (estd. ±30 cm^{-1}) for corresponding progression members, i.e., for the members n+i (A) and m+i-1 (B) (i = 1,...,10).

The possibility that two electronic transitions are involved cannot be discounted. The members of progressions C and D could not be assigned as vibronic components of the $^1A''$ ($^1\Delta$) ← $\tilde{X}$ $^1\Sigma^+$ transition from the present

data. As the higher energy Renner component, $^1A'$ ($^1\Delta$), should be close in energy to the $^1A''$ ($^1\Delta$) state, the C and D progression members may correspond to vibronic transitions to this $^1A'$ ($^1\Delta$) state. Breckenridge and Taube[82] have suggested that, in the analogous absorption system of OCSe, two or more electronic transitions are involved.

The Bond Angle in the $^1A''$ ($^1\Delta$) State

It was not possible to carry out Franck-Condon Effect calculations to determine the difference in molecular geometry between the ground and excited states, as the overlap integrals (c.f. Equation [1.16]) cannot be calculated when the exact analytical forms of the eigenfunctions in the combining states are unknown. However, Dressler and Ramsay[90] have given an approximate method for calculating the change in bond angle between electronic states involved in a transition. In this method, the equation

$$\frac{1}{2} k_\delta' (\Delta\theta)^2 = \Delta E \qquad [5.1]$$

is used, where

$\Delta\theta$ is the difference in bond angle,

k_δ' is the force constant for the bending vibrational motion in the excited state of the transition, and

ΔE is the energy difference between the origin band and the bands of maximum absorption intensity.

This method may be applied to the $^1A''$ ($^1\Delta$) $\leftarrow$ $^1\Sigma^+$ transition by assuming that

(i) the energy of the origin band is ~37600 cm^{-1}, and

(ii) in view of the small frequency change for ν_2 upon electronic excitation, k_δ' may be approximated to the ground state bending

mode force constant k''_δ (2.769×10^4 cm^{-1}/rad.)[18]. Hence

ΔE - 3100 cm^{-1}

and $\Delta\theta$ - 473 radians (~27°),

which gives the OCSe bond angle of the molecule in the $^1A''$ ($^1\Delta$) state as 153°.

Effects due to "quasilinearity"[91, 92, 93] or to "axis-switching"[94] could not be observed in the spectrum, although

(i) for OCSe bond angles of 150°-180°, the value of the rotational constant (A) for rotational motion about the top (a) axis is a sensitive function of the OCSe angle ($A_{153°}^{(calc.)}$ = 17.5 cm^{-1}; ground ($\tilde{X}$) state bond lengths assumed);

(ii) the equilibrium axis-switching angle[94] at an OCSe bond angle of 153° is calculated to be ~8.9° (ground (X) state bond lengths assumed).

The absence of quasi-linear effects in the spectrum, i.e., where the intervals between the vibrational levels associated with the bending of the bent molecule show a minimum at an energy corresponding approximately to that required to straighten the molecule, is taken to indicate that the height of the potential barrier to linearity is large (>3000 cm^{-1}).

5.A.4. Description and Analysis of the 2150 Å - 1820 Å Absorption System of OCSe

5.A.4.1. Description

A banded absorption system of OCSe occurs in the 2150 Å - 1820 Å region, which is much stronger than that in the 2500 Å region. This system has been previously reported by Strausz, Tyerman and Gunning[11] and by Bavia, Di Lonardo, Galloni and Trombetti[12].

The bands of this system were photographed under high resolution (Eagle instrument). All appear very diffuse. Temperature-dependence studies of absorption intensities proved inconclusive.* The bands were assigned to a single progression with frequency interval of 480 cm^{-1} decreasing to 370 cm^{-1} towards higher frequencies. A spectrophotometer (McPherson) trace of this absorption system is reproduced in Fig. 5.3. The measured frequencies and relative intensities of the observed bands are given in Table 5.5. The bands of $OCSe^{80}$ appear equally diffuse as those of $OCSe^{nat}$, and a strong absorption continuum underlies the banded absorption (see Fig. 5.3). Accordingly, the genuine diffuseness of these bands is attributed to (case I) predissociation by electronic transition.

5.A.4.2. Analysis

The vibrational analysis of this absorption is incomplete, as no electronic origin band could be assigned in confidence. The oscillator strength value calculated for this absorption system is 0.8×10^{-2}. A larger oscillator strength value (7×10^{-2}) is reported[33] for the corresponding (1875 Å - 1625 Å) absorption system of OCS. The electronic transition corresponding to the banded absorption is therefore most likely of the type singlet-singlet.

A discussion of the energy ordering of the singlet electronic states arising from the excited electron configuration of OCSe, $\ldots(3\pi)^3(4\pi)$, has been given in Section 5.A.3. The ordering considered most reasonable was

---

*Some difficulty was encountered when recording this absorption with $OCSe^{80}$, as trace quantities of CS_2 were present in the sample. The absorption bands of CS_2 in this region were photographed under high resolution. The measured frequencies and relative intensities of these bands are given in Appendix A.3.

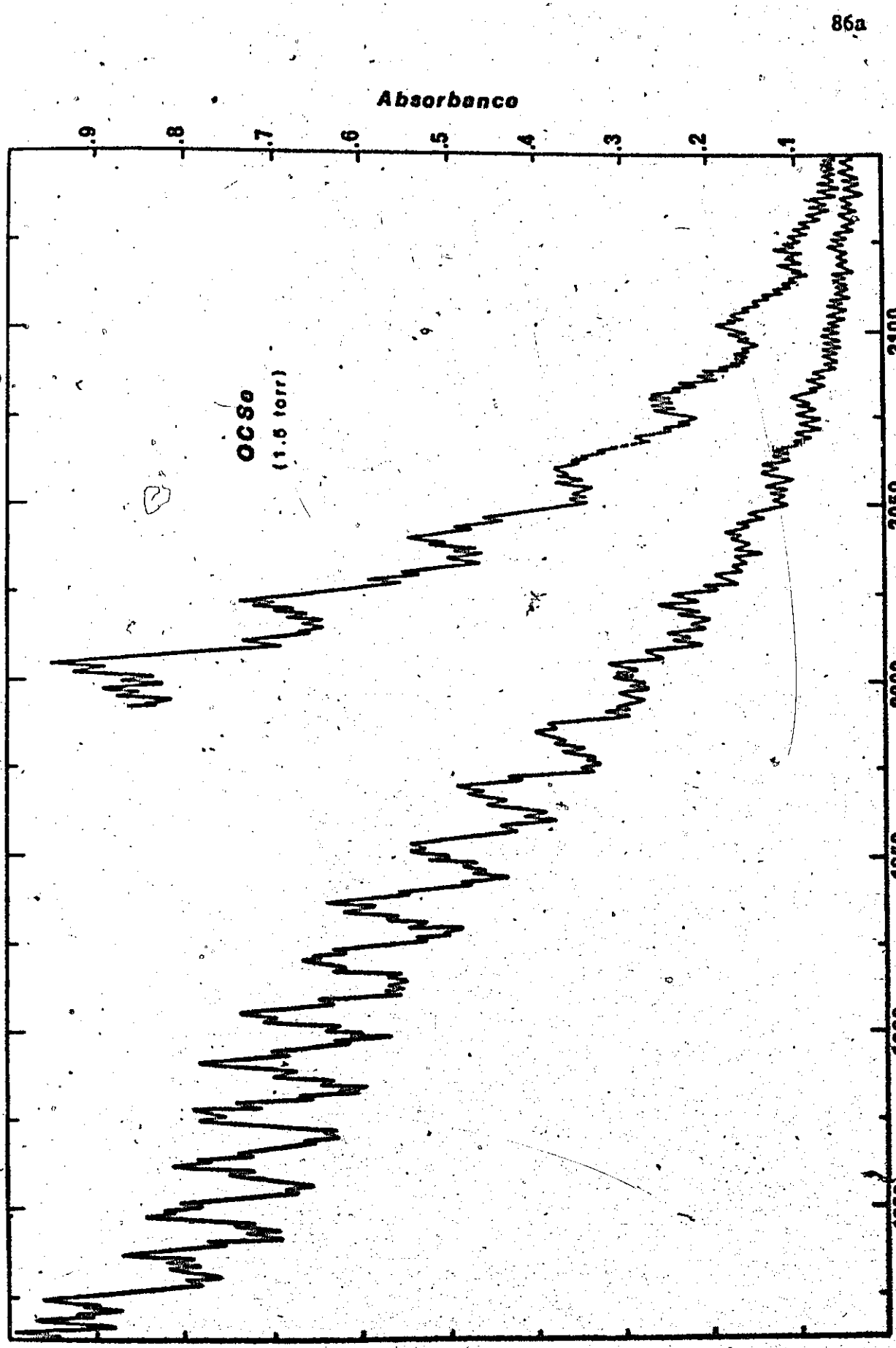

Fig. 5.3. Low resolution absorption spectrum of OCSe in the 1810 Å - 2150 Å region.

TABLE 5.5

MEASURED BANDS OF $OCSe^{nat}$ IN THE 46650 cm^{-1} (2143.6 Å) - 54800 cm^{-1} (1824.8 Å) REGION

Band Frequency* (cm^{-1})	$\nu_{m+i+1} - \nu_{m+i}$ in cm^{-1} (i=0,...,18)	Relative Intensity**	Assignment[a] (Progression number)
46680			
	414	0.28	m
47094			
	491	0.43	m+1
47585			
	487	0.61	m+2
48072			
	467	1.00	m+3
48539			
	461	1.45	m+4
49000			
		1.80	m+5
49121	444	w	not assigned
49444		2.50	m+6
49670	442	w	not assigned
49886		3.10	m+7
50078	451	w	not assigned
50337			
	435	4.00	m+8
50772			
	429	4.90	m+9
51201			
	412	5.40	m+10
51613			
	424	6.40	m+11
52037			
	423	6.70	m+12
52460			
	396	7.35	m+13
52856			
	419	8.85	m+14
53275			
	390	8.95	m+15
53665			
	383	9.15	m+16
54048			
	374	9.40	m+17
54422			
	364	9.70	m+18
54786		10.10	m+19

*Vacuum wavenumbers (cm^{-1}). Estimated measurement accuracy: ±30 cm^{-1}.

**Values are absorbance ratios, i.e., Log I_o/I_A / Log I_o/I_B. B is chosen as the band at 48072 cm^{-1}.

[a]See text.

$$T_o\{^1A''(^1\Delta)\} < T_o\{^1A'(^1\Delta)\},\ T_o\{^1A''(^1\Sigma^-)\} < T_o\{^1\Sigma^+\}$$

The molecule is expected to be linear in the $^1\Sigma^+$ state only of this configuration and in both the $^1\Pi$ and $^3\Pi$ states of the electron configuration $\ldots(3\pi)^3(10\sigma)$ (c.f. Chapter III, Section 3.1.6).

The assignment of this absorption system to the bent-linear transition $^1A''(^1\Sigma^-) \leftarrow \tilde{X}\ ^1\Sigma^+$ is then considered reasonable on the following grounds:

(i) The Franck-Condon intensity distribution among the nineteen members of the progression indicates a large change in geometry.

(ii) The frequency intervals (~480 cm^{-1} - ~370 cm^{-1}) between progression members are similar to those of the 2700 Å - 2200 Å OCSe absorption, where they were assigned to ν_2' (c.f. section 5.A.3.). A similar assignment in this case is considered reasonable. The long progression in ν_2' is consistent with the assignment of a bent conformation excited state.

(iii) In the corresponding (1875 Å - 1625 Å) absorption system of OCS, the frequency intervals between progression members* are reported[32] to be in the range ~560 cm^{-1} to ~500 cm^{-1}. These intervals were assigned to ν_2' ($\nu_{2_{OCS}}'' \sim 520\ cm^{-1}$). A calculation of $\Delta\theta$ (c.f. Equation [5.1]) for this absorption system gives an excited state bond angle of 143° ($\Delta E \sim 7000\ cm^{-1}$ [32], $k_\delta'' = 3.31\times10^4\ cm^{-1}/rad$[18]).

(iv) Where the origin band (0_0^0) energy of the OCSe absorption is taken to be ~46700 cm^{-1} (Bavia, Di Lonardo, Galloni and Trombetti have assigned

*Some bands of this system were photographed in this work. The bands are slightly diffuse and red-degraded, and the frequency intervals between progression members are in the reported range[32] (~560 cm^{-1} - ~500 cm^{-1}).

the origin band at 47055 cm^{-1}), ΔE is ~8100 cm^{-1} and $\Delta\theta$ is ~.765 radians (~44°). This calculation gives a bond angle in the $^1A''(^1\Sigma^-)$ state of ~136°. The absence of quasi-linear effects in the spectrum indicates a potential "barrier" to linearity of >8000 cm^{-1} (c.f. Dixon[91]). If the analysis of the excited state $\{^1A''(^1\Delta)\}$ in the 2700 Å - 2200 Å OCSe absorption system is correct, the relative magnitudes of the potential barriers to linearity in the transitions corresponding to these (2700 Å - 2200 Å and 2150 Å - 1820 Å) OCSe absorption systems (>3000 cm^{-1} and >8000 cm^{-1}, respectively) precludes the assignment of the latter absorption system as corresponding to the transition to the higher energy Renner component $^1A'(^1\Delta)$.

(v) The presence of a close-lying $^1A''(^1\Sigma^-)$ state is consistent with the analysis of the 2700 Å - 2200 Å OCSe absorption system (c.f. Section 5.A.3. and Chapter 3, Section 3.2.1.) and with the predicted (c.f. Fig. 3.3) non-linearity of the molecule in this state.

5.A.5. Description and Analysis of the 1820 Å - 1610 Å Absorption System of OCSe

5.A.5.1. Description

A very strong, banded absorption system of OCSe, much stronger than the lower frequency absorptions previously discussed, occurs in the 1820 Å - 1610 Å region. A low-resolution (McPherson monochromator) trace of this absorption is reproduced in Fig. 5.4. Spectra of the species $OCSe^{80}$ and $OCSe^{78}$ were recorded under the high resolution of the Eagle vacuum instrument. The following absorption features were observed:

(i) a series of strong sharp-headed red-degraded bands (1820 Å - 1711 Å);

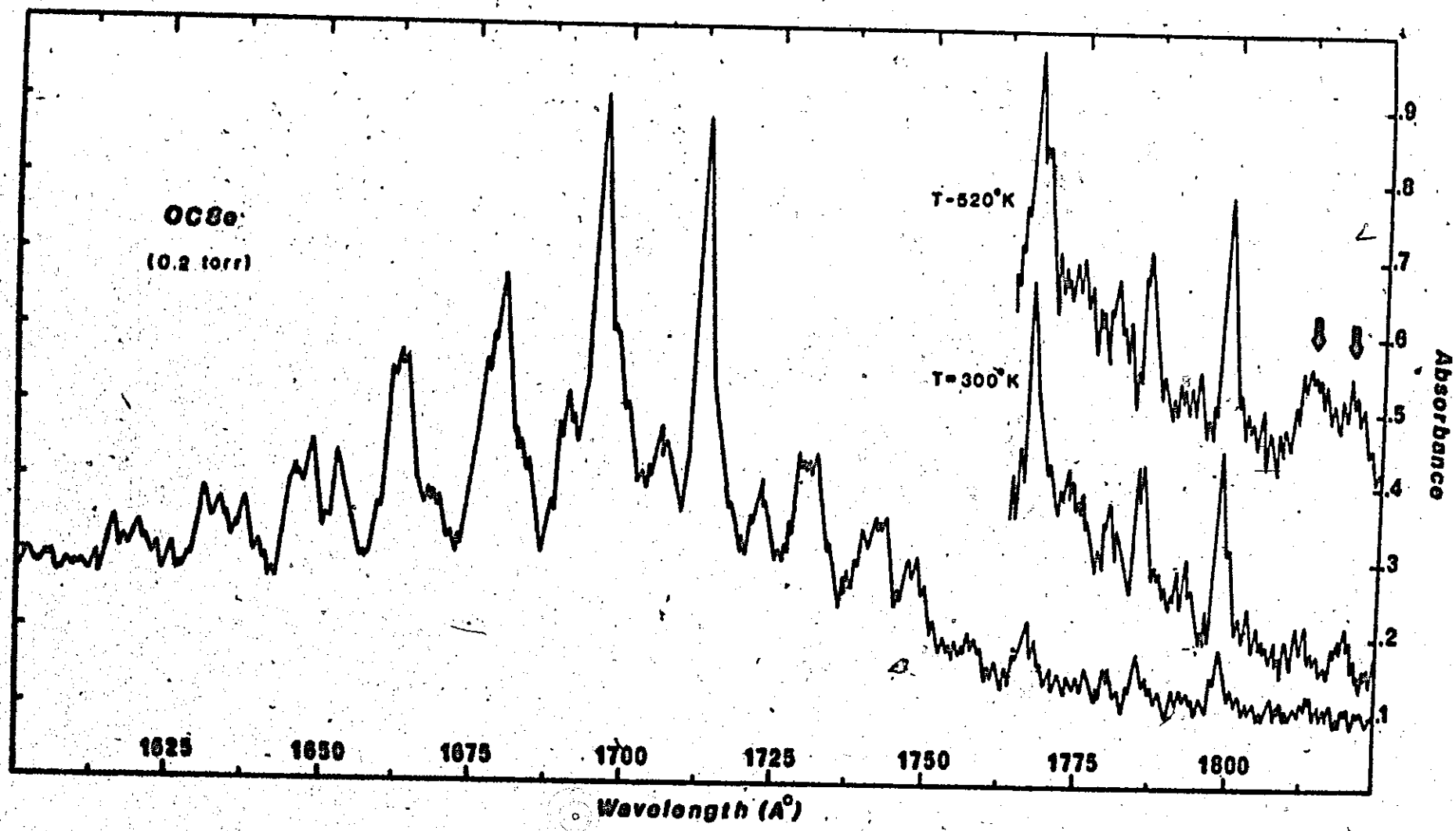

Fig. 5.4. Low resolution absorption spectrum of OCSe in the 1600 Å - 1825 Å region.

FIG 5.5 Spectrogram of a Portion of the 1600 Å - 1825 Å Absorption System of OCSe.

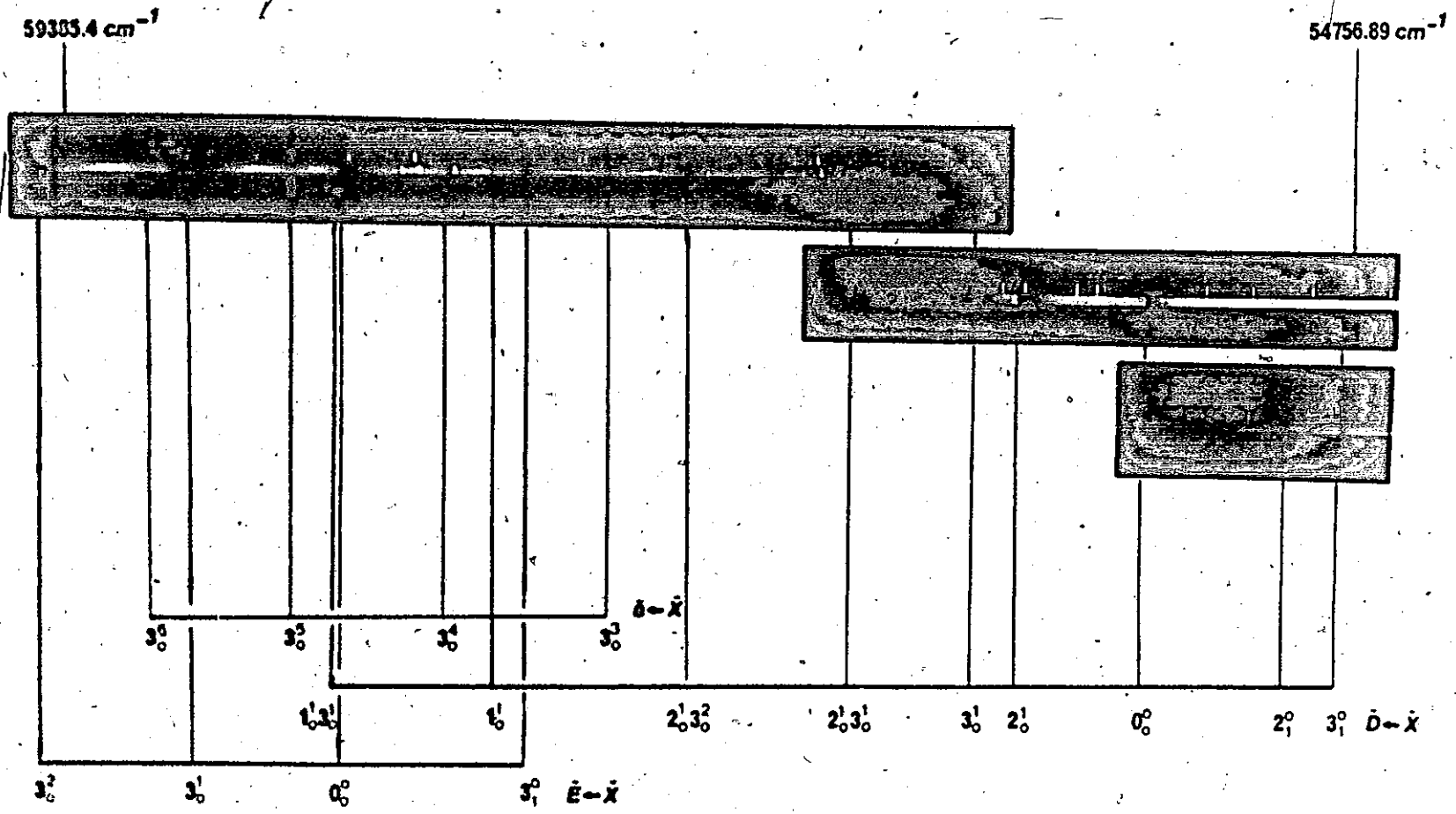
59383.4 cm⁻¹
54756.89 cm⁻¹
δ–X
3⁰₀ 3³₀ 3⁴₀ 3³₀
1¹₀3¹₀ 1¹₀ 2¹₀3²₀ 2¹₀3¹₀ 3¹₀ 2¹₀ 0⁰₀ 2⁰₁ 3⁰₁ D–X
3²₀ 3¹₀ 0⁰₀ 3⁰₁ E–X

(ii) a series of moderately strong, very diffuse bands (1793 Å - 1691 Å);

(iii) a short series of very weak, slightly diffuse, red-degraded bands (~1791 Å); and

(iv) a series of very strong very diffuse bands (1714 Å - 1610 Å).

The vacuum frequencies, isotope shifts, appearances, relative intensities and assignments of the bands of this system are given in Table 5.6, and a portion of the spectrum, photographed under high resolution, is reproduced in Fig. 3.5. No rotational fine structure could be resolved in any of the bands.

5.A.5.2. Analysis

The strong, sharp-headed, red-degraded series of bands observed in the 1820 Å - 1711 Å region of the OCSe absorption spectrum are assigned to vibronic components of the singlet-singlet, linear-linear intravalence shell transition, $\tilde{D}\ ^1\Sigma^+ \leftarrow \tilde{X}\ ^1\Sigma^+$. The following evidence is presented for these assignments.

The measured oscillator strength value of this transition is 1.0×10^{-2}. Accordingly, the analysis is in terms of an allowed singlet-singlet transition.

The intensities of the bands to the low-frequency (red) side of the first strong band at 55595.7 cm^{-1} (80) increase when the gas is heated (cf. Fig. 5.4). These bands, of which the most prominent are at 54951.2 cm^{-1} (80) and 55131.6 cm^{-1} (80), are weak and are observed only at increased pressures of the absorbing gas. The frequencies (55595.7 cm^{-1} - 54951.2 cm^{-1}) = 644.5 cm^{-1} and (55595.7 cm^{-1} - 55131.6 cm^{-1}) = 464.1 cm^{-1} have been observed in the infrared spectrum of OCSe, where they were assigned to ν_3'' and ν_2'', res-

TABLE 5.6

Measured Bands of OCSe in the 54950 cm^{-1} (1819.8 Å) - 63800 cm^{-1} (1567.4 Å) Region

Band Frequency* $OCSe^{80}$	Band Frequency* $OCSe^{78}$	Isotope Shift $\nu_{78}-\nu_{80}$ in cm^{-1}	Description**	Relative Intensity[a]	Assignment Electronic	Assignment Vibronic
54951.2	54949.4	-1.8	sh.,r.d.	$\{^{0.28}_{0.43}$ (298°K) (~540°K)	$\tilde{D} \leftarrow \tilde{X}$	3_1^0
55131.6	55131.7	+0.1	sh.,r.d.	$\{^{0.25}_{0.52}$ (298°K) (~540°K)	$\tilde{D} \leftarrow \tilde{X}$	2_1^0
55379.8			sh.,r.d.	w	$\tilde{D} \leftarrow \tilde{X}$	$2_0^1 3_1^0$
55426.1			sh.,r.d.	vvw	$\tilde{D} \leftarrow \tilde{X}$	3_2^2?
55520.2	55518.5	-1.7	ov.,r.d.	w	$\tilde{D} \leftarrow \tilde{X}$	3_1^1
55540.2			ov.,r.d.	vw	$\tilde{D} \leftarrow \tilde{X}$	2_2^2?
55558.6			ov.,r.d.	w	$\tilde{D} \leftarrow \tilde{X}$	2_1^1
55595.7	55595.4	-0.3	sh.,r.d.	1.00	$\tilde{D} \leftarrow \tilde{X}$	0_0^0 $(^1\Sigma^+ \leftarrow {}^1\Sigma^+)$
55708			r.d.	w	$\tilde{D} \leftarrow \tilde{X}$	$2_1^0 3_0^1$
55757			dif.	0.4	$\tilde{a} \leftarrow \tilde{X}$	0_0^0 $(^3\Pi_{(1)} \leftarrow {}^1\Sigma^+)$
55832			sl.dif.,r.d.	vvw	$\tilde{b} \leftarrow \tilde{X}$	0_0^0? $(^3\Pi_{(0^+)} \leftarrow {}^1\Sigma^+)$
55989.2			ov.,r.d.	w	$\tilde{D} \leftarrow \tilde{X}$	2_1^2
56021.2	56023.4	+2.2	sh.,r.d.	0.83	$\tilde{D} \leftarrow \tilde{X}$	2_0^1
56083.3			ov.,r.d.	w	$\tilde{D} \leftarrow \tilde{X}$	3_1^2

TABLE 5.6 (cont'd.)

Band Frequency* $OCSe^{80}$	Band Frequency* $OCSe^{78}$	Isotope Shift $\nu_{78}-\nu_{80}$ in cm^{-1}	Description**	Relative Intensity[a]	Assignment Electronic	Assignment Vibronic
56116.5			ov.,r.d.	vw	$\tilde{D} \leftarrow \tilde{X}$	$2_2^2 3_0^1$
56165.2	56168.2	+3.0	sh.,r.d.	0.87	$\tilde{D} \leftarrow \tilde{X}$	3_0^1
56303			dif.	0.6	$\tilde{a} \leftarrow \tilde{X}$	3_0^1
56391			sl. dif.,r.d.	vvw	$\tilde{b} \leftarrow \tilde{X}$	3_0^1
56555.3			ov.,r.d.	w	$\tilde{D} \leftarrow \tilde{X}$	$2_1^2 3_0^1$
56588.8	56593.9	+5.1	sh.,r.d.	1.40	$\tilde{D} \leftarrow \tilde{X}$	$2_0^1 3_0^1$
56845			dif.	1.2	$\tilde{a} \leftarrow \tilde{X}$	3_0^2
56877			sl. dif.,r.d.	vvw	$\tilde{D} \leftarrow \tilde{X}$	2_0^3
57155.1	57161.8	+6.7	sl. dif.,r.d.	1.0	$\tilde{D} \leftarrow \tilde{X}$	$2_0^1 3_0^2$
57265.3	57266.0	+0.7	sh.,r.d.	0.8	$\tilde{D} \leftarrow \tilde{X}$	1_0^1
57403.5			dif.	2.0	$\tilde{a} \leftarrow \tilde{X}$	3_0^3
(57721)	57731.3	(+10.3)	ov.	0.6	$\tilde{D} \leftarrow \tilde{X}$	$2_0^1 3_0^3$
(57721)	57721		ov.,dif.	1.6	$\tilde{E} \leftarrow \tilde{X}$	3_1^0
57838.8	57844.3	+5.5	sh.,r.d.	0.6	$\tilde{D} \leftarrow \tilde{X}$	$1_0^1 3_0^1$
57977			dif.	1.3	$\tilde{a} \leftarrow \tilde{X}$	3_0^4
58283			dif.	w	$\tilde{E} \leftarrow \tilde{X}$	3_1^1
58325			dif.	w	$\tilde{E} \leftarrow \tilde{X}$	2_1^1

TABLE 5.6 (cont'd.)

Band Frequency* $OCSe^{80}$	Band Frequency* $OCSe^{78}$	Isotope Shift $\nu_{78}-\nu_{80}$ in cm^{-1}	Description**	Relative Intensity[a]	Assignment Electronic	Assignment Vibronic
58367			dif.	6.6	$\tilde{E} \leftarrow \tilde{X}$ 0_0^0	$(^1\Pi_{(1)} \leftarrow {}^1\Sigma^+)$
58415.7			sh.,r.d.	0.4	$\tilde{D} \leftarrow \tilde{X}$ $1_0^1 3_0^2$	
58551			dif.	1.0	$\tilde{a} \leftarrow \tilde{X}$ 3_0^5	
58850			dif.	w	$\tilde{E} \leftarrow \tilde{X}$ 3_1^2	
58935			dif.	7.0	$\tilde{E} \leftarrow \tilde{X}$ 3_0^1	
59119			dif.	w	$\tilde{a} \leftarrow \tilde{X}$ 3_0^6	
59489			dif.	4.3	$\tilde{E} \leftarrow \tilde{X}$ 3_0^2	
60062			dif.	2.5	$\tilde{E} \leftarrow \tilde{X}$ 3_0^3	
60147			dif.	2.0	$\tilde{E} \leftarrow \tilde{X}$ 1_0^1	
(60608)[c]			dif.,r.d.?	1.4	$\tilde{E} \leftarrow \tilde{X}$ 3_0^4	
(60710)[c]			dif.	1.8	$\tilde{E} \leftarrow \tilde{X}$ $1_0^1 3_0^1$	
(61222)[c]			dif.	0.8	$\tilde{E} \leftarrow \tilde{X}$ 3_0^5	
(61302)[c]			dif.,r.d.?	1.1	$\tilde{E} \leftarrow \tilde{X}$ $1_0^1 3_0^2$	
61850			dif.,r.d.?	0.7	$\tilde{E} \leftarrow \tilde{X}$ $1_0^1 6_0^3$	

*Vacuum wavenumbers (cm^{-1}). For sharp-headed bands, the measured frequency (estimated accuracy ± 2 cm^{-1}) is ν_{Head}. For diffuse bands, the measured frequency (estimated accuracy ± 15 cm^{-1}) is that of the absorption intensity maximum of the band.

TABLE 5.6 (cont'd.)

**sh. = sharp-headed; r.d. = red-degraded; sl. dif. = slightly diffuse; ov. = overlapped.

[a]Values quoted are absorbance ratios, i.e., Log I_o/I_A / Log I_o/I_B. B is chosen as the absorption band at 55595.7 cm^{-1}.

[c]Overlapped by source emission feature at ~1640.4 Å (HeII).

pectively (cf. Section 5.A.1.). The vibronic assignments 0_0^0 (55595.7 cm^{-1}), 2_1^0 (55131.6 cm^{-1}) and 3_1^0 (54951.2 cm^{-1}) are then considered reasonable. The negligible isotope shift (-0.3 cm^{-1}) for the 55595.7 cm^{-1} band supports the 0_0^0 assignment for this band.

Some arguments may be presented for this assignment of a linear $\tilde{D}$ state. These are:

(i) The intensity distribution among the bands assigned to vibronic components of this transition indicates that the molecular geometry in $\tilde{D}$ is little changed from that in the ground ($\tilde{X}$) state. The strongest bands (cf. Table 5.6) are those assigned to 0_0^0, 2_0^1, 3_0^1, $2_0^1 3_0^1$ and 1_0^1. All others are comparatively weak, especially those to the low-frequency side of the 0_0^0 band.

(ii) By application of the Franck-Condon principle, activity of ν_2', the excited state bending vibrational motion, is expected if the molecule is bent in the $\tilde{D}$ state. No long progression in ν_2' is observed. Indeed, while the band assigned to 2_0^1 is strong and that assigned 2_0^3 is very weak, a band corresponding to 2_0^2 is not observed, although the latter component is allowed in both linear and bent conformations.

(iii) For the parallel bent-linear electronic transitions $^1A'(^1\Sigma^+) \leftarrow \tilde{X}\,^1\Sigma^+$, the 0_0^0 and 2_1^0 bands should be separated in energy by $\nu_2'' - \{A - \frac{1}{2}(B + C)\}$, where A, B and C are the excited state rotational constants. For OCSe bond angles in the range 146° - 179°, the molecule OCSe is almost an accidental prolate symmetric top(i.e., A >> B ≈ C). A is calculated to be in the range of 11.2 cm^{-1} (146°) - ~10^4 cm^{-1} (179°), while B and C are both calculated to be ~.13 cm^{-1} for all bond angles in this range. Although ground state bond lengths were used in these calculations, small

changes in these distances affect these values only slightly. Because the frequency interval $\nu(0_0^0) - \nu(2_1^0)$ is, within measurement accuracy limits, exactly ν_2'', the molecule is highly unlikely to be bent in the excited state $\tilde{D}$. The assignment $\tilde{D}(^1A'')$ may also be excluded on the basis of a similar argument.(95)

If the molecule is linear in the excited state $\tilde{D}(^1\Sigma_u^+)$, the vibronic transition 2_1^0 is forbidden by the selection rules derived through application of the Born-Oppenheimer approximation (cf. Chapter 1, Section 1.3.). The observation of the band assigned 2_1^0 may be explained in terms of Herzberg-Teller vibronic coupling. The ground state ($\tilde{X}\ ^1\Sigma^+$) eigenfunction is mixed with the eigenfunction of an excited state of Π symmetry through excitation of $\nu_2''(\pi)$ in $\tilde{X}$ (cf. Chapter 3, Section 3.2.2.).

The strong bands at 56021.2 cm^{-1} (80), 56165.2 cm^{-1} (80), 56588.8 cm^{-1} (80), 57155.1 cm^{-1} (80) and 57721 cm^{-1} (80) are assigned to 2_0^1, 3_0^1, $2_0^1 3_0^1$ and $2_0^1 3_0^2$, respectively. From these assignments, $\nu_2'(80) = 425.5\ cm^{-1}$ and $\nu_3'(80) = 569.5\ cm^{-1}$. Bavia, Di Lonardo, Galloni and Trombetti( ) analyzed the bands at 55595.7 cm^{-1} and 56021.2 cm^{-1} as the origin bands of two electronic transitions. However, the observation of the bands assigned to 2_1^1 (at 55558.6 cm^{-1}(80)) and 3_1^1 (at 55520.2 cm^{-1}(80)) and the similar ν_3' intervals from 0_0^0 and 2_0^1 (569.5 cm^{-1} and 567.6 cm^{-1}) support the analysis presented here.

The vibrational isotope shifts, $(\nu_{78}-\nu_{80})$, for bands in the $2_0^1 3_0^n$ progression, indicate a shift of $\sim +3\ cm^{-1}$/quantum of ν_3'. This shift is in

good agreement with that calculated for quanta of ν_3'' (cf. Section 5.A.2.). Although small, the isotope shift for the band assigned to $2_0^1 3_0^1$ (+6.7 cm^{-1}) is outside the estimated measurement accuracy limits (±4 cm^{-1}) and was quite obvious when photographic enlargements of the ($OCSe^{78}$ and $OCSe^{80}$) spectra were compared.

In the assignment, $\nu_1''(80) = 1669.6\ cm^{-1}$. The negligible vibrational isotope shift (+0.7 cm^{-1}) for the band assigned to 1_0^1 supports this assignment. Excitation of the totally symmetric stretching vibrational motions ν_1' and ν_3' in $\tilde{D}$ is consistent with the assignment of the transition $\tilde{D} \leftarrow \tilde{X}$ to a linear-linear transition.

The false origin band assigned to 2_0^1 (56021.2 cm^{-1}(80)) is a forbidden vibronic component of $\tilde{D} \leftarrow \tilde{X}$, and a Herzberg-Teller vibronic coupling mechanism is invoked to account for its intensity. Under the $C_{\infty v}$ point group, the linear-linear singlet-singlet transitions (from $\tilde{X}$) $^1\Pi \leftarrow \tilde{X}\ ^1\Sigma^+$ and $^1\Sigma^+ \leftarrow \tilde{X}\ ^1\Sigma^+$ only are electric dipolar allowed. The very strong diffuse bands observed in the OCSe spectrum in the region 1714 Å - 1610 Å are assigned to vibronic components of the allowed $\tilde{E}\ ^1\Pi_{(1)} \leftarrow \tilde{X}\ ^1\Sigma^+$ transition. Intensity "borrowing" from this transition is considered a reasonable mechanism whereby the intensity of the $2_0^1 3_0^n$ components of the $\tilde{D} \leftarrow \tilde{X}$ transition may be explained. The assignment of $\tilde{D}$ as being of $^1\Sigma^+$ symmetry follows from the discussion of Chapter 3, Section 3.2.2. because the normal vibration ν_2' in $\tilde{D}$ is of π symmetry.

The structure of the 0_0^0, 3_0^1 and $1_0 3_0^n$ bands should then be different from that in bands assigned $2_0^1 3^n$. (The vibronic transitions $\Sigma^+ \leftarrow \Sigma^+$ and $\Pi \leftarrow \Sigma^+$ are polarized $\parallel$ and $\perp$, respectively.) Since no rotational fine structure could be resolved in any of these bands, a band contour analysis

was not attempted. Also, the bands assigned $2_0^1 3_0^n$ appear very slightly diffuse. This diffuseness is attributed to (Case I) predissociation.

The $\tilde{D}\ ^1\Sigma^+$ state most probably arises from the electron configuration $\ldots(3\pi)^3(4\pi)$. In Section 5.A.3., where the relative energies of the singlet states arising from this configuration were discussed, the $^1\Sigma^+$ state was predicted to lie at slightly higher energies than the $^1A''(^1\Sigma^-)$ and $^1A''(^1\Delta)$ and $^1A'(^1\Delta)$ states. Also, OCSe was predicted to be linear in the $^1\Sigma^+$ state (cf. Table 3.1) from a consideration of the Walsh diagram for ABC-type molecules and from the calculations reported for NCS^- (cf. Fig. 3.3). The assignment $\tilde{D}(^1\Sigma^+)$ is therefore considered reasonable.

The very strong very diffuse series of bands observed in the 1714 Å - 1610 Å region are assigned to correspond to vibronic components of a separate electronic transition viz. $\tilde{E}\ ^1\Pi_{(1)} \leftarrow \tilde{X}\ ^1\Sigma^+$. Vibrational isotope shifts were not determined for these bands, as the estimated measurement accuracy was $\pm 15\ cm^{-1}$. The measured oscillator strength value of this transition is $S \times 10^{-2}$. The bands are the strongest observed in the U.V. and V.U.V. absorption spectrum of OCSe ($\epsilon_{max} \sim 3.8 \times 10^3$ litre $mole^{-1} cm^{-1}$).

The first (lowest energy) strong band observed in this region (at 58367 cm^{-1}) is assigned to the origin (0_0^0) of the $\tilde{E} \leftarrow \tilde{X}$ transition. The weak diffuse band at $(E(0_0^0) - 646)\ cm^{-1} = 57721\ cm^{-1}$ is accordingly assigned 3_1^0. (Temperature-dependence studies of the intensity of this band were inconclusive.)

The vibrational analysis of the bands (cf. Table 5.6) yields, for the $\tilde{E}$ state,

$$\nu' = 1780\ cm^{-1}$$

$$\nu_2' = 422\ cm^{-1}$$

and $$\nu_3' = 568\ cm^{-1}.$$

These values are similar to those obtained from the analysis of the bands of the $\tilde{D} \leftarrow \tilde{X}$ transition, where the similarity of the calculated and observed vibrational isotope shifts allowed an unambiguous assignment of the excited state vibrational frequencies. Although the $\tilde{E}\ ^1\Pi_{(1)}$ and $\tilde{D}\ ^1\Sigma^+$ states must arise from different electron configurations, the similarity of the vibrational frequencies in $\tilde{D}$ and $\tilde{E}$ is not unexpected in view of the (postulated) mixing of the eigenfunctions of these states through the Herzberg-Teller vibronic coupling mechanism.

The Franck-Condon intensity distribution among the vibronic components of the $\tilde{E} \leftarrow \tilde{X}$ transition indicates a small change in molecular geometry in $\tilde{E}$ from that in $\tilde{X}$. Excitation of the totally symmetric vibrational motions ν_1' and ν_3' in $\tilde{E}$ is consistent with the assignment of a linear excited state in the transition.

The moderately strong diffuse absorption bands of OCSe observed in the 1793 Å - 1691 Å region are assigned to the linear-linear electronic transition $\tilde{a}\ ^3\Pi_{(1)} \leftarrow \tilde{X}\ ^1\Sigma^+$. The measured oscillator strength of this transition is 1.7×10^{-2}. The bands assigned to vibronic components of this transition form a progression in which the frequency interval is ~546 cm^{-1}. This interval is assigned to ν_3'. At higher pressures of the absorbing gas, no further bands of this progression could be observed at frequencies < 55757 cm^{-1}. The first member of this progression (at 55757 cm^{-1}) is therefore assigned to the origin band (0_0^0). The diffuseness of the bands is attributed to (Case I) predissociation.

Two very weak, slightly diffuse, red-degraded bands were also observed in the region of the $\tilde{a} \leftarrow \tilde{X}$ origin band. They were observed only at higher pressures (~5 torr OCSe in an absorbing path of 75 cm). They could not be

assigned to vibronic components of any of the previously mentioned transitions. Their frequency interval, 559 cm^{-1}, is assigned to ν_3' in the upper state $\tilde{b}$ of the transition $\tilde{b}\ ^3\Pi_{(0^+)} \leftarrow \tilde{X}$, and the first of these bands, at 55832 cm^{-1}, is tentatively assigned as the origin band of this transition. These features may be bands of a sample impurity. However, a check of the known spectra of the possible impurities CS_2, CSe_2, H_2Se, CO_2 and H_2O revealed no such features at these frequencies.

In the preceeding discussion the $\tilde{a}$, $\tilde{b}$ and $\tilde{E}$ states have been assigned to $^3\Pi_{(1)}$, $^3\Pi_{(0^+)}$ and $^1\Pi_{(1)}$, respectively. The quantity in brackets is the value of the quantum number Ω (cf. Chapter 3, Section 3.3.3.). Arguments are now presented which support these assignments, and which indicate that all of these states arise from the electron configuration $\ldots(3\pi)^3_{core}(2s\sigma)_{Ryd.}$, for which the spin-orbit coupling is intermediate in strength between (Λ,s) and (Ω_c,w) coupling (cf. Fig. 3.5). These are:

(i) As has been previously stated, the bands assigned to $\tilde{E} \leftarrow \tilde{X}$ are by far the strongest observed in the absorption spectrum of OCSe (ϵ_{max} - 3.8×10^3 litre $mole^{-1}cm^{-1}$). The results of Bavia, DiLonardo, Galloni and Trombetti[12] confirm this observation. Of the absorption features which occur in molecular spectroscopy of the U.V. and V.U.V. regions, those which correspond to molecular Rydberg transitions are known to be the most intense. Also, in a given Rydberg series, the first member is, in general, the most intense (cf. Chapter 3, Section 3.4.). For the analogous 1570 Å - 1430 Å absorption system of OCS, ϵ_{max} - 4.1×10^4 litre $mole^{-1}cm^{-1}$. It is considered most reasonable, therefore, to assign $\tilde{E}$ to a singlet Rydberg state of linear OCSe.

(ii) The Franck-Condon intensity distribution among the bands of $\tilde{E} \leftarrow \tilde{X}$ indicates a small change in molecular geometry in $\tilde{E}$ from that in $\tilde{X}$.

The 0_0^0 and 3_0^1 bands are the strongest and the intensity of each succeeding member of the 3_0^n progression falls off markedly. Because the Rydberg orbital is, by definition, non-bonding and the 3π M.O. is weakly bonding (cf. Chapter 3, Section 3.1.2.) the molecular geometries of OCSe in its Rydberg states should be little changed from that in its ground ($\tilde{X}$) state. Although this argument does not exclude the possibility that $\tilde{E} \leftarrow \tilde{X}$ is an intravalence shell transition, the observed intensity distribution in this transition is consistent with this prediction.

(iii) According to the results of the model potential method calculations for OCSe (cf. Table 4.2), the largest T_n value (24080 cm^{-1}) is $T_{2s\sigma}$. The Rydberg states of OCSe which lie lowest in energy, relative to that of the ground state, should then result from the electron configuration $...(3\pi)^3_{core}(2s\sigma)_{Ryd.}$. These states are: $^1\Pi_{(1)}$, $^3\Pi_{(0^+)}$, $^3\Pi_{(0^-)}$, $^3\Pi(1)$ and $^3\Pi(2)$.

(iv) The ionization potential of OCSe (I.P.$_{(OCSe)}$) has been measured, in this work (cf. Section 5.A.8.), to be 81436 ± 100 cm^{-1} (10.1 ev, $\tilde{X}\ ^2\Pi_i$ $OCSe^+$ average). From equation [3.4], $\sigma_{2s\sigma}$ (OCSe) is 57356 cm^{-1}. If the $\tilde{E}$ and $\tilde{a}$ states are correctly assigned, the average of the T_o values for the $\tilde{E} \leftarrow \tilde{X}$ and $\tilde{a} \leftarrow \tilde{X}$ transitions may be taken as being an approximation to $\sigma_{2s\sigma}$. This quantity is 57062 cm^{-1}. The excellent agreement between the semi-empirical $\sigma_{2s\sigma}$-value and the value from the experimental data provides support for the present hypothesis.

(v) The bands of the $\tilde{a} \leftarrow \tilde{X}$ transition are much weaker than those of $\tilde{E} \leftarrow \tilde{X}$. The 0_0^0 band is much weaker than the 0_0^0 band of $\tilde{D} \leftarrow \tilde{X}$, which has been assigned to a singlet-singlet intravalence shell transition. The bands

of $\tilde{a} \leftarrow \tilde{X}$ have been assigned to a single progression in ν_3', an assignment which is compatible with the frequency intervals assigned to ν_3' in other excited states of OCSe and with the predicted linearity of OCSe in the $\tilde{a}$ state (Franck-Condon Principle). Although the measured oscillator strength of the $\tilde{a} \leftarrow \tilde{X}$ transition ($f \sim 1.7 \times 10^{-2}$) is of the magnitude of that of a singlet-singlet transition, the assignment of transitions as singlet ← singlet or triplet ← singlet on the basis of f-values is not a valid procedure in cases where the spin-orbit coupling is strong (this point has been discussed in Chapter 3, Section 3.3.3). The spin-orbit coupling in atomic selenium is strong, and tends toward (j,j) coupling, which is analogous to (Ω_c,ω) coupling in molecules. Accordingly, the spin-orbit coupling in Rydberg states of OCSe should be strong because the Rydberg orbitals are expected to be largely localized on the selenium atom. The intensities of triplet ← singlet transitions of OCSe should then be enhanced in cases where the triplet state arises from a configuration involving a Rydberg orbital.

(vi) The correlation of electronic states, which arise from a $(\pi)^3_{core}(n\sigma)_{Ryd.}$ electron configuration, between the (Λ,s) and (Ω_c,ω) coupling cases, has been discussed in Chapter 3, Section 3.3.3 Also included there was a discussion of the relative intensities and the energy separations of transitions to the zeroth-vibrational energy levels of these states from the ground state. If the states $\tilde{E}(^1\Pi_{(1)})$ and $\tilde{a}(^3\Pi_{(1)})$ both arise from the configuration $(\pi)^3(\sigma)$, then the value of $\{T_o(\tilde{E}) - T_o(\tilde{a})\} = 2610$ cm^{-1}, should be intermediate between the value of X, the singlet-triplet energy separation in pure (Λ,s) coupling, and the value of A, the spin-

orbit coupling constant for the $(\pi)^3$ core configuration of the molecule-ion $OCSe^+$. The value of X for OCSe is unknown. However, for most molecules, $|X| >> |A|$. $A(\tilde{X}\ ^2\Pi_i\ OCSe^+)$ has been measured in this work to be $-1453 \pm 100\ cm^{-1}$. Then, for coupling strengths intermediate between those in the (Λ,s) and (Ω_c,w) cases, $\{T_o(\tilde{E}) - T_o(\tilde{a})\} = 2610\ cm^{-1}$ is considered a reasonable value for the energy separation of the singlet and triplet states of the $(\pi)^3_{core}(2s\sigma)_{Ryd.}$ configuration.

(vii) Where the $^1\Pi_{(1)}$ and $^3\Pi_{(1)}$ states arise from a $(\pi)^3_{core}(\sigma)_{Ryd.}$ configuration, the transitions $^1\Pi_{(1)} \leftarrow \tilde{X}$ and $^3\Pi_{(1)} \leftarrow \tilde{X}$ have been denoted C and B, respectively[96,97]. Towards the (Ω_c,w) limit, the ratio of the intensities of these transitions I_B/I_C should increase to unity (cf. Chapter 3, Section 3.3.3.). The ratio of the oscillator strengths of the $\tilde{a} \leftarrow \tilde{X}$(B) and $\tilde{E} \leftarrow \tilde{X}$(C) transitions is ~0.34, which indicates that the coupling is indeed intermediate between cases (Λ,s) and (Ω_c,ω).

(viii) The corresponding (1570 Å - 1430 Å) absorption system in OCS is remarkably similar in appearance and intensity ($\epsilon_{max} \sim 4.1 \times 10^4$ litre $mole^{-1}cm^{-1}$) to the OCSe spectrum in the 1714 Å - 1610 Å region (cf. Fig. 5.9). This former system has been photographed under high resolution and analyzed (cf. Section 5.B.1.) in terms of transitions to the Rydberg states $^1\Pi_{(1)}$ and $^3\Pi_{(1)}$ of the $\ldots(3\pi)^3_{core}(2s\sigma)_{Ryd.}$ configuration of OCS. All of the bands assigned to these transitions are very diffuse.

(ix) All of the observed bands assigned to the $\tilde{E} \leftarrow \tilde{X}$ and $\tilde{a} \leftarrow \tilde{X}$ (but not $\tilde{D} \leftarrow \tilde{X}$) transitions are very diffuse. This phenomenon is attributed to (Case I) predissociation, i.e., radiationless transition to a neighbouring electronic state which is either dissociative or has a small potential minimum for some displacement coordinate. The strength of

the predissociation indicates that it is homogeneous. $\tilde{E}$ and $\tilde{a}$ must then be of the same symmetry, and, in (Ω_c,w) coupling, of the same Ω-value[98]. The assignment of the predissociating state is discussed in Section 5.A.6.

(x) The bands assigned to the $\tilde{b}\ ^3\Pi_{(0^+)} \leftarrow \tilde{X}\ ^1\Sigma^+$ transition are red-degraded, slightly diffuse and very weak. This assignment, though tentative, is considered reasonable if the assignment of $\tilde{a}\ ^3\Pi_{(1)}$ is correct. The energy separation of the $^3\Pi_1$ and $^3\Pi_{0^+}$ states of the $(\pi)^3(\sigma)$ configuration should be small for weak spin-orbit coupling[97,99], as should the intensity of the $^3\Pi_{(0^+)} \leftarrow \tilde{X}\ ^1\Sigma^+$ transition (cf. Fig. 3.5).

5.A.5.3. Bond Lengths in the $\tilde{D}$ and $\tilde{E}$ States

If the rotational structure of the bands of a spectrum cannot be resolved, several methods may be used to obtain approximate values for the excited state bond lengths. Some of these are: (i) The rules of Clark and Badger[100], which relate the experimentally-determined ground and excited state frequencies and bond lengths, and (ii) Franck-Condon calculations, in which the ratios of the intensities of vibronic transitions are related to changes in the normal coordinates of vibration. In general, these methods yield results which are in poor agreement with bond lengths (and angles) accurately determined by other means. Both of these methods are used in this work to obtain CO and CSe bond lengths in the $\tilde{D}$ and $\tilde{E}$ states of OCSe.

Clark's rule is used here in the form

$$r_e'^3 \upsilon_e' = r_e''^3 \upsilon_e'' \qquad [5.1]$$

where r_e and υ_e are the bond length and the vibrational frequency in a given

electronic state (double prime and prime symbols refer to ground and excited states, respectively). Badger's rule is used here in the form

$$\upsilon_e'(r_e' - d_{ij})^3 = \upsilon_e''(r_e'' - d_{ij})^3 \qquad [5.2]$$

where r_e and υ_e are as before and d_{ij} is a constant. The magnitude of d_{ij} depends on the row of the periodic table to which atoms i and j, which form the bond, belong. Values of d_{ij} have been given in the literature[101]. Some of these are:

Row (atom i)	1	1	1	1
Row (atom j)	1	2	3	4
d_{ij}	0.68	0.94	1.06	1.18

Both of these rules were developed for diatomic molecules, for which they yield only moderately accurate values of excited state bond lengths. When these rules are applied to polyatomic molecules, it is necessary to treat each bond as a separate diatomic molecule. Though the calculations of the vibrational potential energy distribution in OCSe ($\tilde{X}\ ^1\Sigma^+$) (cf. Section 5.A.2.) indicates that the ν_1 and ν_3 vibrational modes are almost completely (86%) localized in the CO and CSe regions, respectively, the results of these bond length calculations for OCSe must be considered to be highly approximate.

A method of calculating excited state bond lengths in triatomic[102] molecules has been given by Coon, DeWames and Loyd. This method, a quantitative application of the Franck-Condon principle, has been adapted in this work for application to linear ABC-type molecules and applied to the $\tilde{D}$ and $\tilde{E}$ states of OCSe. The adapted method is given in Appendix A.4. The totally symmetric normal vibrations (ν_1 and ν_3) only are considered. The assignments and relative intensities of the bands of the $\tilde{D} \leftarrow \tilde{X}$ and $\tilde{E} \leftarrow \tilde{X}$

transitions and the frequencies assigned to ν_1 and ν_3 in both excited states have been given previously. These quantities are used in the Franck-Condon calculations.

The ($\tilde{D}$ and $\tilde{E}$ state) bond lengths for OCSe calculated by each of these methods are given in Table 5.7, together with the excited state rotational constant (B') calculated for each of the Franck-Condon structural possibilities.

Because the bands of $\tilde{D} \leftarrow \tilde{X}$ are red-degraded, it is reasonable to assume that the rotational constant in $\tilde{D}$ is less than that in $\tilde{X}$ (B" = .134 cm^{-1} (80)). A choice must still be made between the Franck-Condon possibilities (i) and (iv). The latter is in agreement with the results from Clark's and Badger's rules in that both bond lengths increase (r_{CO}" = 1.160 Å, r_{CSe}" = 1.711 Å). Also, because the $\tilde{D}$ state results from an electron promotion from the "bonding" 3π M.O. to the antibonding 4π M.O., an increase in both bond lengths is expected. The bond lengths r_{CO} = 1.24 Å and r_{CSe} = 1.73 Å are then considered to be the most reasonable of these calculated for the $\tilde{D}$ state of OCSe.

The higher frequency bands of $\tilde{E} \leftarrow \tilde{X}$ appear to be red-degraded, which suggests that B'($\tilde{E}$) < B"($\tilde{X}$). $\tilde{E}$ has been assigned as a Rydberg state of OCSe. Again, because the promoted electron is removed from the 3π M.O., which was stated in Chapter 3, Section 3.1.2. to be weakly bonding between Se and O, an increase in both bond lengths in $\tilde{E}$ is expected. Also, because the Rydberg orbital is non-bonding, the bond lengths in $\tilde{E}$, and those in the ground state of $OCSe^+$, are expected to be similar. Although the latter quantities have not been determined in this work, a comparison of bond lengths in the ground electronic states of CO_2, CS_2 and N_2O with those in the ground states of CO_2^+, CS_2^+ and N_2O^+, respectively, reveals that the bond lengths in the ionic species are, without exception, increased over those in the molecules[103].

TABLE 5.7

POSSIBLE BOND LENGTHS FOR OCSe IN THE $\tilde{D}$ AND $\tilde{E}$ STATES

$\tilde{D}$ STATE

Calculation	r_{CO} (Å)	r_{CSe} (Å)	B' (cm^{-1})
Clark's rule	1.23	1.78	-
Badger's rule	1.19	1.74	-
Franck-Condon possibilities			
(i)	1.11	1.81	0.127
(ii)	1.69	1.08	0.142
(iii)	1.21	1.61	0.140
(iv)	1.24	1.73	0.126

$\tilde{E}$ STATE

Calculation	r_{CO} (Å)	r_{CSe} (Å)	B' (cm^{-1})
Clark's rule	1.21	1.78	-
Badger's rule	1.18	1.74	-
Franck-Condon possibilities			
(i)	1.14	1.80	.126
(ii)	1.11	1.67	.143
(iii)	1.18	1.62	.142
(iv)	1.22	1.75	.125

The bond lengths (calculated) for the $\tilde{E}$ state are then taken to be $r_{CO} = 1.22$ Å, $R_{CSe} = 1.75$ Å (Franck-Condon (iv)). The values are in poor agreement with those calculated by the rules of Clark and Badger. Again, it is emphasized that the simplicity of the model chosen for these calculations allows little confidence in the accuracy of these results.

5.A.6. Predissociation in the Lower Excited States of OCSe

The diffuseness observed in the U.V. and V.U.V. (2100 Å - 1610 Å region) absorption spectra of OCSe (and OCS) impedes the unambiguous assignment of their spectral features. A mechanism is now proposed to account for this diffuseness of the OCSe spectra.

The absorption continuum underlying the 2150 - 1820 Å and 2700 - 2200 Å absorption systems of OCSe corresponds to the transition $^1\Pi \leftarrow \tilde{X}\ ^1\Sigma^+$. This Π state, which arises from the configuration $\ldots(3\pi)^3(10\sigma)$, is the predissociating state responsible for the diffuseness observed in the spectra corresponding to the $\tilde{E}\ ^1\Pi_{(1)}$, $\tilde{b}\ ^3\Pi_{(0^+)}$, $\tilde{a}\ ^3\Pi_{(1)}$, $\tilde{C}\ (^1A'')$, $\tilde{B}\ ^1A'$ and $\tilde{A}\ (^1A'')$ $\leftarrow \tilde{X}\ ^1\Sigma^+$ transitions (and for the slight diffuseness of the $2_0^1 3_0^n$ bands of the $\tilde{D} \leftarrow \tilde{X}$ transition). It is a dissociative state and its energy converges asymptotically to the ground state dissociation limit, D_{OC-Se}, of OCSe.

The following arguments are advanced in support of this hypothesis. These are:

(i) From a consideration of the (calculated) M.O. energies of OCS (cf. Fig. 3.1), the $^{1,3}\Pi$ states arising from the configuration $\ldots(3\pi)(10\sigma)$ are predicted to lie close in energy to the singlet states arising from the $\ldots(3\pi)^3(4\pi)$ configuration. Also, from the Walsh diagram (cf. Fig. 3.2), OCS is predicted to be linear in these $^{1,3}\Pi$ states. In the simple des-

cription of the bonding properties of the OCS M.O.'s given in Chapter 3, Section 3.1.2., the 10σ (virtual) M.O. was stated to be strongly antibonding between the S and C atoms. A strong possibility then exists that the states arising from a configuration involving this M.O. are either dissociative or have a small potential minimum for the coordinate of extension of the S-C bond. By analogy, these considerations also apply to OCSe.

(ii) The absorption continuum underlying the 2150 - 1820 Å system of OCSe is strong ($f \sim 0.8 \times 10^{-2}$). The absorption continuum which underlies the analogous (1875 Å - 1625 Å) absorption system of OCS ($f \sim 7 \times 10^{-2}$) is also very strong[33]. This suggests that the upper state in the transition responsible for the continuum in OCSe is a singlet state and that the transition is allowed.

(iii) Photodissociation of gaseous-phase OCSe at wavelengths >2200 Å has been reported[11]. The dissociation products are CO ($^1\Sigma^+$) + Se (^1D_g). By application of the Wigner-Witmer rules, the predissociating state must be of $^1\Pi$ or $^1\Sigma^-$ or $^1\Delta$ symmetry. If the assignments of the upper states {$^1A''(^1\Delta)$, $^1A'(^1\Delta)$, $^1A''(^1\Sigma^-)$} of the transitions responsible for the 2700 - 2200 Å and 2150 - 1820 Å absorption systems of OCSe are correct, the predissociating state must then be of $^1\Pi$ symmetry.

(iv) The diffuseness observed in the bands of the $\tilde{E} \leftarrow \tilde{X}$, $\tilde{a} \leftarrow \tilde{X}$ and $\tilde{b} \leftarrow \tilde{X}$ transitions, and in those bands of the $\tilde{D} \leftarrow \tilde{X}$ transitions assigned $2_0^1 3_0^n$ may also be attributed to predissociation by this Π state (cf. Section 5.A.5.). The sharpness of the bands of $\tilde{D} \leftarrow \tilde{X}$ assigned 0_0^0, 3_0^1 and $1_0^1 3_0^n$ is consistent with this interpretation, because the predissociation Σ - Π is forbidden (in the Born-Oppenheimer approximation).

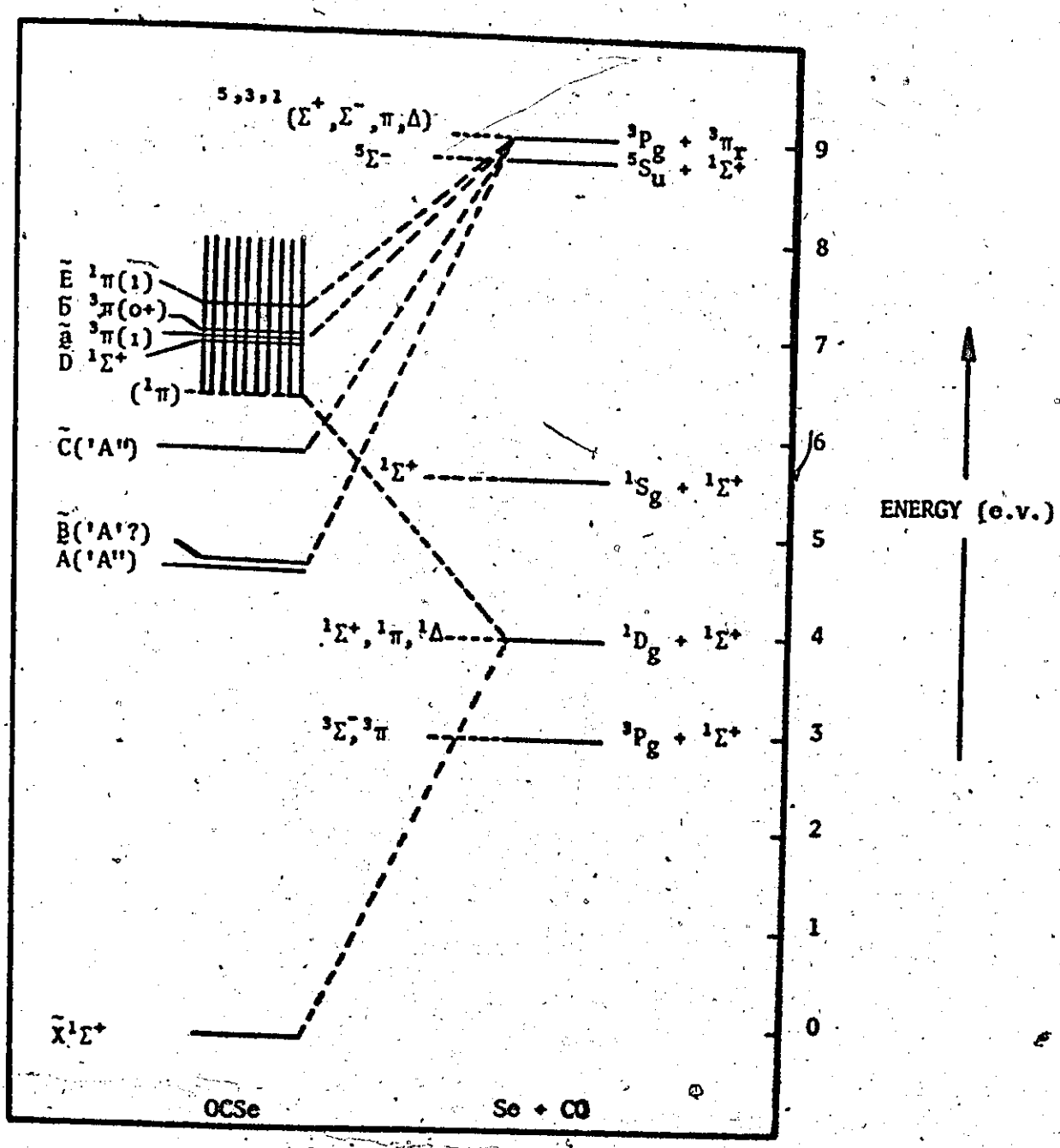

FIG. 5.6. CORRELATION, IN (Λ,S) COUPLING, BETWEEN THE ELECTRONIC STATES OF OCSe AND THOSE OF Se + CO.

(v) The correlation, in (Λ,s) coupling, between the lower-energy excited states of OCSe and those of CO + Se is shown schematically in Fig. 5.6. On the left of this figure are the energies of the observed states of OCSe. The energy of the zeroth vibrational level of the ground (X) state is set to zero. The thermodynamic quantities used in the construction of this diagram are:

$S_{(C)}$ (sublimation energy of carbon): 170.9 kcal/mole[104]

$S_{(Se)}$ (sublimation energy of selenium): 49.4 kcal/mole[104]

$D_{(O_2)}$ (bond energy of O_2): 119.1 kcal/mole[104]

$D_{(CO)}$ (bond energy of carbon monoxide): 9.14 ev[104]

Atomic energy levels of Se I have been given by Ruedy and Gibbs[105]. For the purposes of the diagram, the average of the energies of the $3p_g$ components is used.

Also, $T_o(^3\Pi_r)$ CO = 48687.5 cm^{-1}[106] = 6.04 ev.

The predissociating state $^1\Pi$ and the ground (X) state most probably correlate with $CO(^1\Sigma^+) + Se(^1D_g)$. If this is so, D"(OC-Se) ~ 4 ev. The diffuseness observed in the first (lowest energy) strong band of the $^1A"(^1\Delta) \leftarrow \tilde{X}\ ^1\Sigma^+$ transition (2700 - 2200 Å system) at 37648 cm^{-1} (~4.67 ev) supports the present hypothesis. The latter value is considered to be an upper limit to D(OC-Se), i.e., D(OC-Se) $\leq$ 4.67 ev. D(C-Se) for the diatomic molecule CSe has been reported to be 5 ± 1 ev[104].

No arguments will be presented for the other correlations shown in Fig. 5.6. The effects of spin orbit (Ω_c,ω) coupling and the considerable uncertainty in the values of thermodynamic quantities used in the construction of the diagram render argument (v) somewhat tentative.

5.A.7 Description and analysis of the bands of OCSe in the 60800 cm^{-1} (1567.4 Å) - 68295 cm^{-1} (1464.2 Å) Region

5.A.7.1 Description

A strong, banded absorption system of OCSe occurs in the 1570 Å - 1460 Å region. A McPherson monochromator trace of this absorption is reproduced in Fig. 5.7. The bands of $OCSe^{80}$ and $OCSe^{78}$ have been photographed in this work under the high resolution of the Eagle vacuum spectrograph. A spectrogram of a portion of the $OCSe^{80}$ spectrum in this region is shown in Fig. 5.8.. The absorption features observed in this region are classified, by intensity and appearance, as follows:

(i) A series of moderately strong diffuse bands. These are assigned to vibronic components of the electronic transitions $\tilde{C} \leftarrow \tilde{X}$ (c.f. Fig. 5.7). Bands assigned as members of the principal progression are separated in energy by $\sim$ 527 cm^{-1}. In this progression, which extends from 1553 Å - 1516 Å, the first and second members are the most intense. The diffuseness of the bands is attributed to case I predissociation.

(ii) A series of very strong, sharp, red-degraded bands. These are assigned to a separate electronic transition viz. $\tilde{F} \leftarrow \tilde{X}$. Successive members of the principal progression, of which the second member is the most intense, are separated in energy by $\sim$ 506 cm^{-1}. The principal progression extends from 1549.5 Å - 1514 Å.

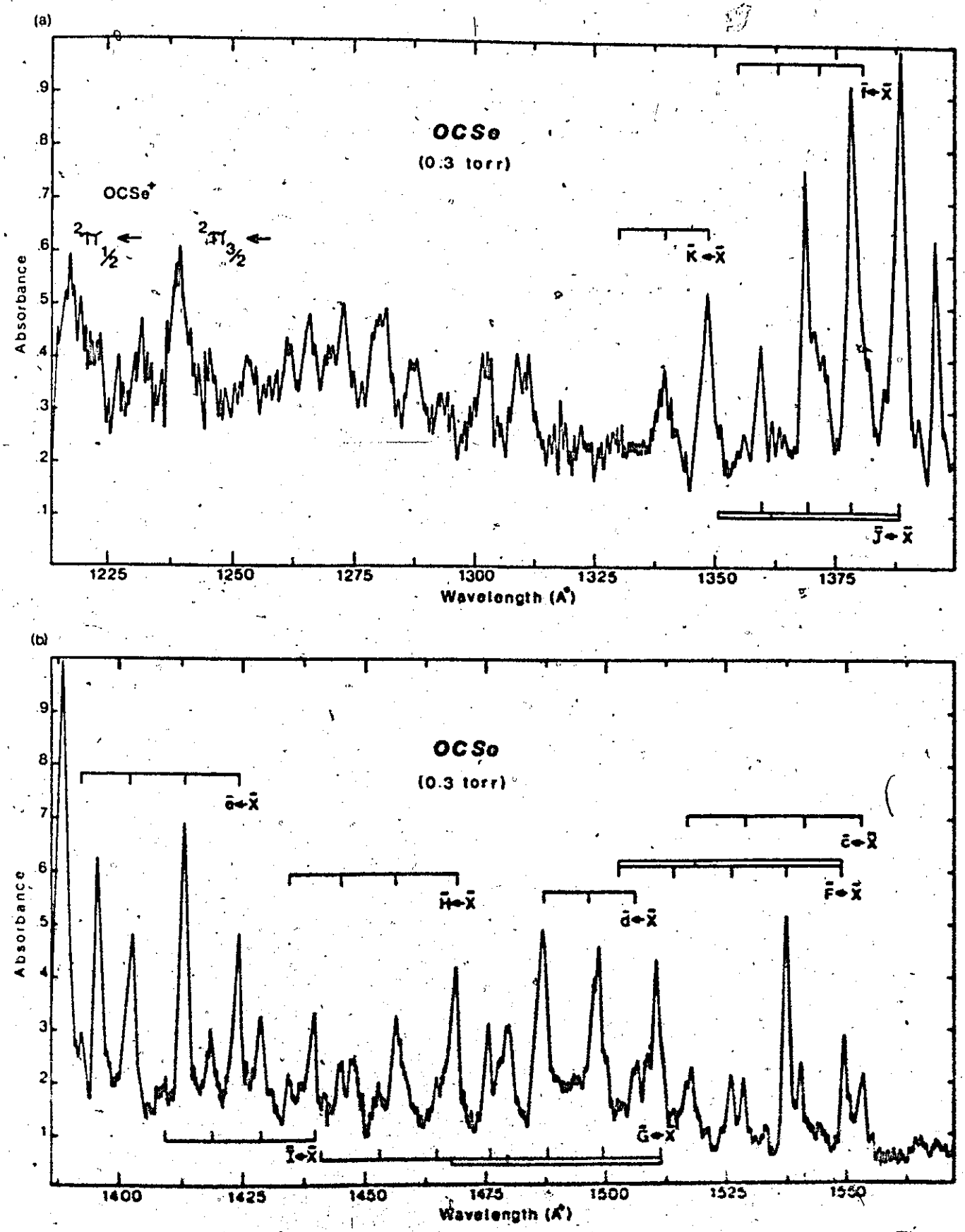

Fig. 5.7. Low resolution absorption spectrum of OCSe in the regions (a) 1212 Å - 1400 Å and (b) 1385 Å - 1570 Å.

FIG 5.8 Spectrogram of a Portion of the OCSe Spectrum in the 1560 A - 1460 A Region.

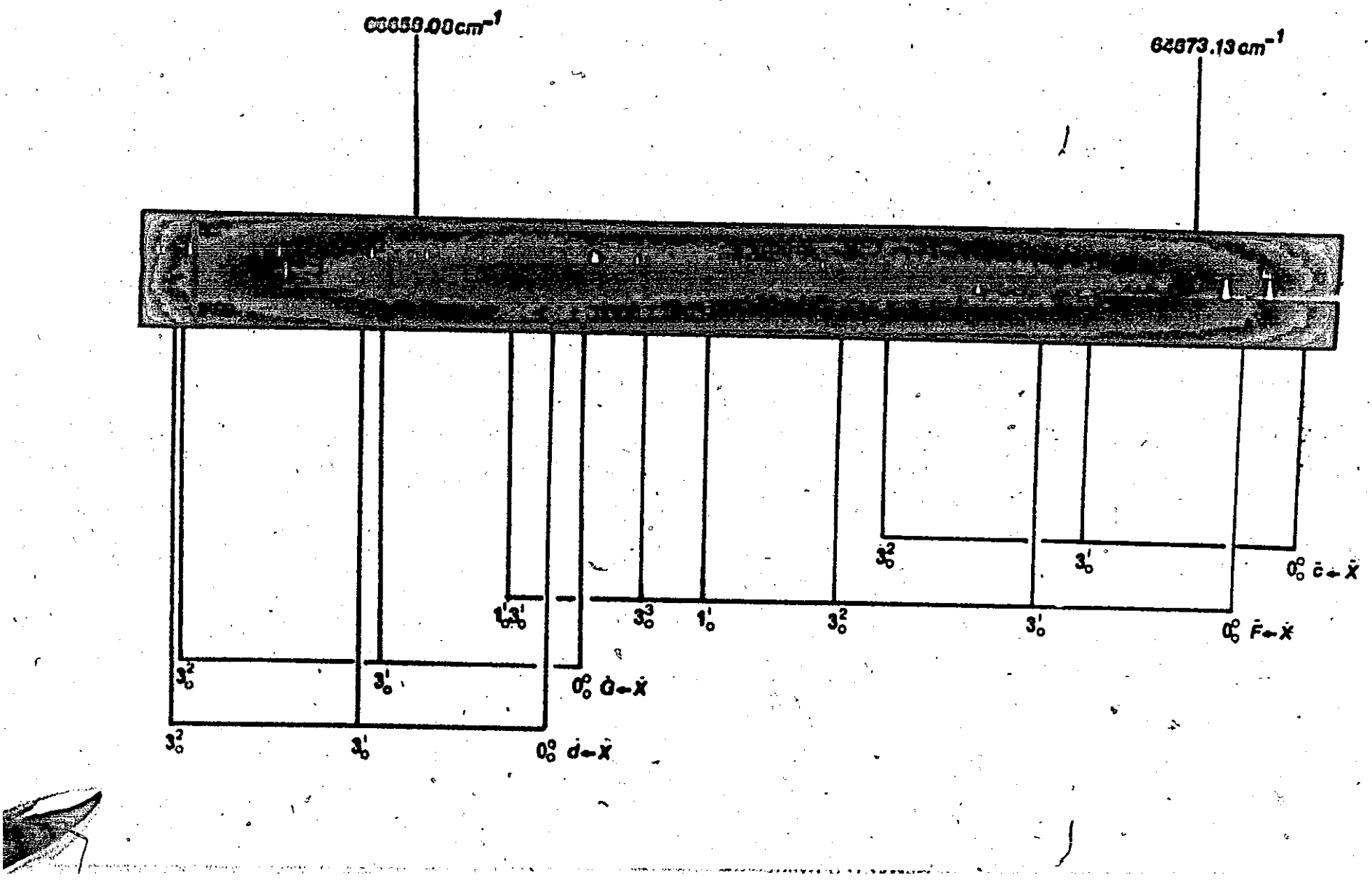
62858.00cm⁻¹
62873.13cm⁻¹
3_0^2
3_0^1
0_0^0 d←X
$1_0'3_0'$
3_0^3
$1_0'$
3_0^2
0_0^0 G←X
3_0^2
3_0^1
0_0^0 F←X
3_0^2
3_0^1
0_0^0 c←X

(iii) A series of strong, red-degraded, slightly diffuse bands, which extend from 1510 Å - 1442 Å. Again, in the principal progression, in which the frequency interval between successive bands is $\sim 522\ cm^{-1}$, the first and second members are the most intense These bands are assigned to the electronic transition $\tilde{G} \leftarrow \tilde{X}$. The slight diffuseness of the bands is attributed to case I predissociation.

(iv) A short series of weak, slightly diffuse, red degraded bands. These are assigned to a single progression in which the frequency interval between successive members is $\sim 498\ cm^{-1}$. The first member is the most intense. These bands are assigned to yet another electronic transition viz. $\tilde{d} \leftarrow \tilde{X}$. The progression extends from 1508 Å - 1486 Å.

(v) A series of moderately strong, slighly diffuse, red-degraded bands which extends from 1467 Å - 1434 Å. These bands, of which the first member is the most intense, are assigned to a single progression belonging to the transition $\tilde{H} \leftarrow \tilde{X}$. The intensity of succeeding members decreases markedly and the frequency interval between the bands is $\sim 539\ cm^{-1}$.

Other absorption bands of OCSe in this region have been assigned to minor progressions belonging to the $\tilde{c} \leftarrow \tilde{X}$, $\tilde{F} \leftarrow \tilde{X}$ and $\tilde{G} \leftarrow \tilde{X}$ transitions. The intensities of bands assigned to the latter progressions are generally less than the intensities of the bands of the corresponding major progressions. The first member of each minor progression is

is the most intense. The interval of ~ 1350 cm^{-1} between the first members of the major and minor progressions is prominent.

In this work, high resolution photographic recording of the OCSe absorption spectrum is complete only to $\lambda > 1464$ Å.

Rotational fine structure could not be resolved in any of the bands of this absorption system.

The vacuum frequencies, vibrational isotope shifts, appearances, relative intensities and assignments of the bands of this system of OCSe are given in Table 5.8.

5.A.7.2 Analysis

The frequencies quoted in this discussion are those measured for $OCSe^{80}$, unless otherwise specified.

The intensities of the very weak bands at 63755 cm^{-1} and 63893 cm^{-1} increase slightly when the temperature of the absorbing gas is increased. The energy separations of these bands from the first (lowest energy) strong bands of the major progression in $\tilde{c} \leftarrow \tilde{X}$ and $\tilde{F} \leftarrow \tilde{X}$ are (64388.6-63755) ~ 634 cm^{-1} and (64537/4-63893) ~ 644 cm^{-1}, respectively. Both of these quantities are within measurement accuracy limits of the ground state frequency, ν_3''. The bands at 64388.6 cm^{-1} and 64537.4 cm^{-1} are assigned as the origin (0_0^0) bands of separate electronic transitions $\tilde{c} \leftarrow \tilde{X}$ and $\tilde{F} \leftarrow \tilde{X}$, respectively. The assignments 63755 cm^{-1} ($3_1^0\ \tilde{c} \leftarrow \tilde{X}$) and 63893 cm^{-1} ($3_1^0\ \tilde{F} \leftarrow \tilde{X}$) follow. The negligible vibrational isotope shifts measured for the origin bands of $\tilde{c} \leftarrow \tilde{X}$ and $\tilde{F} \leftarrow \tilde{X}$ (-2.1 cm^{-1} and -1.4 cm^{-1}, respectively) support the 0_0^0 assignments.

TABLE 5.8

Measured Bands of OCSe in the 63800 cm^{-1} (1567.4 Å) - 68295 cm^{-1} (1464.2 Å) Region.

Band Frequency*		Isotope Shift	Description**	Relative Intensity[a]	Assignment	
$OCSe^{80}$	$OCSe^{78}$	$\nu_{78}-\nu_{80}$ in cm^{-1}			Electronic	Vibronic
63755[b]				v.w.	$\tilde{c} \leftarrow \tilde{X}$	3_1^0
63893			sh., r.d.	0.12	$\tilde{F} \leftarrow \tilde{X}$	3_1^0
64388.6	64386.5	-2.1	dif.	1.00	$\tilde{c} \leftarrow \tilde{X}$	0_0^0 $[^3\Pi(1) \leftarrow {}^1\Sigma^+]$
64466				v.w.	$\tilde{F} \leftarrow \tilde{X}$	2_1^1
64537.4	64536.0	-1.4	sh., r.d.	1.52	$\tilde{F} \leftarrow \tilde{X}$	0_0^0 $[^1\Sigma^+(0^+) \leftarrow {}^1\Sigma^+]$
64915.3	64917.8	+2.5	dif.	1.16	$\tilde{c} \leftarrow \tilde{X}$	3_0^1
64968			ov., r.d.	w	$\tilde{F} \leftarrow \tilde{X}$	$2_1^1 3_0^1$
65043.8	65046.1	+2.3	sh., r.d.	3.04	$\tilde{F} \leftarrow \tilde{X}$	3_0^1
65437.8			dif.	w	$\tilde{c} \leftarrow \tilde{X}$	3_0^2
65549.2	65554.0	+4.8	sh., r.d.	1.04	$\tilde{F} \leftarrow \tilde{X}$	3_0^2
65733.9			dif.	w	$\tilde{c} \leftarrow \tilde{X}$	1_0^1
(65828.8)			v. dif.	w	not assigned	
65892.6	65891.7	-0.9	sh., r.d.	1.12	$\tilde{F} \leftarrow \tilde{X}$	1_0^1
65952.0			dif.	w	$\tilde{c} \leftarrow \tilde{X}$	3_0^3

TABLE 5.8 (cont'd)

Band Frequency* $OCSe^{80}$	Band Frequency* $OCSe^{78}$	Isotope Shift $\nu_{78}-\nu_{80}$ in cm^{-1}	Description**	Relative Intensity[a]	Assignment Electronic	Assignment Vibronic
66051.4			sh.,r.d.	0.56	$\tilde{F} \leftarrow \tilde{X}$	3_0^3
66209.3	66210.8	+1.5	sh.,dif. r.d.	2.48	$\tilde{G} \leftarrow \tilde{X}$	0_0^0 $[^1\Pi(1) \leftarrow {}^1\Sigma^+]$
66291.0	66289.7	-0.3	sh.,dif. r.d.	0.85	$\tilde{d} \leftarrow \tilde{X}$	0_0^0 $[^3\Pi(1) \leftarrow {}^1\Sigma^+]$
66400.6	66401.9	+1.3	sh.,r.d.	0.64	$\tilde{F} \leftarrow \tilde{X}$	$1_0^1 3_0^1$
(66435.3)	n. obs.		sh.,r.d.	v.w.	not assigned	
66661.5	66664.3	+2.8	sh.,dif.,r.d.	w	$\tilde{G} \leftarrow \tilde{X}$	$2_1^1 3_0^1$
66731.4	66732.5	+1.1	sh.,dif.,r.d.	2.64	$\tilde{G} \leftarrow \tilde{X}$	3_0^1
66788.7	66793.7	+5.0	sh.,dif.,r.d.	0.6	$\tilde{d} \leftarrow \tilde{X}$	3_0^1
(66820.0)	n. obs.		dif.	w	not assigned	
67148.5	67147.1	-1.4	dif.	w	$\tilde{F} \leftarrow \tilde{X}$	1_0^2
67255.4	67259.8	+4.4	sh.,diff.,r.d.	1.60	$\tilde{G} \leftarrow \tilde{X}$	3_0^2
67281.9	67287.5	+5.6		0.3	$\tilde{d} \leftarrow \tilde{X}$	3_0^2
67586.1			sh.,dif.,r.d.	1.60	$\tilde{G} \leftarrow \tilde{X}$	1_0^1
67783.5	67789.3	+5.8	sh.,dif.,r.d.	1.2	$\tilde{G} \leftarrow \tilde{X}$	3_0^3
68113.0				1.0	$\tilde{G} \leftarrow \tilde{X}$	$1_0^1 3_0^1$
68151[c]				1.3	$\tilde{H} \leftarrow \tilde{X}$	0_0^0 $[^1\Pi(1) \leftarrow {}^1\Sigma^+]$
68294.4			sh.,dif.,r.d.	0.8	$\tilde{G} \leftarrow \tilde{X}$	3_0^4

* Vacuum wavenumbers (cm^{-1}). For sharp-headed bands, the measured frequency (estimated accuracy ± 2 cm^{-1}) is ν_{Head}. For diffuse bands, the measured frequency (estimated accuracy ± 5 cm^{-1}) is that of the absorption intensity maximum of the band.

** w = weak; sh. = sharp-headed; dif. = diffuse; ov. = overlapped.

[a] Values quoted are absorbance ratios ie. $\log I_0/I_A \Big/ \log I_0/I_B$. B is chosen as the band at 64388.6 cm^{-1}

[b] Measurement from McPherson monochromator recording. Estimated accurate ± 20 cm^{-1}.

[c] The frequencies of other bands assigned to $\tilde{H} \leftarrow \tilde{X}$ and $\tilde{G} \leftarrow \tilde{X}$ are quoted in Table 5.10.

All of the bands assigned to $\tilde{c} \leftarrow \tilde{X}$ are diffuse. The frequency intervals between successive bands assigned to the major progression of this transition are $\sim$526 cm^{-1}. These intervals are assigned to ν_3'. Because the bands are diffuse, the vibrational isotope shift, which is predicted to be $\sim$2 - 3 cm^{-1}/quantum of ν_3' excited, is inside the measurement accuracy limits for all levels of $\tilde{c} \leftarrow \tilde{X}$. However, this ν_3' assignment is consistent with the ν_3' frequencies assigned in other electronic transitions of OCSe, and with the ν_3' assignments of Bavia, DiLonardo, Galloni and Trombetti[12]. As will be shown, the state $\tilde{c}$ is most probably a Rydberg state of linear OCSe. By application of the Franck-Condon principle, activity of ν_1' and ν_3', the excited state totally symmetric stretching vibrational motions, is expected if OCSe is linear in both combining electronic states in the transition. The weak diffuse band at 65733.9 cm^{-1} is assigned to 1_0^1 of $\tilde{c} \leftarrow \tilde{X}$. This ν_1' assignment will be shown to be consistent with the assignments at this frequency in the neighbouring $\tilde{F}$ and $\tilde{G}$ states. From the assignments of the bands at $\tilde{c} \leftarrow \tilde{X}$, the excited state vibrational frequencies are;

$$\nu_1' = 1456.4 \text{ cm}^{-1}$$
$$\nu_3' = 526.7 \text{ cm}^{-1}.$$

The Franck-Condon intensity distribution among vibronic components of $\tilde{c} \leftarrow \tilde{X}$ indicate a small change in geometry upon electronic excitation. Indeed, the vibrational structure associated with the Rydberg transitions of OCSe is highly characteristic viz. a short ν_3' progression and a shorter $\nu_1' + n\nu_3'$ progression. In a given transition, the most intense bands occur in the former progression. These characteristics have been

noted previously in the assignments of the bands of the $\tilde{E} \leftarrow \tilde{X}$ transition (c.f. Section 5.A.4).

The bands assigned to $\tilde{F} \leftarrow \tilde{X}$ are sharp headed and red-degraded. The strength of the predissociation of the bands of $\tilde{c} \leftarrow \tilde{X}$ and $\tilde{G} \leftarrow \tilde{X}$ suggests that the mechanism is that of homogeneous predissociation. Accordingly, the excited states $\tilde{F}$ and $\tilde{c}$, $\tilde{G}$ must be of different symmetry, and, where spin-orbit coupling is strong (Ω_c,ω), of different Ω quantum number[98].

In the preceding discussion, the band at 64537.4 cm^{-1} has been assigned to 0_o^o of $\tilde{F} \leftarrow \tilde{X}$. The frequency interval of $\sim$ 506 cm^{-1} between the sharp-headed bands is assigned to ν_3'. The isotope shift of + 4.8 cm^{-1} for the band assigned 3_o^2 is only slightly outside measurement accuracy limits (± 4 cm^{-1}). This shift is qualitatively very obvious, however, when photographic enlargements of the spectra of $OCSe^{80}$ and $OCSe^{78}$ are compared and it serves to confirm the ν_3' assignments. The sharp-headed band at 658926 cm^{-1} is assigned to 1_o^1, because of: (i) the negligible isotope shift (-0.9 cm^{-1}) measured for this band and (ii) the observation of the band, assigned to $1_o^1 3_o^1$, 508 cm^{-1} to the high frequency side of the 1_o^1 band and (iii) in this assignment, the ν_1' frequencies in $\tilde{c}$ and $\tilde{F}$ are approximately equal, as would be expected for close-lying electronic states.

The very weak band of $\tilde{F} \leftarrow \tilde{X}$ at 64466 cm^{-1}, assigned 2_1^1, allows calculation of ν_2' in $\tilde{F}$ as 392 cm^{-1}.

The bands of $\tilde{G} \leftarrow \tilde{X}$ form the most extensive series in this region of the OCSe spectrum. The first strong band of this series, at 66209.3 cm^{-1}, is assigned to the origin (0_o^o) of $\tilde{c} \leftarrow \tilde{X}$. This band is

overlapped by the rotational structure of the 1-0 band of the fourth positive system of CO . The presence of the latter band, an absorption feature of the helium source continuum used in the photographic work, may obscure the sequence bands which should occur to the low-frequency side of this origin band. Again, because $\tilde{G}$ is most probably a Rydberg state of linear OCSe, the molecular geometry in $\tilde{G}$ is expected to be little changed from that in the ground $\tilde{X}$ state, and the origin band of $\tilde{G} \leftarrow \tilde{X}$ is expected to be strong. The 0_0^0 assignment of this band is therefore reasonable. Also, the small vibrational isotope shift measured for this band ($+ 1.5\ cm^{-1}$) allows confidence in this assignment. The assignments of the bands of $\tilde{G} \leftarrow \tilde{X}$ are consistent with the assignments in the $\tilde{c} \leftarrow \tilde{X}$ and $\tilde{F} \leftarrow \tilde{X}$ transitions, ie. a short progression in a ν_3' interval and a weaker progression of bands assigned to $1_0^1 3_0^n$. The large vibrational isotope shift ($+5.8\ cm^{-1}$) for the 3_0^3 band of $\tilde{G} \leftarrow \tilde{X}$ supports the ν_3' assignment. The isotope shift is $\sim 2\ cm^{-1}$/quantum. The vibrational frequencies in $\tilde{G}$ are, from the present assignments; $\nu_1' = 1376.8\ cm^{-1}$ and $\nu_3' = 522.1\ cm^{-1}$.

The $\tilde{d} \leftarrow \tilde{X}$ and $\tilde{H} \leftarrow \tilde{X}$ transitions both consist of single progressions. The first strong band of each is assigned to the origin band of the transition. The frequency intervals between successive bands, which are $\sim 498\ cm^{-1}$ in $\tilde{d} \leftarrow \tilde{X}$ and $\sim 539\ cm^{-1}$ in $\tilde{H} \leftarrow \tilde{X}$, are assigned to ν_3' in the $\tilde{d}$ and $\tilde{H}$ states, respectively.

It now remains to assign the symmetries of the excited states $\tilde{c}$, $\tilde{F}$, $\tilde{G}$, $\tilde{d}$ and $\tilde{H}$, and to specify the electron configurations from which they arise. To this point (cf. sections 5.A.1-5.A.7), all of the singlet states arising from the configurations--- $(3\pi)^3(4\pi)$, $--(3\pi)^3(10\sigma)$

and-$(3\pi)^3_{core}(2s\sigma)_{Ryd.}$ have been assigned. It was noted in Chapter 3, Section 3.1.2 that the next (to 3π) lowest energy M.O. (9π) lies at $\sim$ 6 e.v. below the 3π M.O. energy in OCS. The $\tilde{c}$, $\tilde{F}$, $\tilde{G}$, $\tilde{d}$ and $\tilde{H}$ states of OCSe then most probably arise from the Core-Rydberg electron configuration ---$(3\pi)^3$(Ryd).

The $\tilde{c}$ and $\tilde{G}$ states are assigned the symmetries $^3\Pi(1)$ and $^1\Pi(1)$, respectively. These states arise from the electron configurations ---$(3\pi)^3_{core}(2p\sigma)_{Ryd}$. Some evidence exists for these assignments viz.

For strong (Ω_c,ω) spin-orbit coupling, the transitions $\tilde{G}\,^1\Pi(1) \leftarrow \tilde{X}\,^1\Sigma^+$ and $\tilde{c}\,^3\Pi(1) \leftarrow \tilde{X}\,^1\Sigma^+$ are both allowed in $C_{\infty v}$ symmetry. The measured oscillator strengths of these transitions are 1.1×10^{-2} and 1.8×10^{-2}, respectively. The ratio of these oscillator strengths is .011/.018 $\sim$ 0.56. It should be noted that this value is lower than the ratio of the oscillator strengths of the $\tilde{a} \leftarrow \tilde{X}$ and $\tilde{E} \leftarrow \tilde{X}$ transitions (0.34) assigned in Section 5.A.4 as spin-orbit (Ω_c,ω) components $^3\Pi(1)$ and $^1\Pi(1)$, respectively, of the configuration ---$(3\pi)^3_{core}(2s\sigma)_{Ryd.}$. The larger value (0.56) in the present case indicates a closer approach to ideal (Ω_c,ω) coupling. From Fig. 3.5, the quantity $T_o\tilde{G}\,^1\Pi(1) - T_o\tilde{c}\,^3\Pi(1)$ should then be smaller in magnitude than $T_o\,\tilde{E}\,^1\Pi(1) - T_o\tilde{a}\,^3\Pi(1)$ These quantities are 1820.7 cm^{-1} and 2610 cm^{-1}, respectively. This qualitative agreement between theoretical prediction and experimental data offers support for the present hypothesis. Also, a value of 1820.7 cm^{-1} for this energy separation is in good agreement with data obtained for other molecules in which selenium is the constituent atom of greatest mass i.e.

(a) The energy separation of the zeroth-vibrational energy levels of the $^1\Pi_u(1)$ and $^3\Pi_u(1)$ states of the $---(\pi_g)^3_{core}(2p\sigma_u)_{Ryd}$ configuration of CSe_2 has been measured[64] to be 2019±40 cm^{-1}.

(b) The spin-orbit coupling constant in the $^2\Pi_i$ ground state of the radical HSe has been reported[107] to be -1815±100 cm^{-1}.

From Table 4.2, $T_{2p\pi}$(calc.) for OCSe is 15943 cm^{-1}. The first ionization potential of OCSe is, from this work, 81436±100 cm^{-1} ($\tilde{X}^2\Pi_i$ $OCSe^+$ average) c.f. section 5.A.8). Then, from equation 3.4, $\sigma(2p\sigma)$ OCSe is 65493 cm^{-1}. If the $\tilde{G}$ and $\tilde{c}$ states are correctly assigned, the average of the T_o-values for the $\tilde{G} \leftarrow \tilde{X}$ and $\tilde{c} \leftarrow \tilde{X}$ transitions may be taken as being an approximation to $\sigma(2p\sigma)$. This quantity is 65298.9 cm^{-1}. The excellent agreement between the calculated and experimental term values supports the present assignments.

All of the bands assigned to $\tilde{G} \leftarrow \tilde{X}$ and $\tilde{c} \leftarrow \tilde{X}$ (but not $\tilde{F} \leftarrow \tilde{X}$) are diffuse. The diffuseness observed in the bands assigned to transitions to lower excited states of OCSe has been attributed to predissociation by a neighbouring dissociative $^1\Pi(1)$ state (c.f. Section 5.A.6).

The bands at $\tilde{c} \leftarrow \tilde{X}$ and $\tilde{G} \leftarrow \tilde{X}$ are not as diffuse as those at $\tilde{E} \leftarrow \tilde{X}$. It is not, however, unreasonable to attribute the diffuseness of the bands of the former transition to predissociation by this $^1\Pi(1)$ state. The analysis of $\tilde{c}$ and $\tilde{G}$ as being of the same symmetry and Ω quantum number is consistent with this interpretation.

The analogous (1420 Å - 1550 Å) absorption system of OCS has been investigated by several authors[33,77,108,109]. This absorption system is remarkably similar in appearance and intensity to the OCSe spectrum in the 1560 Å - 1420 Å region. Kopp[103] has assigned the symmetries of the excited states in four electronic transitions of OCS which

occur in this spectral region. These are: $\tilde{E}\ ^1$ or $^3\Pi(1)$, $\tilde{F}\ ^1$ or $^3\Pi(1)$, $\tilde{I}\ ^1$ or $^3\Pi(1)$ and $\tilde{N}\ ^1\Sigma^+(0^+)$. However, the configurations from which these states arise were not specified. As will be shown in Section 5.B.2., good evidence exists for the assignment of $\tilde{E}$ and $\tilde{F}$ to the states $^3\Pi(1)$ and $^1\Pi(1)$ respectivly, of the $---(3\pi)^3_{core}(2p\sigma)_{Ryd}$ configuration, and for the assignment of $\tilde{N}$ to $^1\Sigma^+(0^+)$ of the configuration $---(3\pi)^3(2p\pi)$.

The measured oscillator strength (2.4×10^{-2}) of the $\tilde{F} \leftarrow \tilde{X}$ transition of OCSe is larger than that measured for either $\tilde{G} \leftarrow \tilde{X}$ (1.8×10^{-2}) or $\tilde{c} \leftarrow \tilde{X}$ (1.1×10^{-2}). This is taken to indicate that $\tilde{F} \leftarrow \tilde{X}$ is also an allowed transition. As has been previously stated, the fact that the bands assigned to $\tilde{F} \leftarrow \tilde{X}$ are sharp-headed indicates that the symmetry, and Ω quantum number, of $\tilde{F}$ is different from that of either $\tilde{c}$ or $\tilde{G}$. In the discussion of the correlation of the states, which arise from the configuration $---(\pi)^3_{core}(np\pi)_{Ryd}$, between the spin-orbit coupling cases (Λ,S) and (Ω_c,ω) (c.f. Chapter 3 Section 3.3.3), it was pointed out that the transition $^1\Sigma^+(0^+) \leftarrow \tilde{X}\ ^1\Sigma^+$ is fully allowed in both coupling cases. $\tilde{F}$, here assigned the symmetry $^1\Sigma^+(0^+)$, most probably arises from the OCSe configuration $(3\pi)^3_{core}(2p\pi)_{Ryd}$. Also, $T_{2p\pi}$ (calc) for OCSe is, from Table 4.2, 16782 cm^{-1}. The separation of the origin energy of $\tilde{F} \leftarrow \tilde{X}$ from I.P.(OCSe) is $\sim$ 16899 cm^{-1}. This agreement of the calculated and experimental term values is obvious support for the present assignment.

The assignments of the symmetries of $\tilde{d}$ and $\tilde{H}$ is somewhat tentative. The measured oscillator strengths of the $\tilde{d} \leftarrow \tilde{X}$ and $\tilde{H} \leftarrow \tilde{X}$ transitions are 3.2×10^{-3} and 8.6×10^{-3}, respectively. Because the bands assigned to these transitions are slightly diffuse, it is probable that these

states ($\tilde{d}$ and $\tilde{H}$) are both of Ω quantum number 1. It is unlikely that either $\tilde{d}$ or $\tilde{H}$ arise from the electron configurations ---$(3\pi)^3_{core}(2p\pi)_{Ryd}$ because, as has been discussed in Chapter 3, Section 3.3.3 the transition (from $\tilde{X}\ ^1\Sigma^+$) to the state $^1\Sigma^+(0^+)$ of this configuration should alone be of observable intensity. Rather, an assignment of these states in terms of the configuration ---$(3\pi)^3_{core}(3d)_{Ryd}$ of OCSe is proposed.

It was stated in Chapter 3, Section 3.3.1 that, for molecules containing a large end-atom, the molecular and large end-atom term values for corresponding Rydberg series members should be similar. For atomic selenium, the largest term value for the d Rydberg series is $\sim$ 13380 cm^{-1} [76]. The average of the T_o- values of the $\tilde{d} \leftarrow \tilde{X}$ and $\tilde{H} \leftarrow \tilde{X}$ transitions is $\sim$ 67221 cm^{-1}. Then I.P.(OCSe)-67721 cm^{-1} = 13715 cm^{-1}. If the latter quantity is taken as an approximation to T_{3d} of OCSe, the agreement between this value and the SeI term value allows some confidence in the present hypothesis.

However, a problem which arises in this assignment is the fact that several --- $(\pi)^3_{core}(nd)_{Ryd}$ configurations, viz.---$(3\pi)^3_{core}(3d\sigma)_{Ryd}$, ---$(3\pi)^3_{core}(3d\pi)_{Ryd}$ and ---$(3\pi)^3_{core}(3d\delta)_{Ryd}$, are possible. The correlation of states, between the coupling cases (Λ,S) and (Ω_c,ω), for the first two of these configurations should be similar to the correlations shown in Fig. 3.5 and Fig. 3.6. For the states which arise from the configuration ---$(3\pi)^3(3d\delta)$, a correlation diagram may also be drawn. If a Hund's rule ordering of these states (in (Λ,S) coupling) is assumed, then

(i) Transitions (from $\tilde{X}\ ^1\Sigma^+$) to the states $^1\Pi(1)$ and $^3\Pi(1)$ only of this configuration should occur with observable intensity and

(ii) The separation of the origin energies of these transitions should be intermediate in magnitude between $|X|$ and $|A|$, and should tend towards $|A|$ as the coupling approaches pure (Ω_c,ω).

The separation of the origin energies of the $\tilde{d} \leftarrow \tilde{X}$ and $\tilde{H} \leftarrow \tilde{X}$ transitions is $\sim 1861\ cm^{-1}$. This quantity is similar in magnitude to the value of $T_o(\tilde{G} \leftarrow \tilde{X}) - T_o(\tilde{c} \leftarrow \tilde{X})$. If the diffuseness of the bands of $\tilde{d} \leftarrow \tilde{X}$ and $\tilde{H} \leftarrow \tilde{X}$ is attributed to predissociation by the dissociative $^1\Pi(1)$ state, then the assignments $\tilde{d}\ ^3\Pi(1)$ and $\tilde{H}\ ^1\Pi(1)$ are reasonable. However, it is not possible, on the basis of the present experimental evidence, to state whether $\tilde{d}$ and $\tilde{H}$ arise from the configuration $---(3\pi)^3_{core}(3d\sigma)_{Ryd}$ or from $---(3\pi)^3_{core}(3d\delta)_{Ryd}$.

5.A.7.3 Bond lengths in the $\tilde{c}$, $\tilde{F}$ and $\tilde{G}$ states

Several methods, by which the band lengths in the excited states of OCSe may be calculated, have been given in Section 5.A.5. These are applied here to obtain estimates of the bond lengths r_{co} and r_{cse} in the excited states $\tilde{c}$, $\tilde{F}$ and $\tilde{G}$. The assignments and intensity data quoted in Table 5.8 have been used in these calculations. Because

(i) all of these states are Rydberg states of linear OCSe and

(ii) The Franck-Condon intensity distributions among vibronic components of $\tilde{c} \leftarrow \tilde{X}$, $\tilde{F} \leftarrow \tilde{X}$ and $\tilde{G} \leftarrow \tilde{X}$ are remarkably similar and

(iii) The Franck-Condon intensity maximum lies close to the origin in each case,

the molecular geometries in $\tilde{c}$, $\tilde{F}$ and $\tilde{G}$ are expected to be similar and to be only slightly changed from the molecular geometry in $\tilde{X}\ ^1\Sigma^+$.

The results of these calculations are shown in Table 5.9. Since the excited electron comes, in each case, from a bonding orbital, bond lengths are expected to increase. The bands assigned to $\tilde{F} \leftarrow \tilde{X}$ and $\tilde{G} \leftarrow \tilde{X}$ are red-degraded. Then, $B'(\tilde{F})$ and $B'(\tilde{G}) < B'(\tilde{X}\,{}^1\Sigma^+)$. An increase in both bond lengths, from those in $\tilde{X}({}^1\Sigma^+)$, is expected in Rydberg states of OCSe (c.f. Section 5.A.5). Accordingly, the bond lengths of Franck-Condon possibility (iv) are chosen in each case as the best approximations to the actual bond lengths in the $\tilde{c}$, $\tilde{F}$ and $\tilde{G}$ states of OCSe. The similarity of these calculated bond lengths to those calculated for the $\tilde{E}$ (Rydberg) state (c.f. Table 5.7) of OCSe should be noted.

5.A.8 Description and Analysis of the Bands of OCSe in the 68295 cm^{-1} (1464 Å) - 82165 cm^{-1} (1217 Å) Region

5.A.8.1. Description

The McPherson monochromator was used, in this work, to record, at low resolution, the absorption spectrum of OCSe vapour in the 1464 Å - 1217 Å region. A recording of the spectrum in this region is reproduced in Fig. 5.7. The absorption bands have been arranged into several progressions in which the frequency interval between successive members is in the range of $\sim$ 530 cm^{-1} - $\sim$ 490 cm^{-1}. The frequency interval of $\sim$ 1350 cm^{-1} is also prominent in the spectrum. The following features are distinguishable (c.f. Fig. 5.7):

(i) Several moderately strong bands of frequency interval of ~530 cm^{-1} which are assigned to the $\tilde{H} \leftarrow \tilde{X}$ transition (cf. Section 5.A.7). The first member of this series is the most intense.

TABLE 5.9

Possible Band Lengths for OCSe in the $\tilde{c}$, $\tilde{F}$ and $\tilde{G}$ States.

$\tilde{c}$ State: Calculation		r_{CO} (Å)	r_{CSe} (Å)	B' (cm^{-1})
Clark's Rule		1.33	1.83	-
Badger's Rule		1.23	1.76	-
Franck-Condon Possibilities	(i)	1.14	1.81	.126
	(ii)	1.10	1.67	.143
	(iii)	1.18	1.61	.142
	(iv)	1.22	1.75	.125

$\tilde{F}$ State: Calculation		r_{CO} (Å)	r_{CSe} (Å)	B' (cm^{-1})
Clark's Rule		1.33	1.85	-
Badger's Rule		1.23	1.77	-
Franck-Condon Possibilities	(i)	1.12	1.83	.125
	(ii)	1.08	1.67	.145
	(iii)	1.20	1.59	.143
	(iv)	1.24	1.75	.124

$\tilde{G}$ State: Calculation		r_{CO} (Å)	r_{CSe} (Å)	B' (cm^{-1})
Clark's Rule		1.32	1.85	-
Badger's Rule		1.23	1.76	-
Franck-Condon Possiblities	(i)	1.12	1.81	.126
	(ii)	1.09	1.68	.143
	(iii)	1.20	1.61	.142
	(iv)	1.23	1.74	.125

(ii) A series of weak bands. These are assigned to correspond to vibronic components of $\tilde{G} \leftarrow \tilde{X}$ (cf. Section 5.A.7). The intensities of these bands decrease to higher energies.

(iii) A short series of moderately strong bands which form a progression of frequency interval of $\sim 511\ cm^{-1}$. These are assigned to the electronic transition $\tilde{I} \leftarrow \tilde{X}$. The first member of the progression is the most intense. These bands extend from 1439 Å - 1408 Å.

(iv) A short series of strong bands, which are assigned to another electronic transition viz. $\tilde{e} \leftarrow \tilde{X}$. The bands are arranged into two progressions. The frequency interval between the bands of the major progression which extends from 1423 Å - 1385 Å, is $\sim 527\ cm^{-1}$. The second member of this progression is the most intense. The first (and most intense) members of the first and second progressions are separated in energy by $\sim 1397\ cm^{-1}$.

(v) A series of very intense bands, which are assigned to the electronic transition $\tilde{J} \leftarrow \tilde{X}$. These bands, which form in progression of frequency interval of $\sim 512\ cm^{-1}$, extend from 1388 Å - 1359 Å, and are, next to the bands of the $\tilde{E} \leftarrow \tilde{X}$ transition, the most intense features observed in the OCSe absorption spectrum. The intensity decreases somewhat uniformly from the first to the last member of the progression.

(vi) Overlapped by the bands of $\tilde{J} \leftarrow \tilde{X}$ are a weak series of bands which form a progression of frequency intervals of $\sim 506\ cm^{-1}$. These bands, which extend from 1381 Å - 1363 Å, are assigned to the transition $\tilde{f} \leftarrow \tilde{X}$.

(vii) A short series of weak bands, which form a progression of frequency interval of $\sim$ 482 cm^{-1}, extends from 1348 Å - 1330 Å. The first member is the most intense. These bands are assigned to the transition $\tilde{K} \leftarrow \tilde{X}$.

(viii) In the region 1330 Å - 1212 Å, the OCSe absorption spectrum consists of a very complex series of overlapping bands. These bands could not be arranged into progressions in a repeated frequency interval. They remain unassigned. However, these bands appear to converge to two strong, broad, equally intense absorption features at 80710 cm^{-1} and 82163 cm^{-1} ($\Delta\nu$ = 1453 cm^{-1}). These latter features are assigned to the limits of the Rydberg series of OCSe i.e. the average of the energies of these absorption features corresponds to the energy of formation (from OCSe) of $OCSe^+$ in its ground ($\tilde{X}\ ^2\Pi_i$) electronic state.

The measured frequencies relative intensities, and assignments of these bands are given in Table 5.10.

5.A.8.2. Analysis

As has been discussed in Section 5.A.7, the absorption spectrum which corresponds to a Rydberg transition of OCSe shows a distinctive intensity distribution and frequency interval pattern. The interval of $\sim$ 500 cm^{-1} has been consistently assigned in this work, and in that of Bavia, Galloni, Di Lonardo and Trombetti[12], to ν_3'. Also, the interval of $\sim$ 1370 cm^{-1} has been assigned previously to ν_1'. All of the excited electronic states here discussed are, most probably, Rydberg states of linear OCSe. They arise from the same "core" electron configuration

TABLE 5.10

Measured Bands of OCSe in the 68295 cm^{-1} (1464 Å) - 82165 cm^{-1} (1217 Å) Region.

Band Frequency* (cm^{-1})	Relative Intensity**	Assignment	
		Electronic	Vibronic
68630	0.9	$\tilde{G} \leftarrow \tilde{X}$	$1_0^1 3_0^2$
68827	w.	$\tilde{G} \leftarrow \tilde{X}$	3_0^5
68896	1.3	$\tilde{H} \leftarrow \tilde{X}$	3_0^1
69223	1.1	$\tilde{H} \leftarrow \tilde{X}$	3_0^2
69362	w.	$\tilde{G} \leftarrow \tilde{X}$	3_0^6
69493	1.8	$\tilde{I} \leftarrow \tilde{X}$	0_0^0
69742	0.4	$\tilde{H} \leftarrow \tilde{X}$	3_0^3
70004	1.8	$\tilde{I} \leftarrow \tilde{X}$	3_0^1
70259	2.8	$\tilde{e} \leftarrow \tilde{X}$	0_0^0 $[^3\Pi(1) \leftarrow {}^1\Sigma^+]$
70522	1.6	$\tilde{I} \leftarrow \tilde{X}$	3_0^2
70786	4.2	$\tilde{e} \leftarrow \tilde{X}$	3_0^1
71022	0.9	$\tilde{I} \leftarrow \tilde{X}$	3_0^3
71301	2.8	$\tilde{e} \leftarrow \tilde{X}$	3_0^2
71656	3.8	$\tilde{e} \leftarrow \tilde{X}$	1_0^1
71839	1.5	$\tilde{e} \leftarrow \tilde{X}$	3_0^3
72046	6.4	$\tilde{J} \leftarrow \tilde{X}$	0_0^0 $[^1\Pi(1) \leftarrow {}^1\Sigma^+]$
72190	w.	$\tilde{e} \leftarrow \tilde{X}$	$1_0^1 3_0^1$
72357	-	$\tilde{t} \leftarrow \tilde{X}$	0_0^0 $[^3\Pi(1) \leftarrow {}^1\Sigma^+]$
72558	5.8	$\tilde{J} \leftarrow \tilde{X}$	3_0^1
72881	-	$\tilde{t} \leftarrow \tilde{X}$	3_0^1

TABLE 5.10 (cont'd)

Band Frequency* (cm^{-1})	Relative Intensity**	Assignment	
		Electronic	Vibronic
73062	4.8	$\tilde{J} \leftarrow \tilde{X}$	3_0^2
73383	-	$\tilde{t} \leftarrow \tilde{X}$	3_0^2
73443	w.	$\tilde{J} \leftarrow \tilde{X}$	1_0^1
73567	2.4	$\tilde{J} \leftarrow \tilde{X}$	3_0^3
74176	3.1	$\tilde{K} \leftarrow \tilde{X}$	0_0^0 [$^1\Pi(1) \leftarrow {}^1\Sigma^+$]
74660	2.1	$\tilde{K} \leftarrow \tilde{X}$	3_0^1
75154	1.2	$\tilde{K} \leftarrow \tilde{X}$	3_0^2
75626			u.a.[a]
75873			u.a
76263			u.a.
67383			u.a.
76775			u.a.
77340			u.a.
77658			u.a.
77730			u.a.
78043			u.a.
78113			u.a.
78570			u.a.
78764			u.a.
79014			u.a.
79258			u.a.
79808			u.a.
80710		Rydberg series limit ($^2\Pi_{3/2}$ OCSe$^+$)	
81208		E ($^2\Pi_{3/2}$ OCSe$^+$) + ν_3' ?.	
82163		Rydberg series limit ($^2\Pi_{1/2}$ OCSe$^+$)	

* Vacuum wavenumbers (cm^{-1}). Estimated accuracy ± 20 cm^{-1}.

** Values are absorbance ratios, ie. $\log^I 0/I_A \,/\, \log^I 0/I_B$. B is chosen as the origin band of c X (64388.6 cm^{-1}((c.f. Fig. 5.7).

[a] u.a. = unassigned.

-- $(3\pi)^3$. Because Rydberg orbitals are, by definition, largely non-bonding, it is hardly surprising that these ν_1' and ν_3' frequencies should be very similar in each of the Rydberg states of OCSe.

The assignments of the ν_1' and ν_3' frequencies in the $\tilde{G}$, $\tilde{H}$, $\tilde{I}$, $\tilde{e}$, $\tilde{J}$, $\tilde{f}$ and $\tilde{K}$ states are consistent with the previous assignments of these quantities. Also, the assignments of the origin (0_0^0) bands of these transitions which, in each case, is the first (lowest-energy) strong band observed in the spectrum corresponding to the transition, is consistent with the Franck-Condon intensity distribution expected for a small change in molecular geometry upon electronic excitation. These assignments are tentative, pending a high resolution study of these absorption features. However, these vibronic assignments are, in general, in agreement with those of Bavia, Di Lonardo, Galloni and Trombetti[12] (c.f. Table 1.3).

The excited states $\tilde{H}$ and $\tilde{G}$ have been previously assigned (c.f. Section 5.A.7). From the available experimental evidence, it is not possible to assign unambiguously the symmetry of the excited state $\tilde{I}$. However, it is possible that $\tilde{I}$ is a component state of the -- $(3\pi)^3_{core}(3d)_{Ryd}$ configuration. The neighbouring $\tilde{d}$ and $\tilde{H}$ states have been assigned (c.f. Section 5.A.7) as states which arise from this configuration. The measured oscillator strength of the $\tilde{I} \leftarrow \tilde{X}$ transition is $\sim 1.5 \times 10^{-2}$.

The separation of the origin energies of the $\tilde{e} \leftarrow \tilde{X}$ ($f \sim 2.6 \times 10^{-2}$) and $\tilde{J} \leftarrow \tilde{X}$ ($f \sim 3.5 \times 10^{-2}$) transitions is 1787 cm^{-1}. (Some bands assigned to these transitions were recorded photographically under high resolution. The bands appear to be sharp-headed and red-degraded.)

The excited states $\tilde{e}$ and $\tilde{J}$ are assigned the symmetries $^3\Pi(1)$ and $^1\Pi(1)$, respectively, because

(i) $T_{3s\sigma}$ (calc.) of OCSe is, from Table 4.2, 10953 cm^{-1}. If the average of the T_o-values for the $\tilde{e} \leftarrow \tilde{X}$ and $\tilde{J} \leftarrow \tilde{X}$ transitions ($\sim$ 71053 cm^{-1}) is taken as an approximation to $\sigma_{3s\sigma}$ (obs.), the energy separation of the I.P. of OCSe and this latter quantity is 10284 cm^{-1} = $T_{3s\sigma}$(OCSe).

(ii) The energy separation of the origin bands of the $\tilde{e} \leftarrow \tilde{X}$, and $\tilde{J} \leftarrow \tilde{X}$ transitions is 1787 cm^{-1}. This value, and the ratio of the measured oscillator strengths of $\tilde{e} \leftarrow \tilde{X}$ and $\tilde{J} \leftarrow \tilde{X}$ (0.74) are consistent with the expected increase in the strength of spin-orbit coupling from that in the configuration $(3\pi)^3_{core}(2s\sigma)_{Ryd}$ (c.f. Section 5.A.5).

(iii) The excited state $\tilde{E}$ has been assigned (in Section 5.A.5) to the component state $^1\Pi(1)$ of the $(3\pi)^3_{core}(2s\sigma)_{Ryd}$ configuration. The bands assigned to $\tilde{E} \leftarrow \tilde{X}$ are the most intense observed in the OCSe absorption spectrum. It is therefore reasonable to assign the very intense bands of the $\tilde{e} \leftarrow \tilde{X}$ and $\tilde{J} \leftarrow \tilde{X}$ transitions to the second (3s) Rydberg s-series member.

The excited states $\tilde{f}$ and $\tilde{K}$ are assigned to $^3\Pi(1)$ and $^1\Pi(1)$ of the configuration -- $(3\pi)^3(3p\sigma)$. The separation of the origin energies of these transitions (1801 cm^{-1}) and the ratio of the measured oscillator strengths of the $\tilde{f} \leftarrow \tilde{X}$ and $\tilde{K} \leftarrow \tilde{X}$ transitions ($\frac{6.8\times10^{-3}}{1.0\times10^{-2}}$ = 0.68) support these assignments. Also, where the average value, 1/2 ($T_o(\tilde{f} \leftarrow \tilde{X})$ + $T_o(\tilde{K} \leftarrow \tilde{X})$) = 73276 cm^{-1} is taken as an approximation to $\sigma_{3p\sigma}$, good agree-

ment is found between this experimental value and the calculated (from Table 4.2) value of $\sigma_{3p\sigma}$ (≈73547 cm^{-1}).

The complex series of absorption bands of OCSe, which occurs in the 1325 Å - 1250 Å region, are not assigned in this work. However, these bands appear to converge to two broad, equally intense features at 80710 cm^{-1} and 82163 cm^{-1}. These features are assigned to the limits of the Rydberg series of OCSe. The energy separation of these fearures (1453 cm^{-1}) is assigned to the spin-orbit coupling constant in the $\tilde{X}^2\Pi_i$ ground state of $OCSe^+$. The equal intensity of these features indicates that the coupling is near the pure (Ω_c,ω) limit.

In e.v. units, I.P. (OCSe) is then ∿ 10.1 e.v. ($\tilde{X}\ ^2\Pi_i$ $OCSe^+$ average). This slight increase over the value of I.P. (SeI) = 9.75 e.v.[76] is consistent with the increase found for I.P. (OCS) = 11.2 e.v.[77] over I.P. (SI) = 10.357 e.v.[76]

The molecular geometry and the vibrational frequencies in the $\tilde{X}\ ^2\Pi_i$ ground state of $OCSe^+$ should then be somewhat similar to valuos for these quantities obtained for the higher energy Rydberg states of OCSe i.e. r_{CO} ∿ 1.23 Å and r_{CSe} ∿ 1.74 Å; ν_1' ∿1350 cm^{-1}, ν_2' ∿390 cm^{-1} and ν_3' ∿ 490 cm^{-1}.

The origin energies and the assignments of the observed Rydberg series of OCSe are given in Table 5.11. Also included in this table are the calculated σ values for the OCSe Rydberg series.

TABLE 5.11

OCSe Rydberg Series. Comparison of Experimental and Calculated Energies.

n	$\nu(0_0^0)\,^1\Pi(1)$ (cm^{-1})	$\nu(0_0^0)\,^3\Pi(1)$ (cm^{-1})	$\Delta\nu$ (cm^{-1})	ν(average) (cm^{-1})	∂(obs.)*	σ_n(calc.)** (cm^{-1})
nsσ:						
2	58367	55757	2610	57062	0.06	57356
3	72046	70259	1787	71153		70483
4	-	-	-	-		75200
∞	82163	80710	1453	81436		
npσ:						
2	66209.3	64388.6	1820.7	65299	0.57	65493
3	74176	72375	1801	73276		73546
4	-	-	-	-		76699
∞	82163	80710	1453	81436		
npπ:	$\nu(0_0^0)\,^1\Sigma^+(0^+)$ (cm^{-1})					σ_n(calc.)* (cm^{-1})
2	64537.4					65381
3	-					73787
∞	82163					

*: The relationship, $T_n = R/(n+\partial)^2$ is used.

**: From I.P. (OCSe) average (81436 cm^{-1})

*: From I.P. to $^2\Pi_{1/2}$ $OCSe^+$ (82163 cm^{-1})

5.B.1 Description and Analysis of the 1565 Å - 1438 Å Absorption System of OCS

5.B.1.1. Description

A very intense, banded absorption system of OCS occurs in the spectral region 1564 Å - 1438 Å. This absorption system has been previously investigated under low resolution by several authors[33, 77, 109]. The bands of this system have been photographed, in this work, under the high resolution of the Eagle instrument. The following features were distinguished in the spectrum:

(i) The dominant feature of this absorption system is a series of very intense, very diffuse bands. These are assigned to a progression in a frequency interval which decreases from ~ 840 cm^{-1} to 725 cm^{-1} for the higher-energy progression members. A minor progression of relatively weak bands may also be distinguished. The first members of the major and minor progressions are separated by the frequency interval of ~ 1742 cm^{-1}.

(ii) A short series of relatively weak red-degraded bands which appear to be sharp-headed. These are assigned to a progression in a frequency interval of ~ 730 cm^{-1}.

(iii) The members of the major progression in series (i) appear to be overlapped by a series of weak diffuse bands. However, the general diffuseness of the spectrum did not allow the measurement and assignment of these bands.

The measured frequencies, descriptions, relative intensities and assignments of the bands of OCS in this region are given in Table 5.12.

TABLE 5.12

Measured Bands of OCS in the 63900 cm^{-1} (1564.9 Å) - 69500 cm^{-1} (1438.8 Å) Region.

Band Frequency* (cm^{-1})	Description**	Relative Intensity[a]	Assignment	
			Electronic	Vibronic
63930	v. dif.	0.26 (298°K) 0.35 (500 K)	$\tilde{E} \leftarrow \tilde{X}$	3_1^0
64094	v. dif.	0.24 (298°K) (500 K)	$\tilde{a} \leftarrow \tilde{X}$	0_0^0? ($^3\Pi(1) \leftarrow {}^1\Sigma^+$)
64788	v. dif.	1.0	$\tilde{E} \leftarrow \tilde{X}$	0_0^0 ($^1\Pi(1) \leftarrow {}^1\Sigma^+$)
65610	v. dif.	1.05	$\tilde{E} \leftarrow \tilde{X}$	3_0^1
65970	sh., r.d.	w	$\tilde{D} \leftarrow \tilde{X}$	0_0^0? ($^1\Sigma^+ \leftarrow {}^1\Sigma^+$)
66428	v. dif.	1.0	$\tilde{E} \leftarrow \tilde{X}$	3_0^2
66530	v. dif.	w	$\tilde{E} \leftarrow \tilde{X}$	1_0^1
66701	sh., r.d.	w	$\tilde{D} \leftarrow \tilde{X}$	3_0^1
67208	v. dif.	0.8	$\tilde{E} \leftarrow \tilde{X}$	3_0^3
67333	v. dif.	w	$\tilde{E} \leftarrow \tilde{X}$	$1_0^1 3_0^1$
67413	sh., r.d.	w	$\tilde{D} \leftarrow \tilde{X}$	3_0^2
67967	v. dif.	0.4	$\tilde{E} \leftarrow \tilde{X}$	3_0^4
68705	v. dif.	0.2	$\tilde{E} \leftarrow \tilde{X}$	3_0^5
69430	v. dif.	0.1	$\tilde{E} \leftarrow \tilde{X}$	3_0^6

TABLE 5.12 (cont'd)

---

* Vacuum wavenumbers (cm^{-1}). Estimated accuracy $\pm$ 30 cm^{-1}. Measurements are from photographic enlargments of the spectrum.

** dif. = diffuse, sh. = sharp-headed.

[a] Values are absorbance ratios ie. $\log {}^{I}0/I_A \Big/ \log {}^{I}0/I_B$. B is chosen as the band at 64788 cm^{-1}.

A low-resolution (McPherson monochromator) recording of the spectrum is reproduced in Fig. 5.9.

5.B.1.2. Analysis

The intensity of the absorption band at 63930 cm^{-1} (but not that of the band at 64094 cm^{-1}) increases as the temperature of the absorbing gas is increased. (c.f. Fig. 5.9). The energy separation of this band and the strong band at 64788 cm^{-1}, 858 cm^{-1}, is close to the value for ν_3'' (OCS) (858.9 cm^{-1})[5]. These bands are assigned to the vibronic components 3_0^1 and 0_0^0 of the electronic transition $\tilde{E} \leftarrow \tilde{X}\ ^1\Sigma^+$. The frequency intervals of from ~ 840 cm^{-1} to ~ 725 cm^{-1} for the other bands assigned to $\tilde{E} \leftarrow \tilde{X}$ can be assigned in confidence to ν_3'. This assignment is consistent with the ν_3' intervals assigned for various excited electronic states of OCS[33, 77]. The intervals between the bands assigned to $\tilde{D} \leftarrow \tilde{X}$ (c.f. Table 5.12) are also assigned to ν_3'. In the assignment of the bands of $\tilde{E} \leftarrow \tilde{X}$, ν_1' ~1742 cm^{-1} (ν_1'' = 2062.2 cm^{-1})[5].

The band at 64094 cm^{-1} is assigned to the origin (0_0^0) band of the transition $\tilde{a} \leftarrow \tilde{X}$. Those [series (iii)] bands, which overlap the intense bands of $\tilde{E} \leftarrow \tilde{X}$, form a progression, with the band at 64094 cm^{-1}, in a frequency interval of ~ 800 cm^{-1}.

The excited states $\tilde{E}$ and $\tilde{a}$ are most probably of the symmetry $^1\Pi(1)$ and $^3\Pi(1)$, respectively, and they arise from the $(3\pi)^3_{core}(2s\sigma)_{Ryd}$ configuration of linear OCSe. The relative intensities and energy separation of the origin bands of the $\tilde{a} \leftarrow \tilde{X}$ and $\tilde{E} \leftarrow \tilde{X}$ transitions

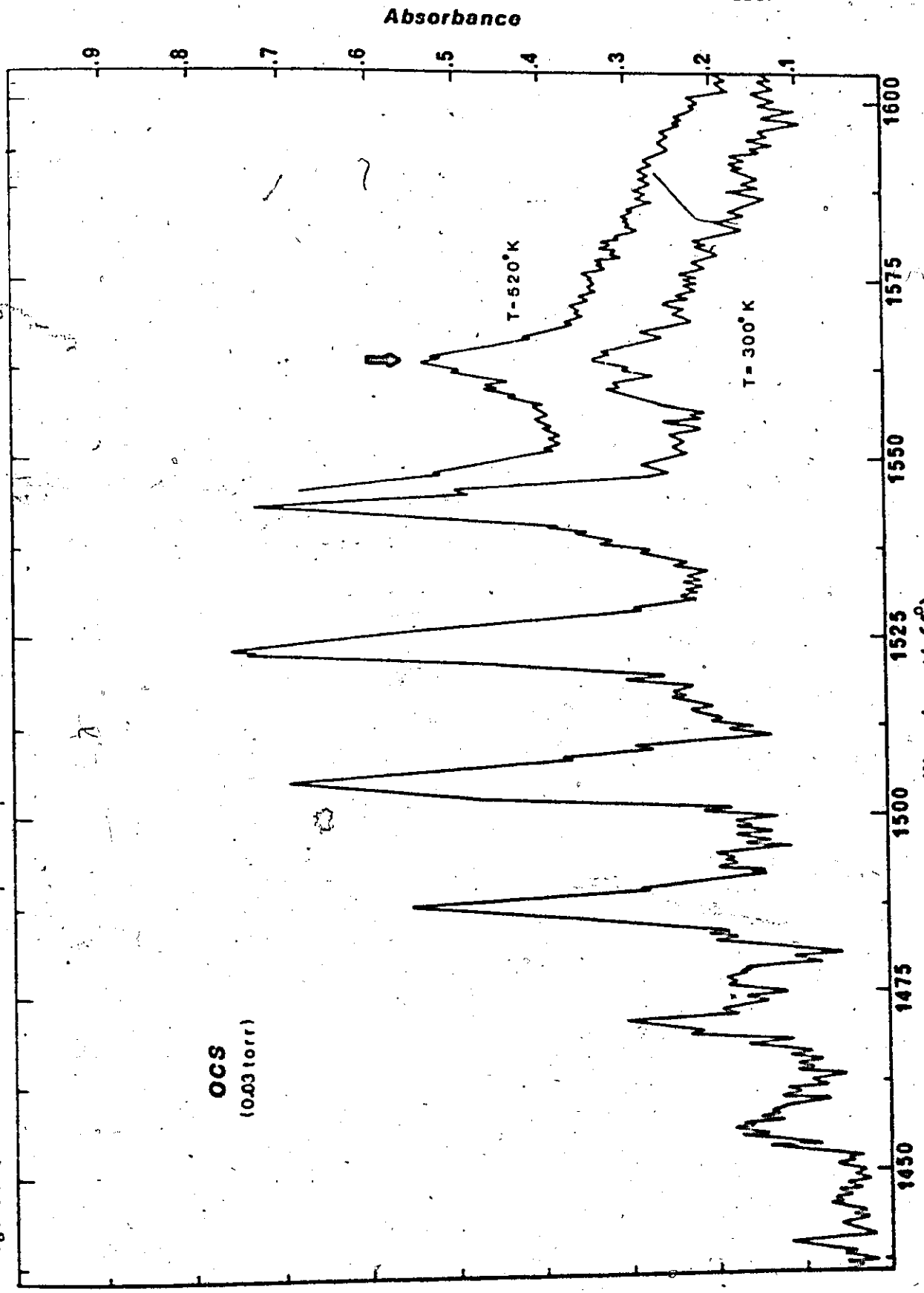

Fig. 5.9. Low resolution absorption spectrum of OCS in the 1435 Å - 1600 Å region.

(0.24 and 694 cm^{-1}) are consistent with this interpretation. [For OCS^+ ($\tilde{X}^2\Pi_i$) A = -370 cm^{-1}(77) and for CS_2^+ ($\tilde{X}^2\Pi_g$), A = -440.4 cm^{-1}(5)]. The bands assigned to $\tilde{E} \leftarrow \tilde{X}$ are the most intense features of the OCS absorption spectrum (ε_{max} = 4.2 X 10^4 liter $mole^{-1}$ cm^{-1}(33)). Also, the agreement between the value of $\sigma_{2s\sigma}$ (obs.) (here taken to be the centroid of the origin energies of the $\tilde{a} \leftarrow \tilde{X}$ and $\tilde{E} \leftarrow \tilde{X}$ transitions, 64411 cm^{-1}) and that of $\sigma_{2s\sigma}$ (calc.) OCS = 66104 cm^{-1} offers support for those assignments.

The sharp-headed red-degraded bands observed in this region are assigned to correspond to vibronic components of a separate electronic transition viz. $\tilde{D} \leftarrow \tilde{X}$. The excited state $\tilde{D}$ is, by analogy with the assignments discussed for OCSe in sections 5.A.4-8, most probably of $^1\Sigma^+$ symmetry and arises from the configuration --$(3\pi)^3$ (4π). Because similar predissociations mechanisms are expected to be operative in OCS and OCSe, the relative sharpness of the bands of $\tilde{D} \leftarrow \tilde{X}$ indicates that the state $\tilde{D}$ is of different Ω-value than the states $\tilde{a}$ and $\tilde{E}$.

Activity of the totally symmetric stretching vibrations ν_1' and ν_3' is consistent with the linear-linear assignments of these transitions.

5.B.2 Rydberg Transitions of OCS

The electronic states $\tilde{a}$ and $\tilde{E}$ of OCS have been shown (c.f. Section 5.B.1) to arise from the configuration --- $(3\pi)^3_{core}(2s\sigma)_{Ryd}$.

Kopp[108] has investigated the OCS spectrum in the 1450 Å - 1350 Å region and has assigned the symmetries of the excited states of four electronic transitions of OCS which occur in this region, viz. $\tilde{E}^1$ or $^3\Pi \leftarrow \tilde{X}^1\Sigma^+$, $\tilde{F}^1$ or $^3\Pi \leftarrow \tilde{X}^1\Sigma^+$, $\tilde{I}^1$ or $^3\Pi \leftarrow \tilde{X}^1\Sigma^+$ and $\tilde{N}^1\Sigma^+ \leftarrow \tilde{X}^1\Sigma^+$. Some evidence is now presented for the assignment of the $\tilde{E}$ and $\tilde{F}$ states (Kopps designation) to Rydberg states of linear OCS. These states are of $^3\Pi(1)$ and $^1\Pi(1)$ symmetry, respectively. They arise from the configuration --- $(\pi)^3_{core}(2p\sigma)_{Ryd}$. The evidence is:

(i) The bands assigned to the (B)$\tilde{E} \leftarrow \tilde{X}$ and (C)$\tilde{F} \leftarrow \tilde{X}$ transitions are double headed. This indicates a $\Delta\Omega = 1$ transition.

(ii) The separation of the origin energies of the $\tilde{E} \leftarrow \tilde{X}$ and $\tilde{F} \leftarrow \tilde{X}$ transitions is 528 cm^{-1}. This value is consistent with that found for $(\nu_C - \nu_B)$ in Section 5.B.1 (694 cm^{-1}) and with the value found[77] for the spin-orbit coupling constant, A, in the ---$(\pi)^3$ core of the OCS^+ molecule-ion (-370 cm^{-1}) if the coupling in the Rydberg states is intermediate between (A,S) and (Ω_c,ω). A similar relationship between the values for $(\nu_C - \nu_B)$ in the first ($2s\sigma$ and $2p\sigma$) Rydberg series members of OCSe and the A constant in the ---$(\pi)^3$ core of $OCSe^+$ has been described in Sections 5.A.4-8 ie. $(\nu_C - \nu_B)\ 2s\sigma > (\nu_C - \nu_B)\ 2p\sigma > |A|$.

(iii) From Table 4.1, $\sigma_{2p\sigma}$ (calc.) OCS is 73990 cm^{-1}. The average of the T_0 - values for the (Kopp's) $\tilde{E} \leftarrow \tilde{X}$ and $\tilde{F} \leftarrow \tilde{X}$ transitions (71172 cm^{-1}) may be taken as an approximation to $\sigma_{2p\sigma}$ (obs.). The reasonable agreement between these quantities is support for the

present assignments.

Also, it is reasonable to assign the excited state $\tilde{N}\ (^1\Sigma^+)$[108] as the state $^1\Sigma^+\ (0^+)$ of the --- $(3\pi)^3_{core}\ (2p\pi)_{Ryd}$ configuration. The agreement between the values of $\sigma_{2p\pi}$ (obs.) OCS, in this assignment (71817 cm^{-1})[108] and the value of $\sigma_{2p\pi}$ (calc.) OCS (from Table 4.2) (73191 cm^{-1}) is support for this hypothesis.

A series of strong absorption bands of OCS $\sim$ 77000 cm^{-1} has been assigned[33] to correspond to the second (here 3s) s-series member of OCS.

Matsunaga and Watanabe[77] have reported the energies of two Rydberg series of OCS, which converge to the first ionization potential of the molecule. These energies are given, approximately, by the relationships:

RI series:- $\nu_n(cm^{-1}) = 90210 - [R/(n + 0.425)^2]$

RII series:- $\nu_n(cm^{-1}) = 90580 - [R/(n + 0.425)^2]$,

where n = 2,3,4,5,6,7 in both equations. The magnitude of the ∂-value (0.425) indicates that both are p-series. The fact that two series, of identical ∂-value, and in which corresponding members are separated by approximately the spin-orbit coupling constant, A, of the $\tilde{X}^2\Pi_i$ ground state of OCS^+ (-372 cm^{-1})[5], indicates that these are pσ-series.

The energies of the Rydberg series of OCS, in these assignments, and the calculated (from Table 4.1) σ_n-values for OCS are compared in Table 5.13.

TABLE 5.13

OCS Rydberg Series. Comparision of Experimental[a] and Calculated Energies.

n	$\nu(0_0^0)\,^1\Pi(1)$ (cm^{-1})	$\nu(0_0^0)\,^3\Pi(1)$ (cm^{-1})	$\Delta\nu$ (cm^{-1})	ν(average) (cm^{-1})	δ^b(obs.)	σ_n(calc.) (cm^{-1})
nsσ:						
2	64788	64094	694	64411		66104
					0.15	
3	77273	76831	442	77052		79509
4	-	-	-	-		84249
⋮						
∞	90580	90210	370	90395		
npσ:						
2	71431(108)	70913(108)	528	71172		73990
					0.36	
3	81210(77)	80840(77)	370	81025		82331
					0.42	
4	84990	84620	370	84805		85562
					0.42	
5	86880	86500	380	86690		87175
					0.43	
6	87950	87570	380	87760		88102
					0.56	
7	88570	88210	360	88390		88685
⋮						
∞	90580	90210	370	90395		

n	npπ: $\nu(0_0^0)\,^1\Sigma^+(0)^+$ (cm^{-1})	σ_n(calc.)[d] (cm^{-1})
2	71817(108)	73191
3	-	82011
⋮		
∞	90580	

TABLE 5.13 (cont'd)

---

[a] : See text for discussion.

[b] : Where the relationship $T_n = R/(n+\delta)^2$ is used.

[c] : From I.P. (OCS) = 90395 cm^{-1} ($\tilde{X}^2\Pi_i$ average).

[d] : From I.P. (OCS) to $^2\Pi_{1/2}$ CSe^+ (90580 cm^{-1})

5.C.1. Description and Analysis of the Absorption Spectrum of CS_2 in the 1500 Å - 1650 Å Region.

5.C.1.1. Description.

The absorption spectrum of CS_2 has been recorded in this region. A low resolution (McPherson monochromator) recording of the spectrum is reproduced in Fig. 5.10. The spectrum consists of two very intense absorption bands, together with some weak satellite bands to the low-frequency side of each of the strong features. Under high resolution, some rotational structure of these bands could be resolved. The bands appear to be very slightly red-degraded and double-headed. The measured frequencies, relative intensities and assignments of these bands are given in Table 5.14.

5.C.1.2. Assignment.

The strong features of 62082.6 cm^{-1} and 62767.5 cm^{-1} are assigned as the origin bands of the electronic transitions (B) $^3\Pi_u(1) \leftarrow \tilde{X}^1\Sigma^+_g$ and (C) $^1\Pi_g(1) \leftarrow X^1\Sigma^+_g$, respectively. These states arise from the configuration --- $(\pi_g)^3(2p\sigma_u)$. The weak bands at 61963.6 cm^{-1} and 62016.2 cm^{-1} are assigned to vibronic components 1^1_1 and 1^2_2, respectively, of the first of these transitions.

These assignments are consistent with the following observations:

(1) The small change in the frequency of ν_1 (~66 cm^{-1}) upon electronic excitation is expected, because the highest filled M.O. and the Rydberg orbital of CS_2 are largely non-bonding. [The C - S bond lengths in the ground electronic states of $CS_2(^1\Sigma^+_g)$ and $CS_2^+(^2\Pi_g)$

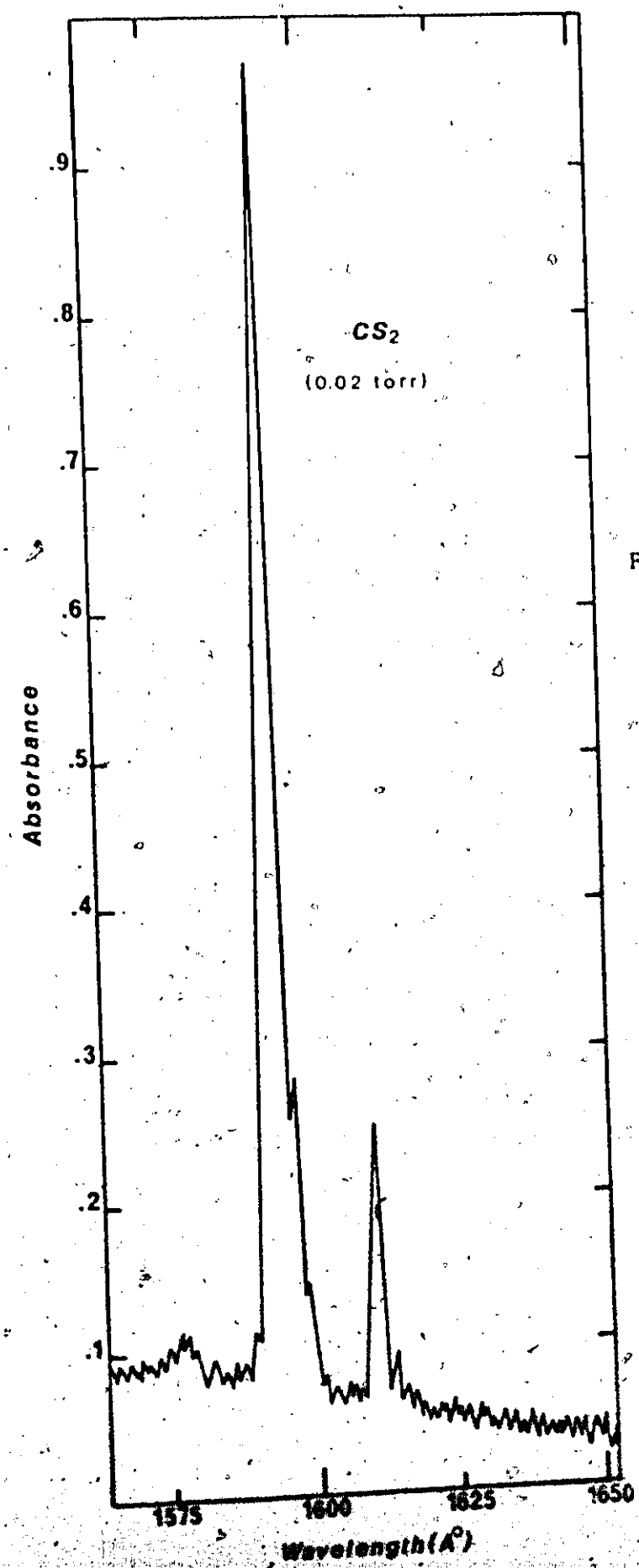

Fig. 5.10. Low resolution absorption spectrum of CS_2 in the 1560 Å - 1650 Å region.

TABLE 5.14

Measured Bands of CS_2 in the 61900 cm^{-1} (1615.5 Å) - 62800 cm^{-1} (1592.3 Å) Region.

Band Frequency* (cm^{-1})	Relative Intensity**	Assignment	
		Electronic	Vibronic
61963.9	v.w.		1_2^2
62016.2	w.		1_1^1
62082.6	1.0	$^3\Pi_u(1) \leftarrow X^1\Sigma^+_g$	0_0^0
62767.5	3.8	$^1\Pi_u(1) \leftarrow X^1\Sigma^+_g$	0_0^0

* Vacuum wavenumbers (cm^{-1}). Estimated accuracy ± 2 cm^{-1}.

** Absorbance ratio $\log I_0/I_A$ / $\log I_0/I_B$. B is chosen as the band at 62082.6 cm^{-1}.

are 1.554 Å and 1.564 Å, respectively. The value of ν_1 in $\tilde{X}(^1\Sigma^+_g)$ CS_2 is 657.98 cm^{-1}](5)

(ii) The energy separation of the origin bands of the C and B transitions is $(\nu_C - \nu_B)$ = 674.9 cm^{-1}. If the spin-orbit coupling in the --- $(\pi_g)^3$ $(2p\sigma_u)$ configuration of CS_2 is intermediate between (Λ,S) and (Ω_c,ω), this value is consistent with the values of the spin-orbit coupling constants, A, measured for the ground electronic states of CS_2^+ (A = -440.4 cm^{-1}) and OCS (A = -372 cm^{-1})(5).

(iii) Greening(64) has calculated $T_{2p\sigma}(CS_2)$ to be 18128 cm^{-1}. The I.P. of CS_2 is 10.079 e.v. ~81290 cm^{-1}(5). Then $\sigma_{2p\sigma}$ (calc.) = 63162 cm^{-1}. The agreement between this value and the value for the centroid of the origin energies of the B and C transitions of CS_2 (62425 cm^{-1}) is support for these assignments.

(iv) The ratio of the intensities of the origin bands of the B and C transitions, I_C/I_B ~0.26, is consistent with the interpretation ie. the coupling is intermediate between (Λ,S) and (Ω_c,ω).

(v) Tanaka, Jursa and LeBlanc(109) have assigned two Rydberg series of CS_2 which converge to the first ionization potential of CS_2. The energies of members of these series are given, approximately, by:

RI:- $\nu_n = 81735 - R/(n + 0.54)^2$ $\quad n = 3,4,5,\ldots$

RII:- $\nu_n = 81299 - R/(n + 0.56)^2$ $\quad n = 3,4,5,\ldots$

The ∂-values for these series indicate that they are p-series The bands of CS_2 at 62082.6 cm^{-1} and 62767.5 cm^{-1} may be the n=2 members of the RII and RI series, respectively.

CHAPTER VI

SUMMARY AND CONCLUSIONS

An efficient method of synthesis of Selenium-isotope carbonyl selenide (OCSe) has been developed in this work. So, also, has a new emission continuum source for absorption spectroscopy of the u.v. and v.u.v. regions.

The ground state fundamental frequencies of vibration of linear OCSe have been determined from an analysis of its infrared absorption spectrum.

The electronic absorption spectra of both of the isotopic species, $OCSe^{80}$ and $OCSe^{78}$, in the u.v. and v.u.v. spectral regions have been recorded under high resolution. Spectra due to both intra-valence shell and Rydberg transitions have been observed. Vibrational analyses have been accomplished and in several cases, the molecular structure in the excited states has been determined by a quantitative application of the Franck-Condon Principle.

The three regions of absorption, which lie at lowest energy, correspond to intravalence shell transitions. For two of these, the experimental results suggest that the molecule is bent in its excited electronic state and that photodissociation of the molecule occurs at these energies.

The Rydberg series of OCSe have been analyzed in terms of the symmetries and electron configurations of the excited (Rydberg) states.

Quantum-mechanical calculations of the term values of Rydberg series members of OCSe (and OCS) have been described and performed.

Although the model chosen for these calculations was conceptually simple, excellent agreement was found between the calculated and observed quantities for both of the molecules OCSe and OCS.

The spin-orbit coupling in the Rydberg states of OCSe (and OCS) has been shown to be intermediate in strength between the cases (Λ,S) and (Ω_c,ω) and to tend towards the latter for higher energy states. The ionization potential of OCSe has been measured.

BIBLIOGRAPHY

1. M. Born and J. R. Oppenheimer, Ann. Physik 84, 457 (1927).

2. E. B. Wilson, Jr., J. C. Decius and P. C. Cross, "Molecular Vibrations", McGraw-Hill Book Co., Inc., New York (1955). p. 283.

3. H. F. Hameka, "Advanced Quantum Chemistry", Addison-Wesley Publishing Co., Inc., Reading, Mass. (1965).

4. H. Eyring, J. Walter and G. E. Kimball, "Quantum Chemistry", John Wiley and Sons, Inc., New York (1960), p. 190 ff.

5. G. Herzberg, "Electronic Spectra of Polyatomic Molecules", D. Van Nostrand Co., Inc., Princeton, N.J. (1966).

6. R. M. Hochstrasser, "Molecular Aspects of Symmetry", W. A. Benjamin, Inc., New York (1966).

7. M. Tinkham, "Group Theory and Quantum Mechanics", McGraw-Hill Book Co., New York (1964).

8. G. W. King, "Spectroscopy and Molecular Structure", Holt, Rinehart and Winston, Inc., New York (1964).

9. G. Herzberg, "Spectra of Diatomic Molecules", D. Van Nostrand Co., Inc., Princeton, N.J. (1950), p. 193 ff.

10. "Report on Notation for the Spectra of Polyatomic Molecules", J. Chem. Phys. 23, 1997 (1955).

11. D. A. Stiles, W. J. R. Tyerman, O. P. Strausz and H. E. Gunning, Can. J. Chem. 44, 1677 (1966).

12. M. Bavia, G. DiLonardo, G. Galloni and A. Trombetti, J. Chem. Soc., Far. Trans. II, 68 (4), 615 (1972).

13. T. G. Pearson and P. L. Robinson, J. Chem. Soc. (London), 652 (1932).

14. R. H. Purcell and F. D. Zahoorbux, J. Chem. Soc. (London), 1029 (1937).

15. O. Glemser and T. Risler, Z. Naturforsch 3b, 1 (1948).

16. M. W. P. Strandberg, T. Wentink, Jr., and A. G. Hill, Phys. Rev. 75 (5), 827 (1949).

17. T. Wentink, Jr., J. Chem. Phys., 29 (1), 188 (1958).

18. T. Wentink, Jr., J. Chem. Phys. 30 (1), 105 (1959).

19. S. J. Cyvin, Spectrochim. Acta 11, 958 (1959).

20. R. S. McDonald and R. C. Lord, Spectroscopy Lab., M.I.T. (unpublished results), (1949).

21. H. Bastius and A. Lissner, Chem. Tech. (Berlin) 11, 82 (1959).

22. N. N. Yarovenko, G. B. Gazieva, V. N. Shemanina and N. A. Fedorova, Zhur. Obschei Khim. 29, 940 (1959).

23. G. W. King, J. Sci. Instru. 35, 11 (1958).

24. A. W. Richardson, Ph.D. Thesis, McMaster University (1966).

25. J. J. Hopfield, Phys. Rev. 35, 1133 (1930).

26. R. E. Huffman, W. W. Hunt, Jr., Y. Tanaka and R. L. Novack, J. Opt. Soc. Am. 51, 693 (1961).

27. R. E. Huffman, Y. Tanaka, J. C. Larrabee, J. Opt. Soc. Am. 52, 851 (1962).

28. J. A. R. Samson, "Vacuum Ultraviolet Spectroscopy", John Wiley and Sons, Inc., New York (1967).

29. G. R. Harrison, ed., "M.I.T. Wavelength Tables", Camebridge, Mass., M.I.T. Press (1963).

30. B. Edlén, J. Opt. Soc. Am. 43, 339 (1953).

31. H. Sponer and E. Teller, Rev. Mod. Phys. 13, 75 (1941).

32. A. D. McLean and M. Yoshimine, "Tables of Linear Molecular Wavefunctions", p. 209, I.B.M. Corp. (1967).

33. J. W. Rabalais, J. M. McDonald, V. Scherr and S. P. McGlynn, Chem. Revs. 71, 73 (1971).

34. E. Clementi, I.B.M. Research Paper R-J-256 (Sept. 1963).

35. E. R. Farnworth, G. W. King and D. C. Moule, Chem. Phys. 1 (1), 82 (1973).

36. Ref. 5, p. 333.

37. Ref. 5, pp. 330-336 incl.

38. F. Hund, "Linenspektren und Periodisches System der Elemente", Springer-Verlag Ohg, Berlin (1927).

39. A. D. Walsh, J. Chem. Soc. 2266 (1953).

40. G. Herzberg and E. Teller, Z. Physik. Chem. B21, 410 (1933).

41. H. Sponer and E. Teller, Rev. Mod. Phys. 13, 90 (1941).

42. R. Renner, Z. Physik. 92, 172 (1934).

43. A. J. Merer and D. N. Travis, Can. J. Phys. 43, 1795 (1965).

44. J. A. Pople and H. C. Longuet-Higgins, Mol. Phys. 1, 372 (1958).

45. R. N. Dixon, Trans. Far. Soc. 60, 1363 (1964).

46. R. N. Dixon, Mol. Phys. 9, 357 (1965).

47. R. N. Dixon, G. Duxbury and D. A. Ramsay, Proc. Roy. Soc. A296, 137 (1967).

48. G. Herzberg and K. K. Innes, Can. J. Phys. 35, 842 (1957).

49. Ref. 8, p. 229 ff.

50. S. R. La Paglia, J. Mol. Spec. 10, 240 (1963).

51. A. D. Walsh, J. Phys. Radium 15, 501 (1954).

52. A. B. F. Duncan, "Rydberg Series in Atoms and Molecules", Academic Press, New York (1971).

53. U. E. Condon and G. H. Shortley, "The Theory of Atomic Spectra", Cambridge University Press (1935), p. 143.

54. R. S. Mulliken, J. Am. Chem. Soc. 86, 3183 (1964).

55. G. Herzberg, J. Mol. Spec. 41, 425 (1972).

56. G. Herzberg, "Atomic Spectra and Atomic Structure", Dover Publications, New York (1945).

57. Ref. 9, p. 333 ff.

58. Ref. 9, p. 295 ff.

59. R. S. Mulliken, Phys. Rev. 57, 500 (1940).

60. R. S. Mulliken and C. Rieke, Rep. Prog. Phys. 8, 231 (1941).

61. Ref. 5, p. 418.

62. O. Redlich, Z. Physik 78, 74 (1932).

63. A. Adel, Phys. Rev. 45, 56 (1934).

64. F. R. Greening, Ph.D. Thesis, McMaster University (1973).

65. A. D. Liehr, Z. Naturforsch 11a, 752 (1956).

66. C. A. Coulson and J. G. Stamper, Mol. Phys. 6, 609 (1963).

67. A. U. Hazi and S. A. Rice, J. Chem. Phys. 54, 3004 (1966).

68. H. Lefebre-Brion and C. M. Moser, J. Mol. Spec. 15, 211 (1965).

69. T. Betts and V. McKoy, J. Chem. Phys. 54, 113 (1971).

70. I. Prigodine and S. A. Rice (eds.), "Advances in Chemical Physics", Vol. XVI, p. 283 (1969).

71. I. V. Abarenkov and V. Heine, Phil. Mag. 11, 529 (1965).

72. J. D. Weeks and S. A. Rice, J. Chem. Phys. 49, 2741 (1968).

73. Ira N. Levine, "Quantum Chemistry", Vol. I, Allyn and Bacon, Boston, Mass. (1970) p. 115.

74. J. C. Slater,"Quantum Theory of Atomic Structure", McGraw-Hill Book Co., Inc., New York (1960), p. 461 ff.

75. Ref. 74, p. 110 ff.

76. C. E. Moore, N.B.S. Circular 467 (1949).

77. F. M. Matsunaga and K. Watanabe, J. Chem. Phys. 46, 11 (1967).

78. G. Runtz, McMaster University, private communication.

79. R. F. W. Bader and P. M. Beddall, Chem. Phys. Let. 8, 29 (1971).

80. M. B. Robin, Contributed Paper P1, Symposium on Molecular Structure and Spectroscopy, Columbus 1971.

81. G. Herzberg, "Infrared and Raman Spectra of Polyatomic Molecules", D. Van Nostrand Co. Inc., Princeton, N.J. (1945), p. 251 ff.

82. W. H. Breckenridge and H. Taube, J. Chem. Phys. 52, 1713 (1970).

83. Ref. 9, p. 295 ff.

84. E. Teller, J. Phys. Chem. 41, 109 (1937).

85. G. Herzberg and H. C. Longuet-Higgins, Disc. Far. Soc. 35, 77 (1963).

86. E.C.Y. Inn, K. Watanabe and M. Zelikoff, J. Chem. Phys. 21, 1648 (1953).

87. R. N. Dixon, Proc. Roy. Soc. 275A, 431 (1963).

88. B. Kleman, Can. J. Phys. 41, 2034 (1963).

89. A. J. Merer, Symposium on Molecular Structure and Spectroscopy, Columbus 1972.

90. K. Dressler and D. A. Ramsay, Phil. Trans. Roy. Soc. A251, 533 (1959).

91. R. N. Dixon, Trans. Far. Soc. 60, 1363 (1964).

92. W. R. Thorson and I. Nakagawa, J. Chem. Phys. 33, 994 (1960).

93. J. W. C. Johns, Can. J. Phys. 45, 2639 (1967).

94. J. T. Hougen and J. K. G. Watson, Can. J. Phys. 43, 298 (1965).

95. Ref. 5, Pg. 202-209.

96. R. S. Mulliken, Phys. Rev. 61, 277 (1942).

97. G. W. King and A. W. Richardson, J. Mol. Spec. 21, 339 (1966).

98. Ref. 5. P. 458 ff.

99. M. L. Ginter and S. G. Tilford, J. Mol. Spec. 34, 206 (1970).

100. Ref. 9, P. 457.

101. Linus Pauling, "The Nature of the Chemical Bond", Cornell University Press, N.Y. (1960) P. 231.

102. J. B. Coon, R. E. De Wames and C. M. Loyd, J. Mol. Spec. 8, 285 (1962).

103. Ref. 5, Pg. 593-598.

104. "Handbook of Chemistry and Physics", The Chemical Rubber Co., Cleveland (1967), Pg. F149-F154.

105. J. E. Ruedy and R. C. Gibbs, 46, 880 (1934).

106. Ref. 9, P. 520.

107. K. C. Smyth and J. I. Brauman, J. Chem. Phys. 56, 5993 (1972).

108. I. Kopp, Can. J. Phys. 45, 4011 (1967).

109. Y. Tanaka, A. S. Jursa and F. J. LeBlanc, J. Chem. Phys. 32, 1205 (1960).

110. J. U. Nef, Ann. Chem. 270, 309 (1892).

111. I. Ugi and R. Meyr, Chem. Ber. 93, 239 (1960).

112. J. L. Hencher, Ph.D. Thesis, McMaster University (1964), P. 141.

113. F. Ansbacher, Z. Naturforsch. 14a, 889 (1959).

APPENDIX A.1

A METHOD FOR SYNTHESIS OF $O^{18}CSe$ FROM O_2^{18}

An efficient method of synthesis of this species has been tested where O_2^{16} and natural selenium were used. It is a variation of the synthesis of the isotopic species $OCSe^{80}$ and $OCSe^{78}$ described in Chapter II, Section 2.3. In this variation, O^{18} is incorporated in the reactant isocyanate.

Phenyl isocyanide (ϕNC) was prepared in reasonable purity by two methods:

(i) that of J. U. Nef[110], which involved the reaction of aniline and chloroform in ethanolic KOH; and

(ii) that of I. Ugi and R. Meyr[111]. This method involved the reaction of potassium tert-butoxide [$(CH_3)_3COK$], phosphorus oxychloride ($POCl_3$) and N-phenyl formamide ($\phi NHCHO$).

The latter method was found to be the more efficient. The infrared spectrum of the purified product matched that of Ugi and Meyr.

Stoichiometric quantities of O_2 gas and Hg were reacted at 350°C to produce red powdered mercuric oxide (HgO). The isocyanide was distilled into this vessel and the mixture was heated to 150°C for 10 min. Oxidation of the isocyanide to the isocyanate by this method is known to be an efficient process. OCSe was then synthesized as previously described.

This method could also be adapted for production of $O^{18}CS$ and $O^{18}CO$ by the substitution of H_2S and H_2O, respectively, for H_2Se in the hydrolysis of the O^{18}-isocyanate.

APPENDIX A.2

CALCULATION OF THE GROUND STATE VIBRATIONAL POTENTIAL ENERGY DISTRIBUTION

The elements $(V_\lambda^\phi)_{\mu k}$ of the potential energy distribution matrix $[V_\lambda^\phi]$ are defined by[112]

$$(V_\lambda^\phi)_{\mu k} = \frac{1}{\lambda_\mu} J_{\mu k}^\phi \phi_k \qquad [A2.1]$$

where, for the μth normal vibration of frequency ν_μ, λ_μ and ν_μ related by the equation

$$\lambda_\mu = 4\pi^2 c^2 \nu_\mu^2 \qquad [A2.2]$$

and $J_{\mu k}^\phi$, an element of the Jacobian matrix $[J^\phi]$, is defined by

$$J_{\mu k}^\phi = \frac{\partial \lambda_\mu}{\partial \phi_k} \qquad [A2.3]$$

ϕ_k is the kth force constant.

For each vibrational frequency ν_μ, the elements of $[V_\lambda^\phi]$ are required to be normalized, i.e.,

$$\frac{1}{\lambda_\mu} \sum_{k=1}^{n_\phi} J_{\mu k}^\phi \phi_k = 1 \qquad [A2.4]$$

where n_ϕ is the number of force constants.

Considering only the totally symmetric normal vibrations, ν_1 and ν_3, of linear carbonyl selenide, the totally symmetric internal coordinates are defined by

$$S_1 = \zeta_2 - \zeta_1 \qquad [A2.5]$$

$$S_3 = \zeta_3 - \zeta_2$$

where ζ_i is the one-dimensional Cartesian displacement coordinate giving the

displacement of atom i from its equilibrium position. The relationships between the elements ζ_i and n_i (the mass-weighted Cartesian displacement coordinates) and between n_i and the normal coordinates Q_i are given by King[8]. The equation

$$[S] = [H][Q] \qquad [A2.6]$$

can be derived[N12] through use of these relationships. In this equation, [S] is the column matrix of S_1 and S_3 and

$$[H] = \begin{bmatrix} h_{11} & h_{13} \\ h_{31} & h_{33} \end{bmatrix} = \begin{bmatrix} -\ell'_{11} + \ell'_{21} - \ell'_{13} + \ell'_{23} \\ -\ell'_{21} + \ell'_{31} - \ell'_{23} + \ell'_{33} \end{bmatrix} \qquad [A2.7]$$

where $\ell'_{ij} = \sqrt{m_i}\,\ell_{ij}$. m_i is the mass of atom i and ℓ_{ij} is an element of the matrix [L] defined by

$$[n] = [L][Q] \qquad [A2.8]$$

The relationship

$$J_{\mu k} = h^2_{k\mu} \qquad [A2.9]$$

can be shown to hold for the totally symmetric normal vibrations (ν_1 and ν_3) of OCSe[24].

The known ground state vibrational frequencies and the atomic masses may be used to calculate the force constants and the [L] matrix elements[24]. In this calculation the model chosen is that of a linear ABC-type triatomic molecule in which the atoms are restricted to motion in the dimension of the molecular axis. Stretching force constants k_{AB} and k_{BC} between adjacent atoms only are considered, i.e., interactions between atoms A and C are assumed to be negligibly small.

APPENDIX A.3

MEASURED BANDS OF CS_2 IN THE 46700 cm^{-1} (2141.3 Å) - 51300 cm^{-1} (1949.3 Å) REGION

Band Frequency* (cm^{-1})	Intensity**
46759.8	vvw
46824.5	vvw
47179.8	vvw
47259.9	vvw
47414.0	vvw
47562.2	w
47598.6	w
47646.6	w
47711.6	vw
47732.6	vw
47784.2	vvw
47906.4	vvw
47980.0	s
48032.3	s
48068.6	vs
48112.3	vw
48140.9	vw
48202	vw
48346.3	vw
48425	w
48445.6	s
48478.0	s
48508	w
48534	w
48857	vs
48877.6	vs
48918.9	vs
48951.2	s

APPENDIX A.3 (cont'd.)

Band Frequency* (cm^{-1})	Intensity**
49048	s
49265	s
49278.8	vs
49358.6	s
49670.0	vs
49703.8	vs
49786.5	s
50059.2	vvs
50100.4	vvs
50192.5	s
50430.6	vvs
50453.5	vvs
50482.9	vvs
50592	s
50800.5	vs
50846.9	vs
50873.6	vs
50901.6	vs
51215	vs
51237	vs
51269	vs

*Vacuum wavenumbers (cm^{-1}). Estimated accuracy ±5 cm^{-1}. All of the observed bands are slightly diffuse and red-degraded.

**These values are estimates, relative to the intensities of neighbouring bands.

APPENDIX A.4

FRANCK-CONDON CALCULATIONS

The Franck-Condon Principle may be applied to obtain a quantitative estimate of the structural changes in molecules upon electronic excitation. The theory developed here is for the case where the symmetry of the molecule is the same in both electronic states involved in a transition.

The oscillator strength of a vibronic transition from the vibrational level v" of the ground electronic state to the vibrational level v' of an excited electronic state may be written as

$$f^{v',v''} = \kappa \sigma^{v',v''} \left| \int \psi_{v'}^{*}(Q')\psi_{v''}(Q'')dQ' \right|^2 \qquad [A4.1]$$

where κ is a constant,

$\sigma^{v',v''}$ is the wavenumber of the vibronic transition; and

Q" and Q' represent, collectively, the normal coordinates for the ground and excited states, respectively.

The total vibration wavefunction $\psi_v(Q)$ can be written as the product of a wavefunction $\phi_i(Q_i)$ for each Q_i, i.e.,

$$\psi_v(Q) = \prod_{i=1}^{n} \phi_i(Q_i) \qquad [A4.2]$$

where n = 3N-5 for a linear molecule with N nuclei. Then

$$f^{v',v''} = \kappa \sigma^{v',v''} \left| \int [\prod_j \phi_j(Q_j')][\prod_i \phi_i(Q_i'')]dQ_1' \ldots dQ_n' \right|^2 \qquad [A4.3]$$

The ground and excited state normal coordinates are related by the equation[102]

$$Q_i'' = \Sigma a_{ij} Q_j' + d_i \qquad [A4.4]$$

If the symmetry of the molecule is the same in both states in a transition, $a_{ij} \neq 0$ only if $r(Q_i'') = r(Q_j')$ and $d_i \neq 0$ only for totally symmetric normal coordinates. For those transitions which originate from the zeroth vibrational level of the ground electronic state, the ground state wavefunction may be assumed to a good approximation to be spherically symmetric. Then the ground state normal coordinates can be taken to be parallel to those of the excited state. Then, equation [A4.4] becomes

$$Q_i'' = Q_i' + d_i \qquad [A4.5]$$

and equation [A4.1] becomes

$$f^{v',0} = \kappa \sigma^{v',0} \mid \bar{M}^{v',0} \mid^2 \qquad [A4.6]$$

where the vibrational transition moment $\bar{M}^{v',0}$ is given by

$$\bar{M}^{v',0} = \prod_{i=1}^{n} M_i(v_i',0) \qquad [A4.7]$$

and $$M_i(v',0) = \int Q_i''(Q_i') \cdot Q_i''(Q_i' + d_i)\, dQ_i \qquad [A4.8]$$

If a progression for only the ith normal vibration in the excited state is considered, then

$$\frac{f^{v_i',0}}{f^{0,0}} = \frac{\sigma^{v_i',0}}{\sigma^{0,0}} \mid \frac{M_i(v_i',0)}{M_i(0,0)} \mid^2 \qquad [A4.9]$$

The $\phi_i(Q_i)$ can be expressed as harmonic oscillator wavefunctions, i.e.,

$$\phi_i(Q_i) = N_{v_i} H_{v_i}(\alpha_i Q_i) \exp\left(-\tfrac{1}{2} \alpha_i^2 Q_i^2\right)$$

α_i and ν_i, the vibrational frequency (in cm^{-1}) of the ith normal vibration are related by

$$\alpha_i^2 = \frac{4\pi^2 c}{h} \nu_i \qquad [A4.10]$$

N_{v_i} is a normalization constant given by

$$N_{v_i} = (\alpha_i/\pi^{1/2} 2^{v_i} v_i!)^{1/2} \qquad [A4.11]$$

and $H_{v_i}(\alpha_i Q_i)$ is a Hermite polynomial of order v_i.

The values of $M_i(v_i',0)$ for harmonic oscillator wavefunctions centred at different points on a given normal coordinate axis have been evaluated in closed form[113]. The most useful values of $M_i(v_i',0)/M_i(0,0)$ are:

$$\frac{M_i(1,0)}{M_i(0,0)} = \frac{\sqrt{2}\,\beta_i^2\,\gamma_i}{(1+\beta_i^2)} \qquad [A4.12]$$

$$\frac{M_i(2,0)}{M_i(0,0)} = \frac{1}{\sqrt{2}(1+\beta_i^2)}\left[\frac{2\beta_i^4\gamma_i^2}{(1+\beta_i^2)} - (1-\beta_i^2)\right] \qquad [A4.13]$$

where $\beta_i = \alpha_i''/\alpha_i'$ [A4.14]

and $\gamma_i = -\alpha_i' d_i$ [A4.15]

If the assignments (v_{ia} and v_{ib}) for two bands of the spectrum differ for only the ith totally symmetric vibrational mode of the excited state, the peak molecular extinction coefficients of these bands (ϵ_a and ϵ_b), the frequencies at which these bands are observed (σ_a and σ_b) and the transition moments for the bands are related by the expression

$$\frac{\epsilon_a}{\sigma_a}\,\frac{\sigma_b}{\epsilon_b} = \left|\frac{M(v_{ia},0)}{M(v_{ib},0)}\right|^2 \qquad [A4.16]$$

The relationship between the extinction coefficients and the absorption intensities of the bands of a spectrum is

$$\epsilon = A/c\ell \qquad [A4.17]$$

where A is the absorbance (cf. equation [2.1]), ℓ the length of the absorbing column of gas (in cm) and c the concentration of the gas in moles/litre.

In this work, absorbance ratios A_a/A_b and band frequencies for any two bands a and b of the spectrum of OCSe could be measured from McPherson monochromator traces (cf. Chapter 2, Section 2.6). Analysis of the spectrum yields the vibrational frequencies of the ν_1 and ν_3 vibrational motions of the ground and excited electronic states. The normal coordinates corresponding to these motions are totally symmetric in linear OCSe.

The normal coordinate changes d_i may then be calculated by use of equations [A4.10] - [A4.17]. Because the R.H.S. of equation [A4.16] is a squared quantity, the signs of the d_i are not determined, i.e., for each totally symmetric normal coordinate Q_i, d_i may be either positive or negative. In linear OCSe Q_1 and Q_3 are totally symmetric, and four possible excited state structures arise from this calculation, each of which could account equally well for the observed intensity distribution.

The calculated d_i, the changes in the normal coordinates upon electronic excitation may be related to changes in bond lengths. In matrix for, equation [A4.4] may be written as

$$[D''] = [Q'] \cdot [D] \qquad [A4.18]$$

The relationship between n_i, the mass weighted Cartesian displacement coordinates and Q_i is, in matrix formulation:

$$[n] = [L]\,[Q] \qquad [A4.19]$$

The method of calculation of the [L] matrix has been described by several authors[8,24]. For the excited state

$$[n'] = [L'] [Q'] = [L'] [Q''] = [D] \qquad [A4.20]$$

Relative to the equilibrium conformation of the ground state ([Q''] = 0), equation [A4.20] becomes

$$[n'] = [L'] [D] \qquad [A4.21]$$

Because the signs of the d_i are undetermined, the negative sign is disregarded. For each atom i, n_i is related to the Cartesian displacement coordinate ζ_i by

$$\zeta_i = (m_i)^{-1/2} n_i \qquad [A4.22]$$

ζ_i is the physical displacement of atom i from its equilibrium position in the ground electronic state upon electronic excitation. The change Δr_{ij} in the equilibrium bond length r_{ij} of the ground state upon electronic excitation is then given by

$$\Delta r_{ij} = \zeta_i - \zeta_i \qquad [A4.23]$$

In linedr OCSe, four possible structures result from this calculation for each excited state (Q_1' and Q_3' are both totally symmetric). Other evidence, both theoretical and experimental, may be available which facilitates a choice between these possibilities.